INFORMATION TO USERS

This material was produced from a microfilm copy of the original document. While the most advanced technological means to photograph and reproduce this document have been used, the quality is heavily dependent upon the quality of the original submitted.

The following explanation of techniques is provided to help you understand markings or patterns which may appear on this reproduction.

1. The sign or "target" for pages apparently lacking from the document photographed is "Missing Page(s)". If it was possible to obtain the missing page(s) or section, they are spliced into the film along with adjacent pages. This may have necessitated cutting thru an image and duplicating adjacent pages to insure you complete continuity.

2. When an image on the film is obliterated with a large round black mark, it is an indication that the photographer suspected that the copy may have moved during exposure and thus cause a blurred image. You will find a good image of the page in the adjacent frame.

3. When a map, drawing or chart, etc., was part of the material being photographed the photographer followed a definite method in "sectioning" the material. It is customary to begin photoing at the upper left hand corner of a large sheet and to continue photoing from left to right in equal sections with a small overlap. If necessary, sectioning is continued again — beginning below the first row and continuing on until complete.

4. The majority of users indicate that the textual content is of greatest value, however, a somewhat higher quality reproduction could be made from "photographs" if essential to the understanding of the dissertation. Silver prints of "photographs" may be ordered at additional charge by writing the Order Department, giving the catalog number, title, author and specific pages you wish reproduced.

5. PLEASE NOTE: Some pages may have indistinct print. Filmed as received.

University Microfilms International
300 North Zeeb Road
Ann Arbor, Michigan 48106 USA
St. John's Road, Tyler's Green
High Wycombe, Bucks, England HP10 8HR

Downloaded from SHAREOK. Persistent Handle URL: https://hdl.handle.net/11244/4306

77-21,407

SOLIZ, Peter, 1944-
A DIAGNOSTIC ANALYSIS OF KINETIC ENERGY BALANCES OF A DEVELOPING CYCLONE OVER THE EAST CHINA SEA DURING AMTEX 1975.

The University of Oklahoma, Ph.D., 1977
Physics, atmospheric science

Xerox University Microfilms, Ann Arbor, Michigan 48106

THE UNIVERSITY OF OKLAHOMA

GRADUATE COLLEGE

A DIAGNOSTIC ANALYSIS OF KINETIC ENERGY BALANCES OF A DEVELOPING CYCLONE OVER THE EAST CHINA SEA DURING AMTEX 1975

A DISSERTATION

SUBMITTED TO THE GRADUATE FACULTY

in partial fulfillment of the requirements for the

degree of

DOCTOR OF PHILOSOPHY

BY

PETER SOLIZ

Norman, Oklahoma

1977

A DIAGNOSTIC ANALYSIS OF KINETIC ENERGY BALANCES OF A DEVELOPING CYCLONE OVER THE EAST CHINA SEA DURING AMTEX 1975

APPROVED BY

DISSERTATION COMMITTEE

ACKNOWLEDGEMENTS

I wish to express my gratitude to Dr. Jay S. Fein for his scientific and personnel counseling throughout this research. My sincere thanks go also to Dr. Yoshi K. Sasaki and Dr. James F. Kimpel, who provided me with their technical advice and encouragement. The review and criticism of this manuscript by Dr. Albert B. Schwarzkopf and Dr. James A. Payne is appreciated.

This dissertation would not have been completed without the assistance of my fellow graduate students, especially Mr. Tom Baxter, Capt. Tom Wildman, Ms. Alvina Hutcheson, and Maj. Wallace Chaplin. I am indebted to Maj. Dennis Moreno and TSgt. Schwartz, who sacrificed their time from duties at the Air Force Global Weather Central in order to supply me with the data used in this research. I wish to acknowledge the assistance of Ms. Jo Ann Oberst and Ms. Joan Kimpel in the preparation of this manuscript.

I will be eternally grateful to my wife, Susan, who not only shared me with this work, but also for providing me with grammatical assistance.

This dissertation was accomplished while attending the University of Oklahoma under the auspices of the Air Force Institute of Technology and sponsored in part by the Atmospheric Sciences Section, National Science Foundation under grant ATM74-23024.

ABSTRACT

A kinetic energy budget of a disturbance which developed in the vicinity of the Air-Mass Transformation Experiment (AMTEX) 1975 is performed using a quasi-Lagrangian approach. Gridded analyses fields for six 12-hour periods are employed in computing the kinetic energy budget of a cyclone, the "AMTEX storm", which developed on about 1200 GMT, 13 February 1975. The objective analysis program, the Pattern Conserving Technique (PCT), used to obtain the gridded fields was developed within the framework of the calculus of variations. PCT, through the application of several variational constraints such as proposed by Sasaki (1970a) and implemented by Baxter (1975), simulates the thought processes and subjective analysis techniques of the human analyst. The analyses fields are further refined by including physical constraints which minimize inertial instability, satisfy hydrostatic balance and insure for mass continuity.

From the resulting horizontal wind analyses vertical motion fields are computed using the kinematic method and are verified for representativeness by subjectively comparing them with synoptic features such as fronts, precipitation reports, cloud analyses, and satellite photographs obtained from the U.S. Air Force Global Weather Central (AFGWC). The vertical motion fields are also compared

with those derived from the quasi-geostrophic omega equation as solved by the Japanese Meteorological Agency (JMA), and the AFGWC, and with vertical motions kinematically computed from subjectively analyzed horizontal winds. The results of the comparison show that the vertical motion fields obtained from PCT exhibit a marked improvement in representing the synoptic situation and related weather features.

The kinetic energy budget of the AMTEX storm was found to produce values of reasonable magnitude when compared with results of similar studies. In some aspects the budget for the AMTEX storm differed qualitatively from budgets of storms studied over the North American Continent. For example, from studies such as Ward and Smith (1976), the advection of kinetic energy into developing cyclones east of the Rocky Mountains provides the storm with a source of kinetic energy. The advection term in the budget for the AMTEX storm was initially negative (sink) and became positive (source) in the latter periods of this study.

The results serve to document from a kinetic energy perspective the large-scale physical processes responsible for the intense cyclogenesis frequently observed in the AMTEX area.

TABLE OF CONTENTS

	Page
ACKNOWLEDGEMENTS	iii
ABSTRACT	iv
LIST OF TABLES	vii
LIST OF FIGURES	viii
CHAPTER	
I. INTRODUCTION	1
II. REVIEW OF THE LITERATURE IN RELATION TO THE PRESENT STUDY	5
III. THE DATA	16
IV. THE ANALYSIS AND COMPUTATIONAL TECHNIQUES	21
V. A SYNOPTIC DISCUSSION	35
VI. RESULTS	39
VII. CONCLUSIONS AND SUGGESTIONS FOR FUTURE RESEARCH	57
BIBLIOGRAPHY	61
APPENDICES	
A. THE KINETIC ENERGY EQUATION	65
B. THE MINIMIZATION OF THE FUNCTIONAL USED IN THE PATTERN CONSERVING TECHNIQUE OF THE OBJECTIVE ANALYSIS	67
C. A VARIATIONAL APPROACH TO HYDROSTATICALLY ADJUSTING OBJECTIVELY ANALYZED HEIGHT AND TEMPERATURE FIELDS	72
D. A VARIATIONAL APPROACH TO THE MASS CONTINUITY PROBLEM	75
E. A SENSITIVITY ANALYSIS	79

LIST OF TABLES

Table		Page
1.	Kinetic energy budgets by period for Smith's (s) and Petterssen and Smebye (P & S). (from Smith, 1973).	83
2.	Kinetic energy balance of various types of cyclonic disturbances. (from Kung and Baker, 1975).	83
3.	Cyclone vicinity budget for the period 1200 GMT, April 12 to 0000 GMT, April 15, summarized with cyclone system budget. (from Smith, 1973).	84
4.	Summary of the data set	85
5.	Summary of "3-D Neph" data.	85
6.	Definition of variables used in Eq. (4.2)	86
7.	Root-mean square errors in radiosonde computed height and density at specified pressure. (from Lenhard, 1973)	87
8.	Definition of variables in Eq. (4.6).	88
9.	Cyclone vicinity budget from study by Smith (1973). . .	89
10.	Kinetic energy budget for AMTEX storm vicinity from 0000 GMT, 13 February to 1200 GMT, 15 February 1975 . .	89
11.	Same as Table 10 except for 0000 GMT, 13 February to 0000 GMT, 15 February	89
12.	Time-mean, avrea-average cyclone vicinity kinetic energy budget for 11-24 April 1970 (from Ward and Smith, 1976).	90
13.	Same as Table 12 except for 13-18 April 1970. (from Ward and Smith, 1976)	90
14.	Kinetic energy budget for AMTEX storm vicinity. Budget quantities are in Wm^{-2}	91

LIST OF FIGURES

Figure		Page
1.	Summary of kinetic energy budgets ($W \cdot m^{-2}$) for general circulation and various synoptic systems. (from Smith, 1973).	92
2.	The analysis grid in vicinity of the AMTEX with observation sites	92
3.	The objective analysis grid used in this study.	93
4.	The standard polar stereographic AFGWC analysis grid. .	94
5.	Vertical resolution of the AFGWC objective analysis model with symbols indicating where parameters are analyzed.	95
6.	How a data point alters a first guess field when a Cressman type of analysis is applied.	96
7.	Outline of the gridded cloud analyses boxes	97
8.	Spatial resolution of the three dimensional cloud analysis program.	98
9.	The objective analysis grid used in this study.	99
10.	The relative location of terms on the staggered grid used for solving Eq. (4.6).	100
11.	Central low pressure of the cyclone which developed in the East China Sea during the AMTEX 1975	101
12.	Examples of curve fitting for kinetic energy changes. .	102
13.	Frequency of cyclone formation. (Trewartha, 1961) . . .	103
14.	Sea level surface analysis with surface fronts, 1200 GMT, 13 February 1975.	104
15.	850-mb height analysis and temperature analysis for 1200 GMT, 13 February 1975.	104
16.	500-mb height analysis and temperature analysis for 1200 GMT, 13 February 1975.	105
17.	300-mb height analysis and isotach analysis for 1200 GMT, 13 February 1975.	105

Figure Page

18. Same as Fig. 14 except for 0000 GMT, 14 February 1975. (Surface) 106

19. Same as Fig. 15 except for 0000 GMT, 14 February 1975. (850-mb) 106

20. Same as Fig. 16 except for 0000 GMT, 14 February 1974. (500-mb) 107

21. Same as Fig. 17 except for 0000 GMT, 14 February 1975. (300-mb) 107

22. Same as Fig. 14 except for 1200 GMT, 14 February 1975. (Surface) 108

23. Same as Fig. 15 except for 1200 GMT, 14 February 1975. (850-mb) 108

24. Same as Fig. 16 except for 1200 GMT, 14 February 1975. (500-mb) 109

25. Same as Fig. 17 except for 1200 GMT, 14 February 1975. (300-mb) 109

26. Same as Fig. 14 except for 0000 GMT, 15 February 1975. (Surface) 110

27. Same as Fig. 15 except for 0000 GMT, 15 February 1975. (850-mb) 110

28. Same as Fig. 16 except for 0000 GMT, 15 February 1975. (500-mb) 111

29. Same as Fig. 17 except for 0000 GMT, 15 February 1975. (300-mb) 111

30. Same as Fig. 14 except for 1200 GMT, 15 February 1975. (Surface) 112

31. Same as Fig. 15 except for 1200 GMT, 15 February 1975. (850-mb) 112

32. Same as Fig. 16 except for 1200 GMT, 15 February 1975. (500-mb) 113

33. Same as Fig. 17 except for 1200 GMT, 15 February 1975. (300-mb) 113

34. The JMA 700-mb vertical motions for 0000 GMT, 14 February 1975 114

Figure		Page
35.	The AFGWC 775-mb vertical motions for 0000 GMT, 14 February 1975.	114
36.	775-mb vertical motions computed kinematically from subjectively analyzed horizontal winds for 0000 GMT, 14 February 1975.	115
37.	The PCT 775-mb vertical motions for 1200 GMT, 13 February 1975.	115
38.	Same as Fig. 37 except for 0000 GMT, 14 February 1975 .	116
39.	Same as Fig. 37 except for 1200 GMT, 14 February 1975 .	116
40.	Same as Fig. 37 except for 0000 GMT, 15 February 1975 .	117
41.	Same as Fig. 37 except for 1200 GMT, 15 February 1975 .	117
42.	The DMSP (Defence Meteorological Satellite Program) satellite photograph valid 0332 GMT, 14 February 1975 .	118
43.	Precipitation analysis for the period from 0000 GMT, 14 February to 0600 GMT, 14 February 1975	119
44.	Same as Fig. 34. (JMA 700-mb ω_s) except for 1200 GMT, 14 February 1975.	120
45.	Same as Fig. 35. (AFGWC 775-mb ω_s) except for 1200 GMT, 14 February 1975.	120
46.	Same as Fig. 36. (Subjective 775-mb ω_s) except for 1200 GMT, 14 February 1975.	121
47.	Cloud analysis for the 800- to 700-mb layer from AFGWC's 3-D Neph analysis model. Valid 1200 GMT, 14 February 1975.	121
48.	Central pressure of major cyclone as a function of time in six hour increments. (from Smith, 1973). . . .	122
49.	Same as 48 except for AMTEX storm	122
50.	Sea level analysis for 1200 GMT, 15 April 1970.	123
51.	The 500 mb height and temperature analysis for 1200 GMT, 15 April 1970	123
52.	The 300 mb height and isotach analysis for 1200 GMT, 15 April 1970	123

Figure Page

53. The kinetic energy budget terms for the AMTEX storm vicinity as a function of time. (---Surface to 100 mb. ——500 mb to 100 mb) 124

54. The kinetic energy budget terms for the AMTEX storm vicinity as a function of time. (——Surface to 500 mb) 124

55. The 300-mb isotach analysis and the generation of kinetic energy for a 100-mb layer centered at 300 mb for 0000 GMT, 15 February 1975. 125

56. The DMSP satellite photograph valid 0351 GMT, 13 February 1975. 126

57. Temperature - dew point spread analysis for 0000 GMT, 13 February 1975. 127

58. Vertical change in kinetic energy with respect to pressure ($\frac{\partial k}{\partial p}$) from surface to 850 mb. Valid 0000 GMT, 14 February 1975. 128

59. The energy cycle of the atmosphere as estimated by Oort (1964a). 129

60. Horizontal distribution of the vertically integrated generation of kinetic energy for 0000 GMT, 14 February 1975. 130

61. The sensitivity of budget terms to % changes in the geostrophic wind as first guess for the wind analysis . 131

A DIAGNOSTIC ANALYSIS OF KINETIC ENERGY BALANCES OF A DEVELOPING CYCLONE OVER THE EAST CHINA SEA DURING AMTEX 1975

CHAPTER I

INTRODUCTION

During the winter months, off the east coasts of the North American and Asian continents, rapid development of sub-synoptic cyclones is frequently observed to occur as cold, dry continental air flows southeastward over warm coastal waters. Within a short time these cyclones intensify into dangerous synoptic-scale lows that pose a potential threat to life and property. The source of energy for their rapid and intense development is thought to be derived partly from the transfer of latent and sensible heat by the sea to the atmosphere. To study these and other processes associated with air-mass modification and subsequent cyclone development, the Air-Mass Transformation Experiment (AMTEX), a sub-program of the Global Atmospheric Research Program (GARP), was conducted in an area that has a particularly high frequency of cyclogenesis during the winter months.

The site chosen to measure the processes involved in air-mass modification is in the East China Sea where a chain of

islands with existing reporting stations or with facilities for conducting observations is present. In addition to these islands (the Southwest Islands of Japan) the area is well traveled by commercial ships which are another source of data. To supplement these data sources research ships were dispatched to areas where data requirements could not otherwise be met. The major factor, however, which makes this area favorable for studying air-sea interactions is the presence of a current of warm ocean water, the Kuroshio or Japan Current.

One of the objectives of AMTEX is to study the relationship between fluxes of energy from the ocean and the generation of medium-scale cyclones. Although a great deal may be learned from the data gathered by AMTEX about the smaller scale disturbances, such as cumulus and organized clusters of cumulus (~50-300 km scale), the AMTEX data must be supplemented by the synoptic data, which is of greater areal extent, in order to study more adequately the behavior of the medium (~1000 km) and large scale (> 3000 km) disturbances. Together these data could then serve as the basis for studying the modification of the cold air mass in the perspective of the sub-synoptic scale or synoptic-scale energetics.

A study of the energy cycle of a cyclone, including the generation and destruction of potential energy by thermal energy sources such as radiation, latent and sensible heat fluxes from the sea surface, and release of latent heat through condensation, may be attempted only after techniques for analyzing the data have been developed. The more restricted problem of kinetic-energy

relationships can be investigated early in the development of such techniques. Although a kinetic energy study cannot quantify the relative importance of the various energy sources for generation of available potential energy, it will add to the understanding of a most important phase of the energy cycle of a cyclone. This logical first step in documenting the energetics of an extra-tropical disturbance would describe quantitatively the evolution and distribution of the storm's kinetic energy. Additionally, the analysis techniques developed to accomplish such a study would aid immeasurably in dealing with the second more difficult task of producing a potential energy budget study.

A diagnostic analysis of kinetic energy balances is essential in extending knowledge of the role of cyclonic disturbances in the earth's general circulation. In studying a single storm, one can only speculate about the overall role of extra-tropical cyclones. One can, however, provide results from the kinetic energy study which are vital in verifying output from forecast models. Diagnostic kinetic energy budgets provide a basis for quantitative comparison with forecast models, which ultimately leads to improved modeling of the atmospheric process and improved accuracy of forecasts.

The general objective of this research is to examine the kinetic energy budget of a rapidly developing cyclone over the East China Sea during the 1975 AMTEX. With the exception of the sub-grid scale and dissipation terms, which are evaluated as a residual, all the terms in the kinetic energy equation are

computed explicitly for various times in the development of the cyclone in the period from February 13 at 0000 GMT to February 15 at 1200 GMT. To attain the general objective, the following tasks have been performed:

1. Objectively analyzed, gridded data, to be used for the budget calculations, are evaluated with other analyzed fields of data for their ability to represent synoptic features.
2. The kinetic energy budget results are compared to results of other research to test the representativeness of the storm studied. Gross differences are explained.
3. The relative importance of the various terms responsible for local changes in kinetic energy are evaluated for different stages of the storm's development.
4. The role of medium-scale cyclones in the general circulation is investigated by comparing results from this budget with those values attributed to the general circulation.

In the next chapter a brief review of the more current studies which delve into the kinetic energy of various phenomena is presented. The nature of the data used in this research is described in Chapter III, while its application and computational methods are given in Chapter IV. In the final three chapters a synoptic history of a cyclone which developed in the East China Sea between February 13 and 14, 1975, is discussed, followed by the results of the kinetic energy budget and concluding remarks.

CHAPTER II

REVIEW OF THE LITERATURE IN RELATION TO THE PRESENT STUDY

The early works in atmospheric energetics sought to examine energy transformations in the earth's atmosphere which maintain the general circulation. Lorenz (1955) developed the concept of available potential energy from the ideas proposed by Margules (1903). Lorenz (1967) recognized the importance of the large-scale eddies in the general circulation. As a result, many of the studies of available potential energy and kinetic energy were applied to open systems where boundary transports made a significant contribution to the energy budget of an area. With the better understanding of the general circulation as a common goal, later kinetic energy budget studies varied in technical approach as well as in their immediate objectives.

Sechrist and Rudy (1969) analyzed kinetic energy changes of a major cyclone which occurred over the United States. In their study they computed Term A and Term B of the kinetic energy equation, derived in Appendix A,

$$\underbrace{\frac{\partial \bar{K}}{\partial t}}_{A} + \underbrace{\bar{\vec{V}}\cdot\nabla\bar{K} + \bar{\omega}\frac{\partial \bar{K}}{\partial p}}_{B} + \underbrace{\bar{\vec{V}}\cdot\nabla\bar{\varphi}}_{C} = \underbrace{\overline{\vec{V}\cdot\nabla K'} + \overline{\omega'\frac{\partial K'}{\partial p}} + \overline{\vec{V}'\cdot\nabla\varphi'}}_{D} + \delta \equiv R \ , \quad (2.1)$$

where K is the kinetic energy defined by $K = \frac{|\vec{V}|^2}{2}$; where $\vec{V}$ is the horizontal wind vector; φ is the geopotential height; and $\omega = \frac{dp}{dt}$ is the vertical component of the wind velocity. δ is the frictional dissipation of kinetic energy, and R is defined as the "residual". The overbar is a spacial average;

$$(\bar{}) = \frac{1}{A} \int_A ( ) \, dA \, , \tag{2.2}$$

where A is the grid area. That is, the overbar terms are grid point variables considered to be representative over a grid area. In the existing literature, R, the residual, is often referred to as the "dissipation" term. In reality the term represents the sum of frictional dissipation, subgrid-scale processes, and errors involved in calculating the large (grid)-scale terms on the left-hand-side of Eq. (2.1).

Using Eq. (2.1), Sechrist and Rudy discussed whether net conversion of available potential energy resulted or whether there was net dissipation. By not calculating explicitly term C, the conversion term, they avoided the most difficult task of computing the divergence of the horizontal wind field and vertical motions. Their goal was to show the relative importance of barotropic and baroclinic instability in the life cycle of the cyclone. They defined local changes in kinetic energy due to preexisting energy advected into the storm as barotropic instability. Baroclinic instability was used in the classical sense, i.e., the conversion from available potential energy to kinetic energy.

From the results of their calculations they arrived at the

following conclusions: first, that the advection term contributed more significantly in the initial stages of development; second, that the conversion process must have become more dominant in subsequent periods of development; and third, that the conversion process began first at low levels then later at successively higher levels. Although their approach was rather simple and incomplete in determining the various terms in Eq. (2.1), their conclusions were justified by their results.

Some investigators (e.g. Kung, 1975) have attempted to study more directly the effect of barotropic instability on kinetic energy budgets. By defining an area mean, $[x]$ and a departure from the mean, x^*, a variable x may be given as

$$x = [x] + x^* \ . \tag{2.3}$$

The kinetic energy equation for eddy quantities is then written by Kung as:

$$\left[\frac{\partial K_E}{\partial t}\right] = -[\nabla\cdot\vec{V}K_E]-\left[\frac{\partial \omega K_E}{\partial p}\right]-\left[(u^*\omega^*)\frac{\partial [u]}{\partial p}\right]+[v^*\omega^*]\frac{\partial [v]}{\partial p} - [\vec{V}^*\cdot\nabla\varphi^*]-[E^*] \tag{2.4}$$

where u and v are eastward and northward wind components and E^* is dissipation of kinetic energy at the eddy scale. Kung's (1975) study dealt with the kinetic energy budget of the tropical circulation over the Western Pacific. A similar technique was used by Kung and Tsui (1975) for the kinetic energy budget of a storm area over central Oklahoma. The use of the term "eddies" by these investigators implies the classical definition (Lorenz 1967). However, in the classical definition the average is taken

with respect to longitude. The validity of this approach in studying barotropic exchange of kinetic energy is therefore open to some question.

In a more straight-forward approach, Petterssen and Smebye (1971) studied the kinetic energy budget of two developing winter cyclones over the United States. In one case the cyclone developed in the absence of any significant amount of baroclinicity. There were initially, however, large values of positive vorticity advection. In the second case the opposite features were observed: a strong baroclinic zone with no appreciable vorticity advection.

Smith (1973b) compared the kinetic energy budget results of Petterssen and Smebye with his own study of cyclone development over the United States in mid-April of 1964. For three periods of the storm's life cycle Smith computed all terms in the kinetic energy equation explicitly with the exception of the dissipation term. In this particular study he found that the kinetic energy changes increased with height so that the larger changes occurred in the upper troposphere. In the layer from the surface to 800 mb his results revealed that gains in kinetic energy due to the conversion process were nearly in balance with the residual term. Advection or a positive flux of kinetic energy, especially in the upper layers, played a significant role in the maintenance of the cyclone development.

Smith's budget differs markedly from that of Petterssen and Smebye, as seen in Table 1. The differences can be justified, at least qualitatively, by the argument that differences in synoptic

situations can produce significantly different results in a kinetic energy budget. In spite of the obvious weakness in using a limited number of kinetic energy budget studies of individual cyclones to compare with a kinetic energy budget of the general circulation, Smith proceeded to demonstrate how the terms of the kinetic energy equation of a "mean cyclone system" might compare with those of the general circulation. Smith's "mean cyclone system" was defined as his Eulerian computational grid which encompassed most of the North American continent. By incorporating the results of several other studies and combining them with his own, he produced an interesting comparison of the kinetic energy budget for the general circulation and for a cyclone system representative of his study and that of Petterssen and Smebye (see Fig. 1). Also noteworthy is his budget for the "cyclone vicinity" in the lower left-hand corner of Fig. 1. The definition of the areal coverage of the cyclone system studied was shown to strongly affect the resulting budget.

Kung and Baker (1975) overcame the problem of generalizing about the role of synoptic scale disturbances in the middle-latitude's global circulation by analyzing a data set over the United States spanning five years. They categorized the disturbances and evaluated mean energy budgets. They verified the suggestion from the earlier studies that cyclones exhibit different energy balances at various stages of development. Kung and Baker accomplished this by examining budgets for the categories classified as developing, mature, occluded, etc. A comparison between

Tables 1 and 2 reveals the extent to which this study agrees with those of Petterssen and Smebye, and Smith. Smith's study of the cyclone vicinity, as well as that of Sechrist and Rudy (1969), indicated a significant import of kinetic energy for all stages of the storm's life cycle, while the studies of Kung and Baker and of Petterssen and Smebye showed an export. In fact the generation term in all but Smith's study appears sufficient to maintain the kinetic energy level. The differences in the results can of course be explained by noting the varying degree of cyclonic development in the cases studied and by the effect of averaging many cases as in Kung and Baker's study.

The difficulty in accurately estimating the conversion term has been discussed in the studies mentioned above. The problem lies in producing a computational model to objectively analyze wind fields from data which include observational errors of about 10 percent and are relatively scarce in space and time. Thompson (1961) noted that a 10 percent measurement error in the observed wind field could lead to a 100 percent error in the computed values of divergence. This kind of error is cumulative when one uses the so-called kinematic technique to integrate the continuity equation to compute vertical motion. However, because of the problems encountered in the vertical integration, alternate techniques have been devised.

One such technique involves solving the so-called "omega equation", one form of which is

$$\sigma\nabla^2\omega + f\eta\frac{\partial^2\omega}{\partial p^2} = f\frac{\partial}{\partial p}[\vec{V}\cdot\nabla\eta] - \nabla^2(\vec{V}\cdot\nabla\frac{\partial\Phi}{\partial p}) - (\frac{R}{C_p})\nabla^2 Q \ , \qquad (2.5)$$

where σ is a static stability term which can be at most a function of pressure only, $\omega \equiv \frac{dp}{dt}$, f is the Coriolis parameter, η is the absolute vorticity, R is the universal gas constant, C_p is the specific heat of air at a constant pressure, Q is the diabatic heating rate, and φ is the geopotential height of the pressure surface, p. The horizontal velocity, $\vec{V}$, is often approximated by its non-divergent component and may be expressed in terms of a stream function ψ by

$$V_r = k \times \nabla \psi \quad . \tag{2.6}$$

A similar form of the omega equation is derived by Haltiner (1971).

Although this technique circumvents many of the problems associated with the kinematic technique, the assumptions made in deriving the quasi-geostrophic equation are too limiting and incomplete in a physical sense. Notably, terms involving time derivatives in the divergence equation and the divergence itself have been set to zero. In addition only the rotational part of the wind is used in the advection term, and the relative vorticity is replaced by its geostrophic value. The vertical advection of vorticity is dropped, as is the relative vorticity, when compared to f in the divergence term. These approximations can all be justified by scale analysis for medium to large scales of motion for which the Rossby number, $R_o \lesssim 10^{-1}$, where

$$R_o \equiv \frac{V}{fL} \ , \tag{2.7}$$

and V and L represent the characteristic horizontal velocity and

the characteristic horizontal scale, respectively (Haltiner, 1971). In order to describe more fully the vertical motion of smaller scales one must resort to a different technique.

Panofsky (1951) describes the advantages and disadvantages of the adiabatic, vorticity, and kinematic techniques for evaluating vertical motions. Smith (1971) compares the values of vertical motions derived from the kinematic technique with those by Krishnamurti (1968a, 1968b), who experimented with several forms of the omega equation by varying the degrees of simplification through the assumptions made in its derivation. Smith found that vertical motion derived from the kinematic technique compared favorably with values derived from a form of the omega equation which included the terms for friction, sensible and latent heating, and a number of other parameters (Krishnamurti, 1968b). Both techniques were compared to observed precipitation and cloudiness. In his study Smith found it necessary to use an adjusted vertical motion field to account for the cumulative bias errors in the estimates of divergence.

One adjustment technique which Smith applied to the vertical motions was derived by O'Brien (1970). O'Brien employed a variational formulation which led to an objective scheme for adjusting divergence and vertical motion profiles constrained by upper and lower boundary conditions on the vertical motion, ω. The calculus of variation methods was first applied to meteorological problems by Sasaki (1958). Recently he has proposed an alternate adjustment technique which solves a variational functional constraining

the wind fields by the integrated continuity equation. This technique is more fully discussed in another section.

Kung (1975, 1974, 1973) has taken yet another approach to computing ω's for a kinetic energy budget study. He analyzed the horizontal wind data through the use of a least squares fit to an approximating polynomial. Kung experimented by varying the degree of the polynomial until a profile satisfying predetermined criteria resulted. Mass continuity is usually only approximately realized by this technique.

Once the technical difficulty of producing a "good" vertical motion field is overcome, the study of the kinetic energy balance is rather straightforward as noted in Eq. (2.1). With the exception of the residual, R, all the other terms can be computed directly. The conversion term can be rewritten as

$$- \vec{V} \cdot \nabla \varphi = - \nabla \cdot \vec{V} \varphi - \frac{\partial \omega \varphi}{\partial p} - \omega \alpha \qquad (2.8)$$

where $-\omega\alpha$ may be regarded as the release of available potential energy and the other two terms represent work done on the boundaries.

The only source for kinetic energy, KE, is available potential energy, APE. APE represents a part of the existing total potential energy which can be converted to kinetic energy. That quantity is given by the difference between the total potential energy of the atmosphere, TPE, and the minimum value TPE, TPE_o, that can be achieved through adiabatic redistribution.

$$APE = TPE - TPE_o \qquad (2.9)$$

This minimum is reached when the atmosphere's density becomes horizontally stratified and statically stable. Lorenz (1955) describes more fully the concept of APE and its relationship to KE. He summarizes the important properties of APE in the following statements:

"(1) The sum of the available potential energy and the kinetic energy is conserved under adiabatic flow.

(2) The available potential energy is completely determined by the distribution of mass.

(3) The available potential energy is zero if the stratification is horizontal and statically stable."

Eq. (2.1) gives no indication of the possible sources for APE generation. The role of the various diabatic processes involved in the generation and destruction of APE, which ultimately becomes the source of the atmosphere's KE, is both quantitatively and qualitatively explained by Dutton and Johnson (1967). The rate of change of APE is proportional to the rate of heating by the diabatic processes, Q.

$$Q = -\nabla\cdot R_S - \nabla\cdot R_L + F_Q + T_Q + L \qquad (2.10)$$

where R_S and R_L are the radiational heating of the solar and infrared components, F_Q is the effect of frictional dissipation, T_Q is the effect of sensible heating, and L is the effect of latent heating.

In the above kinetic energy studies, the source for the generation of available potential energy, APE, was never considered even in a qualitative sense. However, in performing a kinetic energy study in a region where one might suspect certain dominant sources

for the generation of APE, one might speculate on those possible sources by indirect means. An example of this situation is off the east coasts of the Asian and North American continents where cyclonic development is observed to occur over the vicinity of warm ocean currents. Those regions are believed to be a source for sensible and latent heat fluxes.

The Air-Mass Transformation Experiment (AMTEX) of 1975 offers the opportunity to examine the conversion processes of APE to KE in a rapidly developing cyclone over the East China Sea. Here the influence of the warm Kuroshio current, through sensible and latent heat fluxes during cold air outbreaks in winter, is thought to play a dominant role in the frequent cyclone development in that area during that season. By means of the combination of the special data obtained from the AMTEX region and the normal synoptic data of the surrounding area, one can accomplish a budget study which should show quantitatively the magnitudes of the various terms responsible for local changes in kinetic energy.

CHAPTER III

THE DATA

Radiosonde observations (RAOBS) and surface data used in this study were provided for stations indicated in Fig. 2 by the AMTEX. The RAOB data include measurements of wind speed and direction, temperature, relative humidity, and height for the standard pressure levels from 1000 mbs to 100 mbs. These data were checked for gross coding and decode errors as well as for hydrostatic consistency using a computer program developed by Inman (1969) for the National Severe Storms Forecast Center. The surface data obtained from the AMTEX along with all surface data within the analysis grid (see Fig. 3) were subjectively checked for horizontal consistency as well as for coding errors.

The data for the area surrounding AMTEX have been provided by the Air Force through the Air Force Global Weather Central (AFGWC). These RAOBS were similarly decoded and checked by AFGWC for hydrostatic consistency. In addition to those data points indicated in Fig. 3, military aircraft reports have been obtained from AFGWC which supplement the regular synoptic upper air RAOB data. These data were hand screened for errors. Because of the nature of these data, special care had to be exercised in their application. The technique used to apply aircraft data will be discussed

below. Other surface data used in the analyses included any roving ship reports which were received by AFGWC. Some supplemental data have been obtained from Asheville. Satellite-derived RAOBS were also obtained from AFGWC, but their validity was questionable and they were therefore not used in this study. The temporal and vertical resolution of the data are summarized in Table 4.

From Fig. 3 one can easily recognize the potential for large errors in an objective analysis due to the sparsity of data in large regions over the ocean. In this respect the aircraft reports provided the analyses with much-needed data. However, aircraft data are asynoptic in time. In other words, aircraft observations are not made at the regularly spaced time intervals for which RAOBS are taken. Although a data assimilation scheme would probably have been the best approach in incorporating these data (see Ritchie, 1975), this research did not attempt such a procedure. For this project it was sufficient to take reports within some small interval of time of synoptic data and apply them to that particular synoptic time. The aircraft reports were then assigned a standard pressure level by AFGWC's validation model where they were incorporated into the objective analysis.

Initial gridded values for the height, temperature, and dewpoint have been obtained from AFGWC's operational objective analysis model. AFGWC employs a multi-level objective analysis technique (MULTAN) described by Moreno (1974). The AFGWC grid and vertical resolution are given in Figs. 4 and 5. The analysis

technique is similar to one which has been used by the Numerical Meteorological Center (NMC) (Gilchrist and Cressman, 1954). It has been referred to as the successive approximation method or a Cressman analysis.

Briefly, MULTAN starts with a six- or twelve-hour forecast of heights as its first guess. These gridded fields are modified by applying successively the observed height data. This technique is illustrated in Fig. 6. An analysis is first obtained for the 300 mb level because of its operational significance and also because of the large number of aircraft reports near this level. Using the 300 mb analysis and forecast values in combination by means of a statistically derived set of regression equations, MULTAN successively analyzes the lower levels, then re-analyzes the 300 mb level and the higher levels. This method of analyzing multiple levels insures some vertical consistency.

AFGWC also provided initial vertical velocities computed using the quasi-geostrophic omega equation,

$$\sigma\nabla^2\omega + f^2 \frac{\partial^2\omega}{\partial p^2} = f_o\left[\frac{\partial}{\partial p} J(\psi,\eta) - \nabla^2(\vec{\underline{V}}\cdot\nabla \frac{\partial\psi}{\partial p})\right] , \qquad (3.1)$$

where $\vec{\underline{V}}$ is mean wind for the layer, and f_o is a mean value of the Coriolis parameter, ψ is the stream function and is computed from

$$\nabla^2\psi = \frac{g}{f}\nabla^2 z - \frac{g}{f^2}\nabla z\cdot\nabla f , \qquad (3.2)$$

where g is acceleration of gravity, and z is the height of a pressure surface.

The gridded data for the AFGWC three-dimensional nephanalysis,

3-D Neph (Coburn, 1971) boxes 11, 12, 19 and 20, (see Fig. 7) have been obtained from Environmental Technical Applications Center (ETAC). Table 5 summarizes the type of information available for this research from the 3-D Neph. These data were used primarily as a subjective aid in determining the validity of the computed vertical motion patterns. The 3-D Neph is an operational program at AFGWC which processes a collection of data including cloud information which is obtained from the Defense Meteorological Satellite Program (DMSP). A number of these satellites are capable of providing updated cloud information for a given area several times a day. The satellite data available for cloud interpretation include:

H, high resolution (2 NM) visual (sensed at 0.4 to 1.1 micrometer)

V, very high resolution (1/3 NM) (sensed at 0.4 to 1.1 micrometer)

I, high resolution infrared (sensed at 8 to 13 micrometers)

W, very high resolution infrared.

Sheer quantity of these data prohibits an analysis at the 1/3 NM resolution.

The Nephanalysis is performed on a grid with about a 48 km horizontal spacing, which represents one eighth of the basic AFGWC numerical grid depicted in Fig. 4. The grid is extended vertically through 15 levels from 150 feet above ground level to 40,000 feet (Fig. 8). The analysis is performed every three hours for the entire northern hemisphere, merging satellite data with more

conventional data such as surface observations and aircraft reports. In this way areas which have had no recent satellite coverage are continually updated by cloud intelligence derived from other sources.

CHAPTER IV

THE ANALYSIS AND COMPUTATIONAL TECHNIQUES

The data described above are analyzed on a grid which is a subset of the AFGWC octagonal grid (see Fig. 4) and is illustrated in Fig. 9. The grid is on a polar stereographic map projection true at 60 degrees north. The grid spacing at 60 degrees north is 190.5 Km, half the AFGWC mesh. Two grids are used in this study. The grid in Fig. 9 is the analysis grid, on which the variables height, temperature, dewpoint depression, and wind components are analyzed. Values for divergence and vertical velocities are computed for the same grid. Within this grid are outlined other grids of the same mesh size which are used to compute the various terms in the kinetic energy equation. This set of grids is employed in following the storm in time and in performing the actual kinetic energy budget study.

The size and position of the second grid are determined by the following criteria. The right and lower (southern) vertical boundaries (walls) of the grid are based solely on features at the surface and are chosen so that they enclose the last closed isobar. Since the disturbance tilts to the northwest, the upper air features are used to complete the selection of the vertical boundaries. The 500-mb trough defines the grid's leftmost extent.

Finally, the upper (northern) vertical boundary is selected so that the storm is near the center of the grid. There is no unique method, nor does this procedure profess to offer a method, for defining the area of a synoptic disturbance; rather it provides one with a consistent means of following the storm volume as it moves during the period of study.

To produce a gridded analysis from irregularly distributed data, one may choose from many objective analysis schemes. The objective analysis usually adopted for a kinetic energy budget study involves the local fitting of a polynomial surface or the application of a successive corrections method. For this study an analysis technique described by Baxter (1974) which preserves certain characteristics of the first guess has been employed. The pattern conservation technique (PCT) simulates many of the thought processes of a good analyst. The human analyst will usually have a first guess field which may be a forecast or a recent past analysis. Using the first guess field as a guide he fits the new data to the first guess, attempting as much as possible to preserve the shapes of contours and magnitudes of gradients. Where data and first guess fields differ significantly the analyst may remove the data on the grounds that the data may be in error, or he may wish to accept the data based on other supporting evidence. In this case he can alter the magnitudes while preserving the contours.

The objective of PCT is to simulate the logic of the analyst by applying the available information with varying degrees of

confidence. The information and characteristics of the analysis which will be considered are: (1) the data; (2) the AFGWC analysis for the same time (the first guess); (3) the gradient of the first guess in eight directions from a grid point; and (4) the Laplacian of the first guess. An analysis which satisfies the above constraints is achieved by the use of a formalism in the calculus of variations. The integral which we wish to minimize may be written as

$$J = \iint_A [\alpha(X - \tilde{X})^2 + \beta(\nabla X - \nabla\tilde{X})^2 + \gamma(\nabla^2 X - \nabla^2\tilde{X})^2]dx\ dy\ , \quad (4.1)$$

where J is the functional; α, β and γ are prescribed weights; X is the analyzed gridded variable; $\tilde{X}$ is the observed, or first guess, gridded variable; and A is the horizontal area over which the analysis is performed. This formalism fits the definition of a weak constraint as given by Sasaki (1970a).

The resulting analysis of the data is influenced by each of the three terms in Eq. (4.1) according to the weight assigned to them. The first term determines the effect of the data on the analysis. Although the analysis is performed on a grid, some grid points do not have data assigned to them. For these points a first guess is assigned, normally with a lower weight than that given to grid points to which data have been assigned. The second term serves to preserve gradients of the first guess, while the third term, a Laplacian, preserves the curvature. These last two terms have the effect of spreading the influence of data into data-void areas on the grid.

Eq. (4.1) may be written in finite difference form as

$$J = \sum_{i=1}^{I} \sum_{j=1}^{J} [A_{i,j}(X^*_{i,j} - X_{i,j})^2 + B_{i,j}(\mu^*_{i,j} - \mu_{i,j})^2$$

$$+ B_{i,j-1}(\mu^*_{i,j-1} - \mu_{i,j-1})^2 + C_{i,j}(\nu^*_{i,j} - \nu_{i,j})^2$$

$$+ C_{i-1,j}(\nu^*_{i-1,j} - \nu_{i-1,j})^2 + E_{i,j}(\alpha^*_{i,j} - \alpha_{i,j})^2$$

$$+ E_{i+1,j-1}(\alpha^*_{i+1,j-1} - \alpha_{j+1,j-1})^2 + F_{i,j}(\beta^*_{i,j} - \beta_{i,j})^2$$

$$+ F_{i-1,j-1}(\beta_{i-1,j-1} - \beta_{i-1,j-1})^2 + D_{i,j}(L^*_{i,j} - L_{i,j})^2] \qquad (4.2)$$

where the above scalar variables are all defined in Table 6. The resulting Euler-Lagrange equations and their derivation are given in Appendix B.

In order to duplicate the analyst's removal of data which appears to be in error, PCT solves the above minimization equation several times. After each minimization process the weight of the data is re-evaluated by noting the change in the last guess field affected by a given piece of data. If a particular report causes too large a change in the guess field or its differential properties, PCT will consider the report to be in error and will lower the value of its weight, A_{ij}, to reflect a lack of confidence in the value of the data. This process is repeated after

each cycle, which makes it possible for a report to have part or all of its original weight restored as the influence of other data changes the analysis.

An obvious weakness in this type of two-dimensional objective analysis is that there is no explicit attempt to link the fields vertically. To insure at least hydrostatic consistency the scalar variables, height and temperature, are adjusted using another variational formalism. To adjust the temperature and height fields the following functional is minimized.

$$J = \sum_k \sum_i \sum_j [\tilde{\alpha}(\bar{T} - \tilde{\bar{T}})^2 + \tilde{\beta}(\Delta z - \tilde{\Delta z})^2 + \lambda(K'\bar{T} - \Delta z)] , \qquad (4.3)$$

where $\tilde{\alpha}$ and $\tilde{\beta}$ are the observational weights given to $\bar{T}$ and Δz, respectively; Δz is the adjusted height thickness between adjacent levels; $\bar{T}$ is the adjusted mean temperature of the layer; $K' \equiv \frac{R}{g} \log_e(\frac{p_{k-1}}{p_k})$, R is the universal gas constant, g is the gravitational constant, p_k is the pressure of the k-th level; and λ is the Lagrange multiplier. The "~" quantities are the observed values. The resulting Euler-Lagrange equations are derived in Appendix C. Solving for Δz and $\bar{T}$ yields

$$\Delta z = \frac{\tilde{\alpha}\,\tilde{\bar{T}} + K'\tilde{\beta}\,\tilde{\Delta z}}{(\frac{\tilde{\alpha} + K'^2\,\tilde{\beta}}{K'})} \qquad (4.4)$$

and

$$\bar{T} = \frac{\tilde{\alpha}\,\tilde{\bar{T}} + K'\tilde{\beta}\,\tilde{\Delta z}}{\tilde{\alpha} + K'^2\,\tilde{\beta}} . \qquad (4.5)$$

The observational weights, $\tilde{\alpha}$ and $\tilde{\beta}$, are functions of height. They can be considered to be a measure of the relative confidence

in the grid point values of temperature and height which result from the interpolation of irregularly spaced RAOB data. A non-hydrostatic relationship may be introduced in performing the objective analysis, or may result from a misrepresentation of the "true" atmosphere by the RAOB. Measurement errors in RAOBS were studied by Lenhard (1970, 1973). He calculated how the errors in temperature are distributed with decreasing pressure. The value of the relative weights for this study are based on Lenhard's results shown in Table 7. This final adjustment yields the three dimensional fields of height and temperature.

From the hydrostatically adjusted height fields a geostrophic wind is computed for each level to serve as first guess for the wind analysis. The pattern-conserving technique used for scalars is modified to analyze simultaneously both horizontal components of the wind. In addition the vorticity and divergence of the winds is constrained for reasons to be given below. The functional minimized is given by

$$J = \sum_{i=1}\sum_{j=m} [A_{i,j}(\mu^*_{i,j} - \mu_{i,j})^2 + A_{i,j}(v^*_{i,j} - v_{i,j})^2 +$$

$$D_{i,j}(d^*_{i,j,k} - d^*_{i,j,k-1})^2 + Q_{i,j}(q^*_{i,j} - q_{i,j})^2 +$$

$$E_{i,j}(e^*_{i,j} - e_{i,j})^2 + \hat{E}_{i,j}(\hat{e}^*_{i,j} - \hat{e}_{i,j})^2 +$$

$$F_{i,j}(f^*_{i,j} - f_{i,j})^2 + \hat{F}_{i,j}(\hat{f}^*_{i,j} - \hat{f}_{i,j})^2 +$$

$$G_{i,j}(g^*_{i,j} - g_{i,j})^2 + \hat{G}_{i,j}(\hat{g}^*_{i,j} - \hat{g}_{i,j})^2 +$$

$$H_{i,j}(h^*_{i,j} - h_{i,j})^2 + \hat{H}_{i,j}(\hat{h}^*_{i,j} - \hat{h}_{i,j})^2] \quad . \qquad (4.6)$$

The above symbols are defined in Table 8. Fig. 10 illustrates the relative location on the staggered grid where their values are defined.

The third and fourth terms on the right side of Eq. (4.6) represent the constraints on the divergence and vorticity, respectively. The analyzed divergence, d^*_k, at a level, k, is constrained to match the divergence, d^*_{k-1}, of a lower level, k-1, weighted by $D_{i,j}$. This constraint acts as a low-pass filter in the vertical, similar to the horizontal low-pass filters described by Sasaki (1970a). The divergence constraint filters high wave numbers in the vertical and could be considered to represent a minimization of

$$\alpha\left(\frac{\partial(\nabla\cdot\vec{V})}{\partial p}\right)^2 ,$$

where α is the weight which is assigned to this filtering constraint.

The analyzed relative vorticity, q*, of the wind field is constrained to match the geostrophic relative vorticity computed from the gradient of the analyzed height field. In addition, the absolute vorticity of the guess field, given by $(q_{i,j} + f_{i,j})$, is altered where necessary to insure that the condition for inertial instability does not exist. This is necessary since the occurrence of areas of negative absolute vorticity immediately triggers unstable motion, which mixes the atmosphere laterally until the area of negative absolute vorticity is reduced. A more complete explanation of this phenomenon is given in most dynamics texts, e.g., Holton, (1972). For this reason the situation given by

Eq. (4.7c) below was modified by setting $(q_{i,j} + f_{i,j}) = 0$.

$$(q + f) > 0 \quad \text{stable} \tag{4.7a}$$

$$(q + f) = 0 \quad \text{neutral} \tag{4.7b}$$

$$(q + f) < 0 \quad \text{unstable} \tag{4.7c}$$

It is worthwhile at this point to justify the liberal use of the geostrophic assumption in obtaining the analyzed horizontal wind components. To begin with, the assumption is quite valid for the area of the grid in Fig. 9 where the kinetic energy budget will be accomplished. However, for lack of a better starting point for the PCT analysis program, the geostrophic winds were used for the entire grid. To compensate for the weakness of the geostrophic assumption in the low latitudes, actual data in low latitudes were weighted considerably higher than data in high latitudes in comparison with the weights on the other constraints.

Because of observational errors in the wind data, as discussed in an earlier section, and because of the inability to represent perfectly irregularly distributed data on a regularly spaced grid, there will be errors in the analyzed gridded wind fields. These errors will lead to fictitious net mass inflow or outflow when the divergence of the horizontal wind is integrated for a column of the atmosphere which is represented by ten grid-points from sea level surface to the top of the atmosphere. To achieve mass continuity a variational approach similar to one used by McGinley (1973) and McFarland (1974) is employed. The variational formalism, for which a minimum is sought, is given by

$$J = \iiint [\alpha(\tilde{u}-u)^2 + \alpha(\tilde{v}-v)^2]dx\ dy\ dp + \iint [\lambda \int (\overline{\frac{\partial u}{\partial x} + \frac{\partial v}{\partial y}})\, dp + \omega_o]dx\ dy \quad (4.8)$$

where α is the observational weight on the observed wind fields and is a function of pressure; λ is the Lagrange multiplier and is not a function of pressure; the bar, "————", indicates a mean divergence for the layer, dp; and ω_o is the lower boundary value of the vertical motion. Whereas McGinley used a terrain-induced ω as the lower boundary condition, in this study terrain- or frictionally-induced vertical motions are minimal when compared to those imposed by the significant pressure falls observed at the surface and associated with the rapid development of the cyclone studied. The relationship between ω_o and pressure tendency, $\frac{\partial p}{\partial t}$, is given by the definition for ω

$$\omega \equiv \frac{dp}{dt} = \frac{\partial p}{\partial t} + \vec{V}_z \cdot \nabla p + w \frac{\partial p}{\partial z} \quad . \quad (4.9)$$

For $z = 0$,

$$\omega_o = \frac{\partial p}{\partial t}\Big|_{z=0} + \vec{V}_o \cdot \nabla p + w_o \frac{\partial p}{\partial z} \quad . \quad (4.10)$$

If one imposes the kinematic boundary condition that at $z = 0$, $w = 0$, as well as the assumption that

$$\vec{V}_o \cdot \nabla p < \frac{\partial p}{\partial t}\Big|_{z=0} \quad , \quad (4.11)$$

then

$$\omega_o \approx \frac{\partial p}{\partial t}\Big|_{z=0} \quad . \quad (4.12)$$

The assumption (4.11) has been justified by means of a scale analysis.

Derivation of the Euler-Lagrange equations, given by Eqs. (4.13), (4.14), and (4.15), and derived in Appendix D is accomplished by applying the first variation to Eq. (4.8).

$$2\tilde{\alpha}\,(u - \tilde{u}) - \frac{\partial\lambda}{\partial x} = 0 \tag{4.13}$$

$$2\tilde{\alpha}\,(v - \tilde{v}) - \frac{\partial\lambda}{\partial y} = 0 \tag{4.14}$$

$$\int_{p_o}^{o} \overline{\left(\frac{du}{dx} + \frac{\partial v}{\partial y}\right)}\, dp + \omega_o = 0 \ . \tag{4.15}$$

Solving for u and v in Eqs. (4.13) and (4.14), respectively, yields

$$u = \tilde{u} + \frac{1}{2\tilde{\alpha}}\frac{\partial\lambda}{\partial x} \tag{4.16}$$

and

$$v = \tilde{v} + \frac{1}{2\tilde{\alpha}}\frac{\partial\lambda}{\partial y} \ . \tag{4.17}$$

Operating on Eq. (4.16) by $\frac{\partial}{\partial x}$ and Eq. (4.17) by $\frac{\partial}{\partial y}$ and then substituting into (4.15) results in Eq. (4.18), where λ is the only dependent variable.

$$\int_{p_o}^{o} \left(\frac{1}{2\tilde{\alpha}}\nabla^2\lambda\right) dp = -\left[\int_{p_o}^{o} \overline{\left(\frac{\partial\tilde{u}}{\partial x} + \frac{\partial\tilde{v}}{\partial y}\right)}\, dp + \omega_o\right] \ . \tag{4.18}$$

Solving for $\nabla^2\lambda$ and expressing in discrete form, one may write

$$\nabla^2\lambda = \frac{-4\left\{\sum_{k=1}^{L}\left[\left(\frac{\partial\tilde{u}}{\partial x} + \frac{\partial\tilde{u}}{\partial y}\right)_k + \left(\frac{\partial\tilde{u}}{\partial x} + \frac{\partial\tilde{u}}{\partial y}\right)_{k+1}\right]\frac{\Delta p_k}{2} - \omega_o\right\}}{\sum_{k=1}^{L}\left[\frac{\Delta p_k}{\alpha_k} + \frac{\Delta p_k}{\alpha_{k+1}}\right]} \ . \tag{4.19}$$

Given the proper boundary conditions for λ, discussed in Appendix D, Eq. (4.19) may be solved numerically using an iterative technique such as the simultaneous relaxation method described by Haltiner (1971) on page 113. From Eq. (4.19) the curvature of λ may be interpreted as being proportional to the observed wind field's ($\tilde{u}$ and $\tilde{v}$) deviation from mass continuity. The gradient of λ is then used in Eqs. (4.16) and (4.17) to adjust $\tilde{u}$ and $\tilde{v}$ to satisfy the mass continuity constraint.

To illustrate the effectiveness of this technique in producing "reasonable" vertical motion patterns, in the following section the resulting fields will be compared with those derived independently by others. Vertical motion fields produced using the variational adjustment technique described above, henceforth referred to as Sasaki's technique, are compared with fields produced by the Japanese Meteorological Agency and with ω's obtained from AFGWC. Both use a form of the quasi-geostrophic omega equation. A comparison with ω's derived from subjectively analyzed wind fields will also be shown. All the fields will be compared subjectively with other gridded analysis data such as cloud amounts, cloud types, and sensible weather obtained from the AFGWC "3-D Neph" analysis, with surface precipitation reports, and with satellite photographs.

The kinetic energy relation given by Eq. (2.1), derived in Appendix A, is the basis for this kinetic energy budget study. With the exception of Term D, each term in (2.1) and $-\omega\alpha$, the expression for the conversion from APE to KE, are computed for

several layers of the atmosphere. The layers are represented by the levels at which an analysis was performed. Fig. 4.2 illustrates how the layers are defined and the vertical resolution of the analyzed variables. To obtain kinetic energy changes of the storm, Eq. (2.1) is integrated for the volume of the atmosphere which includes the disturbance. Eq. (2.1) becomes

$$\underbrace{\left[\frac{\partial \bar{K}}{\partial t}\right]}_{A} = \underbrace{-\left[\bar{\vec{V}}\cdot\nabla\bar{K}\right] - \left[\frac{\bar{\omega}\partial\bar{K}}{\partial p}\right]}_{B} - \underbrace{\left[\bar{\vec{V}}\cdot\nabla\varphi\right]}_{C} + \underbrace{[R]}_{D} , \tag{4.20}$$

where the bracket [ ] on a variable, X, represents a mean value for a limited area. For example,

$$[X] = \frac{1}{gS}\int_{p_o}^{} \int_{S} X \, dS \, dp , \tag{4.21}$$

where S is the area of the region.

The kinetic energy change given by Term A in (4.20) is computed explicitly using the following finite representation of the expression for kinetic energy in a volume. The volume is defined by a gridded field i = 1 to I, j = 1 to J in the horizontal and k = 1 to L in the vertical. Kinetic energy in the volume is given by

$$[K] = \frac{1}{g}\sum_{i}\sum_{j}\sum_{k}\frac{(u^2_{i,j,k} + v^2_{i,j,k})}{2}\Delta p_k . \tag{4.22}$$

The non-linear rate of the cyclone's development, illustrated by Fig. 11 which shows the analyzed central pressure in time, makes the finite differencing for rate of change in kinetic energy extremely inaccurate when using a time difference of 24 hours. For this reason, once [K] is calculated for all the periods to be

studied, a best fit curve from a second degree polynomial is computed and the term $[\frac{\partial K}{\partial t}]$ is obtained using this curve. In Fig. 12 are plotted several examples of the way in which the curve fits the value of the changing kinetic energy. The advection term, Term B, in Eq. (4.20) is computed using the wind components, u and v, which are normal to the sides of the region.

$$B_x = \frac{-\frac{1}{g}\sum_{i}^{I}\sum_{j}^{J}\sum_{k}^{L} u_{i,j,k}(K_{i+1,j,k} - K_{i-1,j,k})\Delta x_{i,j}\ \Delta y_{i,j}\ \Delta p_k}{XY} \qquad (4.23)$$

represents the integrated advection through the left and right sides of the grid, where i takes on the values one through I; j is one through J; X is the sum of the Δx's; and Y is the sum of the Δy's. Similarly, for the upper and lower sides of the grid

$$B_y = \frac{-\frac{1}{g}\sum_{i}^{I}\sum_{j}^{J}\sum_{k}^{L} v_{i,j,k}(K_{i,j+1,k} - K_{i,j-1,k})\Delta x_{i,j}\ \Delta y_{i,j}\ \Delta p_k}{XY} . \qquad (4.24)$$

For the vertical advection term in Term B,

$$B_p = \frac{-\frac{1}{g}\sum_{i}^{I}\sum_{j}^{J} \omega_{i,j,k}(K_{i,j,k-1} - K_{i,j,k})\Delta x_{i,j}\ \Delta y_{i,j}\ \Delta p_k}{XY} , \qquad (4.25)$$

where k takes on the value of the pressure surface at which the vertical advection is computed.

The generation of kinetic energy, Term C, is computed with the use of the following finite difference summations. From the analyzed geopotential and the analyzed u-component of the wind, the generation of kinetic energy is given by

$$C_x = \frac{-\frac{1}{g}\sum_{i}^{I}\sum_{j}^{J}\sum_{k}^{L} u_{i,j,k}(\varphi_{i+1,j,k} - \varphi_{i-1,j,k})\Delta x_{i,j}\ \Delta y_{i,j}\ \Delta p_k}{XY} , \qquad (4.26)$$

and for the v-component

$$C_y = \frac{-\frac{1}{g}\sum_i^I \sum_j^J \sum_k^L v_{i,j,k}(\varphi_{i,j+1,k} - \varphi_{i,j-1,k})\Delta x_{i,j}\ \Delta y_{i,j}\ \Delta p_k}{XY}, \quad (4.27)$$

where $\varphi = gz$, the geopotential height of the pressure surface. The values for the conversion of available potential energy to kinetic energy are computed simply by the following expression

$$[\omega\alpha] = \frac{\frac{1}{g}\sum_i^I \sum_j^J \omega_{i,j,L}\ \alpha_{i,j,L}\ \Delta x_{i,j}\ \Delta y_{i.j}\ \Delta p_L}{XY}. \quad (4.28)$$

Once the values for Terms A, B, and C in Eq. (4.20) are computed, Term D, which represents those processes described in Chapter III is computed as a residual to balance Eq. (4.20).

This completes the description of the numerical techniques to be used in the kinetic energy study. In the following chapter a synopsis of the principal weather features of the storm studied is presented. The analyzed vertical motion patterns are compared subjectively with the synoptic features and with vertical motion fields produced subjectively and by the Japanese Meteorological Agency (JMA) and AFGWC.

CHAPTER V

A SYNOPTIC DISCUSSION

Climatic studies of the East China Sea reveal a frequency maximum of cyclogenesis in this area during the winter months. Fig. 13 depicts the results of a climatic study by Trewartha (1961). The area of development of the cyclonic disturbance in the early period of the 1975 AMTEX was in the vicinity of one observed maximum. The surface layers of the troposphere in the early period of AMTEX typified a winter situation for Eastern Asia. A small portion of the cold anticyclone over eastern Siberia had broken off a few days before the start of AMTEX and flooded the East China Sea with cold continental polar air, but the air had modified by the time the observations for AMTEX began. The similarities between AMTEX conditions and the typical winter flow extend into the upper troposphere. In the winter the zone of westerlies is sufficiently south to be affected by the Tibetan Highlands. The obstructive effect causes the flow to bifurcate, with subsequent merging in an area of confluence east of Tibet. The upper level trough for this time of year is positioned along the eastern reaches of the Asian continent. This upper level pattern characterized the flow for the early period of AMTEX 1975.

At 1200 GMT, 13 February 1975, Figs. 14-17, a wave formed

on an old and ill-defined front which had oscillated in an area between 25°N and 20°N southeast of Taiwan. In the preceeding two days a wave on this quasi-stationary front had been analyzed repeatedly in various positions by the analysts of both the AFGWC and the JMA. At the time stated above, however, a short wave embedded in the westerly flow, earlier on the lee of the Tibetan Plateau, was moving across the southern mainland of China. This minor wave provided upper level support to the eventual development of the surface system. Reported rainshower activity at Ishigaki and Miyako, the two southwestmost reporting stations in AMTEX (Fig. 2), provided added support to the presence of a subsynoptic scale disturbance in its embryonic stage.

By 0000 GMT, 14 February, Figs. 18-21, the surface pressure in the vicinity of the disturbance had dropped from 1012 mb at 1200 GMT, 13 February, to 1006 mb while moving northeastward to an area northwest of Okinawa. Now a marked area of convergence lay across the chain of islands from Taiwan to Nase. The frontal position was readily discernible by the wind reports: from southwest at 20 to 30 kts along the islands; from the northwest at 20 kts by ship observations in the area west of the islands. A closed low at 850 mb was now present over the East China Sea, with the flow at that level characterized by strong cold air advection. At 500 mb the short wave had amplified while moving to a position along the inland margins of the Chinese coast.

During the next twelve hours, Figs. 22-25, the storm experienced a 7-mb drop in central pressure. The surface position of

the low was east of Okinawa but spanned a considerably larger area with widespread areas of precipitation in the two northern quadrants of the storm. Convective precipitation was observed along the frontal system as it moved across the southwest Japanese Islands. Deepening of the 850 mb low continued as the cold air advection persisted throughout the lower and middle troposphere. The 500 mb trough was positioned slightly off the southern China coast with its axis extending northeastward over Korea and merging with the major long wave to the north of Japan.

The next twenty-four hours, Figs. 26-33, were characterized by continued central pressure drops in the storm. No longer a sub-synoptic scale disturbance, the low moved rapidly to the northeast. At 0000 GMT, 15 February, the storm's central pressure was 985 mb, and by 1200 GMT the cyclone had deepened to 979 mb. Corresponding drops in heights were observed in association with the low at 850 mb. By 1200 GMT analysis of the storm continued to show a definite tilt toward the northwest. The upper-level short wave had moved into phase with the major synoptic-scale wave.

The changing thermal structure of the atmosphere was also detectable by the increased intensity of the jet stream at 300 mb. During the first two periods of the study, 1200 GMT, 13 February and 0000 GMT, 14 February, Figs. 17 and 21, the southern branch of the jet at 300 mb was over the mainland of China with maximum winds of 140 kts. By 1200 GMT, 14 February, the jet maximum increased to over 160 kts and was directly over AMTEX in the East China Sea. A broad ribbon of winds in excess of 200 kts

was analyzed on February 15 at 1200 GMT (Fig. 33), extending from the base toward the leading edge of the 300 mb trough.

To capture this general type of synoptic situation with an increased density of observational data was one goal of AMTEX. Although observations were taken through 28 February 1975, for the purpose of the kinetic energy budget study, the objective analyses of winds, heights, and temperatures were carried out only through 1200 GMT, 15 February 1975. By this time the storm was well out to sea. In the following chapter the results of the kinetic energy budget are presented.

CHAPTER VI

RESULTS

A. A comparison of PCT vertical motion fields (ω's) with other independently produced ω's.

In order to evaluate the representativeness of the gridded wind fields which were used to compute the kinetic energy budget, a comparison of the PCT-analyzed vertical motion fields was made with the following:

(1) ω's derived from the quasi-geostrophic omega equation as computed by the JMA and the AFGWC,

(2) ω's computed from subjectively analyzed winds by the kinematic technique using a data base identical to the one used in PCT,

(3) synoptic features such as fronts and areas of convective activity,

(4) regions of cloudiness as photographed by the Defense Meteorological Satellite Program (DMSP) satellite or analyzed by the AFGWC 3-D Neph.

Fig. 34 shows the 700-mb ω field from 0000 GMT, 14 February 1975 obtained by the JMA using the quasi-geostrophic omega equation. Superimposed are the surface fronts and centers of high and low pressure from Fig. 19. The JMA's ω field for this date is

generally supported by the synoptic situation at the surface. The cold front extending from the low pressure over northern Japan through the Sea of Japan and South Korea is well defined by an elongated area of upward vertical motion along the frontal zone. The low in the East China Sea is very nearly in the middle of the computed center of maximum upward vertical motion. However, the location of the newly developed front is not obvious from the vertical motions in the area.

Fig. 35 shows the AFGWC 775-mb ω field for the same time, also obtained using a form of the quasi-geostrophic omega equation. The notable features include an area of maximum upward vertical motion of -2 μb/sec, associated with the newly developed wave cyclone over the East China Sea at approximately 28°N, 133°E, with a secondary, weaker maximum approximately over Shanghai. An area of upward vertical motions extends along and ahead of the surface cold front which lies over the Sea of Japan and Korea. Upward vertical motions are also seen along the newly developed cold front in the East China Sea. A tongue of downward motion should be noted over mainland China just west of Taiwan.

Fig. 36 shows the 775-mb ω field for 0000 GMT, 14 February obtained by the kinematic method applied to subjectively analyzed wind fields. The single center of maximum upward vertical velocity is approximately mid-way between the two centers observed on the AFGWC and JMA analyses shown in Figs. 34 and 35. This center lies west of the analyzed cold front and gives positive indication of the cold front in the East China Sea, but the

ω fields give no indication of the front in the Sea of Japan. This analysis is in disagreement with the area of positive vertical motion to the west of Taiwan indicated in the two previous analysis.

Figs. 37 through 41 are the 775-mb ω fields for 1200 GMT, 13 February 1975 through 1200 GMT, 15 February 1975, respectively, obtained by the kinematic method applied to the objective wind analyses employed in this study and discussed in Chapter IV. In Fig. 38 is given the 0000 GMT, 14 February ω field. There is generally good agreement between this field and those from the JMA and AFGWC (Figs. 34 and 35). There is, however, significantly more detail in this field, particularly with respect to the convectively active developing wave cyclone in the East China Sea where the upward vertical motion is about -4 μb/sec. In addition, the area of downward vertical motion extending along the China coast is supported by the DMSP satellite photograph, Fig. 42, valid at 0332 GMT, 14 February 1975.

The qualitative differences between this analysis and the subjectively derived ω field shown in Fig. 36 are striking. It is of interest to note that the data base for the two analyses is identical. The only difference is that in the former case the horizontal winds were objectively analyzed using PCT, and in the latter subjectively analyzed by a competent and experienced analyst. These horizontal wind analyses are very similar, but the resulting computed ω's are significantly different, underscoring the well-accepted statement made earlier that kinematically derived ω's are

very sensitive to small differences in the horizontal wind fields.

The extreme maximum of upward vertical motion over the AMTEX area shown in Fig. 38 corresponds to a period of extensive shower activity during the following six hours. Fig. 43 is an isohyet analysis (dashed lines) of rainfall from 0000 GMT, 14 February to 0600 GMT, 14 February. The solid lines are isopleths of ω for 0000 GMT, 14 February taken from Fig. 38. The justification for analyzing the elongated isohyets is drawn largely from the DMSP photograph (Fig. 42). A line of convective activity associated with the surface front is readily discernible from point A to point B in Fig. 42, and this line is highly correlated with the PCT-derived ω's. The clear region along the coastal area of Eastern China where the land/water contrast made gridding quite accurate is also noteworthy. Here the kinematic PCT ω's show an area of downward vertical motion with the axis oriented along the clear area. Both the JMA and AFGWC ω fields had downward motions in this area, but in both cases the areas were too broad and included area C and D on the DMSP where overcast cloud conditions existed. An area where the PCT-derived ω's are not well correlated with the DMSP is the area of downward motions toward the southeastern coast of Japan. However, there are indications on the DMSP of breaks in the clouds along this axis of downward motion.

In Fig. 44 the JMA 700-mb quasi-geostrophic ω field for 1200 GMT, 14 February 1975 is depicted with corresponding frontal positions and pressure centers taken from Fig. 22. An axis of upward vertical motion lies off the eastern coast of Japan where a

weakening front is positioned. The intensifying cold front associated with the deepening low to the southeast of the Japanese Island of Shikoku is not apparent in the JMA's vertical motion pattern. The position of this low pressure center is found to correspond to the area of upward vertical motion with a maximum of -2 μb/sec. The upward motion extends along and to the north of the associated warm front. Behind the cold front, the subsiding colder air is marked by an extensive area of downward vertical motion.

Fig. 45, the AFGWC 775-mb quasi-geostrophic ω field, shows no qualitative difference from the JMA ω patterns. There is slightly more indication in the ω pattern of the cold front south of Japan. A diffuse region of maximum upward vertical motion, about -4 μb/sec, is seen in the northeast quadrant of the analyzed surface low. This region lies just to the east of the intense short wave at 500 mb which is associated with the surface low (see Fig. 24). The upward vertical motions are due partially to the strong positive vorticity advection by the short wave. Downward vertical motions are prevalent behind the cold front as was the case in the JMA ω's.

The subjectively analyzed ω field is shown in Fig. 46. It is similar to the JMA and AFGWC analyses except that the magnitude of the maximum upward motion is about double and the maximum is displaced to a position somewhat west of the low pressure center.

Fig. 39 shows the analyzed ω field produced by PCT for 1200 GMT, 14 February. Although it is in general agreement with the other analyses, certain differences are apparent. The area of maximum upward vertical motion is just to the northeast of the cyclone

triplepoint with a maximum of about -4 μb/sec. Upward vertical motion prevails along much of the analyzed front. The major difference occurs over the Japanese Island of Kysuhu where very strong downward vertical motions are present. Inspection of the surface divergence field shows a corresponding area of strong positive surface divergence in this region. The surface winds indicate that the divergence is forced by the effects of orography. Inspection of the 3-D Neph analyses, Fig. 47, indicates primarily clear or scattered clouds between 800 mb and 700 mb in the vicinity of the center of maximum downward vertical motion. There are, however, a few 3-D Neph grid points analyzed as broken or overcast in this area as well as in the axis of downward motion which extends to the southwest into mainland China south of Shanghai. The axis of upward motion along the front is supported by broken or scattered clouds.

The obvious improvement in the ability of the PCT ω's to represent the synoptic scale features with striking correlation, such as displayed in Figs. 38 and 42, adds to the confidence in the representiveness of the PCT analyzed fields and in the energetics to be derived using them.

B. Kinetic energy budget results and comparison with other studies.

A comparison of kinetic energy budgets should be made only in a qualitative sense unless the objective is to show an improvement in results using one technique rather than another. Then the same storm or storms, the same data, and a standard for comparison

must be used. The comparison which follows attempts to show only that the techniques adopted for this research produce qualitatively sound values for all the terms computed in the kinetic energy budget. The studies chosen for the comparison are two of the more recently published ones and are similar in many aspects to the kinetic energy budget of this work.

A kinetic energy study by Smith (1973) was made for a period of cyclogenesis over North America in April 1964. Table 3 shows the averaged results from 1200 GMT, 12 April to 0000 GMT, 15 April. The time spanned in the study includes the storm's development and continues through its occluded stage. Smith's "storm vicinity" was determined entirely by the surface features of the cyclone. It was defined as a right circular "cylinder" shaped volume, the base of which was determined by the last closed surface isobar. To facilitate comparison, Smith's results were retabulated, summing the horizontal and vertical components of kinetic energy fluxes as is done in the present study (Table 9).

Table 10 was compiled by averaging the results of kinetic energy budgets from the six twelve-hour periods of AMTEX. This seventy-two-hour period, henceforth referred to as the AMTEX storm, encompasses the developmental stage of the storm and extends through the early stages of the storm's decay. Smith's calculations, on the other hand, included the final decaying stages of the storm. The central pressure of each storm was plotted (Figs. 48 and 49) to show which periods of each storm's cycle were included in the calculation of the mean budgets (Table 9 and 10). To illustrate

must be used. The comparison which follows attempts to show only that the techniques adopted for this research produce qualitatively sound values for all the terms computed in the kinetic energy budget. The studies chosen for the comparison are two of the more recently published ones and are similar in many aspects to the kinetic energy budget of this work.

A kinetic energy study by Smith (1973) was made for a period of cyclogenesis over North America in April 1964. Table 3 shows the averaged results from 1200 GMT, 12 April to 0000 GMT, 15 April. The time spanned in the study includes the storm's development and continues through its occluded stage. Smith's "storm vicinity" was determined entirely by the surface features of the cyclone. It was defined as a right circular "cylinder" shaped volume, the base of which was determined by the last closed surface isobar. To facilitate comparison, Smith's results were retabulated, summing the horizontal and vertical components of kinetic energy fluxes as is done in the present study (Table 9).

Table 10 was compiled by averaging the results of kinetic energy budgets from the six twelve-hour periods of AMTEX. This seventy-two-hour period, henceforth referred to as the AMTEX storm, encompasses the developmental stage of the storm and extends through the early stages of the storm's decay. Smith's calculations, on the other hand, included the final decaying stages of the storm. The central pressure of each storm was plotted (Figs. 48 and 49) to show which periods of each storm's cycle were included in the calculation of the mean budgets (Table 9 and 10). To illustrate

further the influence of not taking the decaying stage of the AMTEX storm into account in Table 10, Table 11 was computed using only the first five periods. Note the effect of the early decaying stage, 1200 GMT, 15 February, on the mean generation term. Before adding the sixth period, the mean net generation term was 22.8 W m^{-2} (Table 11), and with its inclusion (Table 10) the mean net generation term was 19.9 W m^{-2}. Comparison of the other terms also reveals changes.

The two studies compare favorably with respect to order of magnitude of the terms in the budget but differ in the mechanisms responsible for maintaining the net energy balance. The most notable difference is the contribution of the advection of kinetic energy to the budget. In Smith's (1973) study of cyclogenesis on the lee of the Rocky Mountains, the western intrusion of the jet maximum into the upper levels of the troposphere provided the storm with a large percentage of its kinetic energy. For the AMTEX storm the generation term provided most of the storm's kinetic energy, and in the mean for the five periods, kinetic energy advection was out of the storm. More will be said later concerning the physical implications of this observation.

Another kinetic energy study with statistics for a storm vicinity (defined in a manner analogous to Smith's) was computed for a period of synoptic short-wave activity over North America by Ward and Smith (1976). The period 11-24 April, 1970, was characterized by a number of cyclones tracking through their computational area. Table 12 contains their time mean, area-

average kinetic energy budget. It is the ensemble statistics for four cyclone vicinity budgets. For one particular storm, a separate table (13) is also given. An interesting difference in Ward and Smith's kinetic energy budget was the role played by advection of kinetic energy. Their study, like Smith's (Table 9), showed the advection term as an external source of kinetic energy to the system, while for the early stages of the AMTEX cyclone, advection was negative, out of the storm vicinity.

Although there is no doubt that some barotropic mechanisms were at work to transfer kinetic energy from the jet to the storm (Table 13), barotropic exchange was not likely the sole source of kinetic energy. Had Ward and Smith included the upper levels of their storm, which had a westward tilt, they might have found that the subsiding cold air behind the low added a positive contribution to generation of kinetic energy. In other words it is very likely that more kinetic energy was being generated within the "true storm vicinity" than is indicated by their results.

The difference in the upper level flow is sufficient to explain the disparity in the sign of the value of net generation between Ward and Smith's cyclone and the AMTEX storm. Figs. 50, 51, and 52 are representative of the general upper level flow for Ward and Smith's study. Using their definition of "storm vicinity", one would compute a kinetic energy budget for 15 April which would be centered over Nebraska. In this region the 500- and 300-mb flows indicate a divergence of the height contours. Air leaving the tight gradient at the base of the trough would be deflected

into the high since a temporary imbalance in the pressure gradient force and the Coriolis force would be present. This supergradient flow was responsible for the negative value of the generation term.

The order of magnitude of the residual in the present study is comparable to that found in other studies before time averaging has its effect. In Ward and Smith's study (1976) several extensive areas of +20 W m^{-2} appeared, with maximum values of +40 W m^{-2} for the 400- to 200-mb layer. In a study of cyclone development over the Central United States (Kornegay and Vincent, 1976), surface to 100-mb integrations of the kinetic energy equation resulted in similarly large values of the residual. A more detailed study from a kinetic energy perspective of the structure of the AMTEX storm follows.

C. Physical description of the kinetic energy budget for the "AMTEX storm."

Figs. 53 and 54 show the storm area's kinetic energy budget terms as a function of time, integrated over the upper troposphere (500 mb to 100 mb) and the lower troposphere (surface to 500 mb), respectively. Fig. 53 includes the surface to 100-mb integrated values. In this study the upper troposphere overwhelmingly affected the net kinetic energy budget of the storm system. This is not a surprising observation since the kinetic energy of the upper atmosphere is typically an order of magnitude greater than that of the lower atmosphere. As seen in Fig. 53, the upper troposphere generally accounts for the greater part of the net

change in the various terms of the budget for the entire storm volume. This can also be seen by the increase in the scale of the ordinate (by an order of 10) when the values for the lower layer (Fig. 54) are plotted.

In the upper atmosphere during the early periods of the storm the strong advection of kinetic energy translating the wind maximum out of the storm region predominated and resulted in negative tendencies. By the third and fourth periods a quasi-balance between the positive generation term and the negative advection of kinetic energy was established and the tendency became slightly positive. During the final stages of the storm the residual term became the dominating influence, and the negative residual, implying a sink of kinetic energy, led to a return of negative kinetic energy tendencies. Since the tendency term reflects the combined effects of the other terms, it is instructive to consider some of the temporal fluctuations.

The generation term in the upper atmosphere increases between the first two periods of the storm, remains fairly constant during the intermediate periods, then decreases again in the last two periods. This temporal variation may be explained by the character of the upper level flow. As the upper level short wave entered the computational grid, between the first and second periods, an area of strong confluence developed over the storm volume. At this point the active mechanism responsible for the increase in the generation term was the subgradient wind, which resulted from the winds entering the area of confluence. A subgradient

wind has a cross-isobaric component from higher to lower pressures and therefore is responsible for generation of kinetic energy. During the fifth period there was a sharp drop in the kinetic energy generation term, which continued into the sixth and last period of this study. The supergradient flow on the downwind side of the storm produced cross-isobaric flow towards higher pressure, resulting in an area of destruction and reducing the net integrated value of the generation term for the volume. This argument is supported by the superposition of the jet maximum and the generation term, shown in Fig. 55.

In contrast to the effect of the wind maximum to the east of the storm area in the early stages of its development, an upper tropospheric wind maximum on the inflow boundary of the storm in the late period resulted in a change from negative advection in the early stages to positive advection in the later periods of the study. The change in sign of the advection term occurred between the fourth and fifth periods in agreement with the time when the storm volume passed through the jet maximum. The observed reversal of the role of the advection term and the downward trend of the generation term, as discussed above, are related in the sense that both are consistent with the storm's position in the flow.

Identification of the specific physical mechanisms responsible for the source of kinetic energy implied by a positive residual during the first period is beyond the scope of this research. There are several possible subgrid-scale sources which in combination, or perhaps singly, could account for the large positive

residual. One possibility relates to the subgrid-scale effects of cumulus activity. Examination of a DMSP satellite photograph (Fig. 56) did reveal an extensive area of cumulo-form cloud over the eastern mainland of China, and the AFGWC dewpoint spread analysis of this same area (Fig. 57) confirmed the existence of heavy cloud cover.

A second possibility is related to the effect of the Tibetan Plateau on the flow. One might postulate the existence of a turbulent wake, as in the simpler case of flow past a solid body for Reynolds numbers considerably above the critical value (Landau and Lifshitz, 1959). For flow around the Tibetan Plateau, with a characteristic wind velocity of 20 m/s, a kinematic coefficient of viscosity for the atmosphere of 5 m^2/s , and a characteristic length of 1.5×10^6 meters (the approximate diameter of the Tibetan Plateau), the Reynolds number is 6.0×10^6, considerably above the critical value for turbulence of 2.4×10^4. Although flow around the Plateau is infinitely more complex than the model described by Landau and Lifshitz (pp. 136-147), the concept may provide some insight into the manner in which a turbulent wake would act to produce a subgrid-scale source of kinetic energy. Landau and Lifshitz derive an expression for the averaged turbulent fluctuation:

$$u \sim (FU/\rho)^{1/3} \times^{-2/3} , \qquad (6.1)$$

where F is the drag force, ρ the density of the fluid, U the velocity of the fluid incident upon the obstacle, and x is the distance from the body. Using Eq. (6.1) one can show that a

decrease of about 10% in the value of u occurs between three and four Plateau diameters. Within this distance lies the AMTEX area. It is conceivable, therefore, that processes similar to those described by Landau and Lifshitz could be present in this part of the world, creating a subgrid-scale source for kinetic energy in the AMTEX area.

The above discussion was offered only as a possibility and not as proof of the existence of a turbulent wake. For it must be noted that the second period's observed decrease in the value of the residual does not appear to support the turbulent wake argument as a subgrid-scale source. Because the general pattern of the upper level flow was not noticeably different during the two periods and the budget's computational area remained the same, perhaps the best explanation for the initial large positive residual is convective activity, and the contribution of errors in determining the terms of the budget also may be significant.

Values of the residual during the second, third, and fourth periods were nearly zero (recall the quasi-balance between advection and generation). The fifth and sixth periods were characterized by a large negative residual, implying a sink of kinetic energy. The dissipation of kinetic energy in the vicinity of jet activity has been observed in other studies (Smith, 1973; Kung and Baker, 1975). Theory for dissipation in the vicinity of strong vertical shear is offered by Kung (1966). Why the negative residuals appeared only during the last two periods cannot at this time be explained satisfactorily. Inspection of the vertical and

horizontal shear areas yields no insight into the physical mechanisms responsible for the negative residual. The possibility remains that errors are magnified by the increased intensity of this situation and by the decrease of data to adequately represent the active processes in this area of the grid.

Although the lower layers of the atmosphere had only a minor impact on the overall kinetic energy budget of the AMTEX storm, the small changes in the kinetic energy content of the lowest layers were significant when considering the effects on the dynamics of the developing storm. In the AMTEX storm the kinetic energy of the lowest layer nearly tripled between the initial and final periods of the study, yet its percent contribution to the kinetic energy content changed by about 10% (from 4% to 14%) of the net integrated value. These changes take on special significance when it is considered that most human activity is concentrated in the lowest layers of the atmosphere.

From Fig. 54, the surface to 500-mb time variation of the kinetic energy budget, several important relationships among the terms can be deduced. The first is the quasi-balance between the generation of kinetic energy and the advection term, which was dominated by its vertical component. This quasi-balance is consistent with the following physical relations. Where inflow (convergence) into low pressure is present, generation of kinetic energy results, implying upward vertical motions. This means that advection of kinetic energy out of the layer occurs and is especially strong near the baroclinic zone where the increase of

kinetic energy in the vertical is greatest. In the area behind the front where cold air is subsiding and the vertical velocity is downward, the change in kinetic energy with pressure may be negative, as in the above case, but its magnitude is much less. Fig. 58 illustrates this point.

The behavior of the curves representing temporal fluctuations of the budget terms in the lower layer are all physically meaningful. For example, the rapid increase in kinetic energy content, beginning with the second period and extending through the fourth period, is a consequence of the slight dominance of the generation term over the advection term through those same periods. Additionally, the residual term was positive, therefore acting as a source in the early periods. As the kinetic energy increased, the residual tended toward zero and became negative by the fifth period. This reflects the tendency of the dissipation to increase as a sink in conjunction with the increased vertical shear, which is implied by the larger kinetic energy values. Note that unlike the situation in upper layers, the lower boundary condition for the lower layer is that kinetic energy diminish to zero at the surface.

Several differences in the characteristics of the upper and lower layers of this storm are noteworthy. Interpretations of the upper layer curves are in general subject to greater conjecture, while in the lower layer the relationship of the curves to physical processes seems clearer. Various combinations of budget terms were generally highly correlated in the lower layer,

whereas strong correlation in the upper atmosphere was evident only during certain periods. This is particularly true of the correlation between kinetic energy and the residual, and between advection and generation of kinetic energy. A possible explanation is suggested by the significantly better data coverage at the surface, resulting in a decrease in the error limits of the budget terms for the lower layer. A second possibility is the changing and complex relationship observed between the storm volume and the jet stream structure.

Although numbers, such as those in Table 10, are often the object of kinetic energy budget presentations, the time mean does not yield sufficient insight into a storm's life cycle. It does, however, suggest the role which sub-synoptic and synoptic-scale cyclones developing in the East China Sea might play in maintaining the energy cycle of the general circulation.

The energy cycle of the atmosphere is represented schematically by Fig. 59 (taken from Lorenz, 1969, as estimated by Oort, 1964). The present research was directed at studying the lower branch of the cycle; that is, the conversion of available potential energy to kinetic energy. A study of one cyclone which includes only a small fraction of the earth's atmosphere and even less of the temporal scale of the general circulation cannot begin to answer the question of the role of synoptic disturbances in the general circulation. The large value of the generation term (19.9 W m^{-2}) in Table 10, as compared with that of Fig. 58 (2.3 W m^{-2}), suggests that wide local variations in the conversion

of available potential energy to kinetic energy (Fig. 60) could be expected to offset each other when averaged over larger areas and for a variety of synoptic situations. An example of local variations is given in Fig. 60 which represents the vertically integrated generation of kinetic energy for the analysis grid. The integrated value of the generation term for the entire volume was +9.7 W m^{-2}, while a value of 28.7 W m^{-2} was computed for the storm vicinity.

While Figs. 53 and 54 provide one with a graphic means of representing an otherwise "busy" table of numbers, some detail may be lost. For this reason the tables from which the graphs were derived are included (Table 14).

CHAPTER VII

CONCLUSIONS AND SUGGESTIONS FOR FUTURE RESEARCH

This research was directed at examining the kinetic energy budget of a rapidly developing cyclone over the East China Sea in winter during the 1975 AMTEX. The data gathered by the 1975 AMTEX were limited in space and time and therefore not sufficient for a complete study of the cyclone's life cycle. To overcome this shortcoming, the 1975 AMTEX data were complemented by data from the regular synoptic data network, and the resulting data base was then analyzed on a gridded map applying objective analysis methods.

The objective analysis techniques which were applied to the data were developed within the sphere of the calculus of variations. The pattern conserving technique employs variational constraints which simulate the thought processes of a good human analyst while incorporating physical constraints which are meteorologically sound. The wind analyses produced by PCT were further refined by another variational formalism, the mass continuity constraint, while the temperature and height fields were adjusted for hydrostatic consistency. These objective analysis techniques were programmed to run on a computer in concert with the data management programs in order to produce gridded analyses of parameters

which represent the synoptic features of AMTEX accurately and demonstrate an improvement over fields analyzed by others.

The analysis procedure is not without weaknesses. For example, in regions where data coverage is sparse, the first guess wind, which is geostrophic, will not be significantly altered. The result is that for areas with cyclonic curvature, a geostrophic wind is an overestimate of the true value of the wind. This affects the kinetic energy budget by yielding too large a magnitude for the advection term while not contributing to the generation term in any way. In other words, the geostrophic wind does not contribute to generation or to destruction of kinetic energy.

Several aspects of the AMTEX storm's life cycle revealed by the kinetic energy budget study are especially noteworthy:

1. The integrated storm kinetic energy budget is determined almost exclusively by the contribution of the upper troposphere. Although the contribution of the lower troposphere to the overall budget may be minor, small changes in the kinetic energy content of the lower troposphere are significant in terms of their effect on human activity in the lowest layer of the atmosphere.
2. At upper levels, during the cyclone development stage, a quasi-balance is observed between the horizontal advection (sink) and the generation (source) terms. The physical processes described mathematically by

these terms are both related to the upper tropospheric jet and its position in relation to the storm. This result differs from those of kinetic energy studies over the continental United States (Smith, 1973), in which the horizontal advection is the apparent source of kinetic energy during development. This difference is apparently due in part to the unrealistic definition of storm volumes in previous studies over the United States.

3. In the lower troposphere a quasi-balance between vertical advection and generation is observed during virtually all periods. This is shown to be related to the juxtaposition of strong vertical motion, warm air, and large vertical gradients of kinetic energy.
4. As a result of the differences in the physical processes in the upper and lower troposphere as described in (2) and (3) above, the character of the tendency of kinetic energy in these two layers also differs. The temporal variations of the kinetic energy of the upper troposphere are fairly complex. In the lower troposphere, however, the kinetic energy tendency during all periods studied is positive, resulting in continually increasing kinetic energy. This is consistent with the observed development of the surface cyclone during this time.
5. The AMTEX storm vicinity is quite active energetically

when compared to magnitudes of energy conversions attributed to the general circulation. To compensate for the AMTEX storm's large kinetic energy generation one can assume that there are other areas of the world which are generally energetically quiescent or that there are areas which are actively converting kinetic energy to available potential energy.

The results from this research are the first to attempt to document from a kinetic energy point of view the large-scale physical processes responsible for the intense cyclogenesis frequently observed in the AMTEX area. However, this is only a first step in gaining a more complete understanding of the area's energetics and of the storms which develop within the East China Sea. Since this research brings to focus the dominant role of the upper troposphere in the kinetic energy budget, future research must address the question the role of the various diabatic processes which are responsible for the generation of available potential energy, ultimately the source for kinetic energy. If surface fluxes, as has been suggested by many researchers, play a significant role in providing energy to disturbances which develop in the warm oceanic waters, the mechanisms which transport the available potential energy to the upper troposphere must be identified. An available potential energy budget would accomplish such a task.

BIBLIOGRAPHY

Baxter, T. L., 1975: Meteorological analysis models. Final Report, Ocean Data Systems, Inc.

Coburn, A. R., 1971: Improved three dimensional nephanalysis. Air Force Global Weather Central Technical Memorandum 71-2, 73 pp.

Dutton, J. A. and D. R. Johnson, 1967: Theory of available potential energy and a variational approach to atmospheric energetics. Advances in Geophysics, Vol. 12, Academic Press, 333-463.

Gilchrist, B. and G. P. Cressman, 1954: An experiment in objective analysis. Tellus, 6, No. 4, 309-318.

Haltiner, G. J., 1971: Numerical Weather Prediction. John Wiley and Sons, Inc., 317 pp.

Hess, S. L., 1959: Introduction to Theoretical Meteorology. Holt Rinehart and Winston, New York, 362 pp.

Holton, J. R., 1972: An Introduction to Dynamic Meteorology. Academic Press, 319 pp.

Inman, R. L., 1968: Objective detection and correction of errors in radiosonde data. Tech. Memo. ERLTM-NSSL 40, 48 pp.

Kornegay, F. C. and D. G. Vincent, 1976: Kinetic energy budget analysis during interaction of tropical storm Candy (1968) with an extratropical frontal system. MWR, 104, 849-859.

Krishnamurti, T. N., 1968a: A diagnostic balance model for studies of weather systems of low and high latitudes, Rossby number less than 1. MWR, 96, No. 4, 197-207.

_____, 1968b: A study of a developing wave cyclone. MWR, 96, No. 4, 208-217.

Kung, C. E., 1973: Note on design of an optimized computation scheme for kinematic vertical motion fields. MWR, 101, No. 9, 685-690.

_____, 1974: An analysis of kinetic energy balance over the Marshall Islands area. Proc. Internat. Tropical Meteor. Meeting, Nairobi, Kenya, Amer. Meteor. Soc., Part I, 72-80.

_____, and P. J. Smith, 1974: Problems of large-scale kinetic energy balance--a diagnostic analysis in GARP. BAMS, 55, No. 7, 768-777.

_____, 1975: Balance of kinetic energy in the tropical circulation over the Western Pacific. QJRMS, 101, 293-312.

_____, and W. E. Baker, 1975: Energy transformations in middle-latitude disturbances. QJRMS, 101, 793-815.

_____, and T. L. Tsui, 1975: Subsynoptic-scale kinetic energy balance in the storm area. JAS, 32, 729-740.

Kurihara, Y., 1961: Accuracy of winds-aloft data and estimation of error in numerical analysis of atmospheric motions. J. Meteor. Soc. Japan, 39, 331-345.

Landau, L. D. and E. M. Lifshitz, 1959: Fluid Dynamics. Translation by J. B. Sykes and W. H. Reid, Pergamon Press, Addison-Wesley Publishing Co., Inc., 431 pp.

Lenhard, R. W., 1970: Accuracy of radiosonde temperature and pressure height determination. BAMS, 51, 842-846.

_____, 1973: A revised assessment of radiosonde accuracy. BAMS, 54, 691-693.

Lorenz, E. N., 1955: Available potential energy and the maintenance of the general circulation. Tellus, 7, No. 2, 31-41.

_____, 1967: The Nature and Theory of the General Circulation of the Atmosphere. World Meteorological Organization, 161 pp.

Margules, M., 1903: Uber die energy der sturme. Jahrbuck Zentralanstalt Meteorologie. Translation by C. Abbe 1-26; in Smithson. Misc. Coll., 51, 553-595.

McFarland, M. J., 1974: Variational optimization analysis of temperature and moisture advection in a severe storm environment. Ph.D. Thesis, University of Oklahoma.

McGinley, J. A., 1973: Environmental energy fields associated with severe storms. Master's Thesis, University of Oklahoma, 129 pp.

Moreno, D., 1973: AFGWC macro-scale upper air analysis model (revised). Air Force Global Weather Central Technical Memorandum, 73-1, 75 pp.

O'Brien, J. J., 1970: Alternative solutions to the classical vertical velocity problem. JAM, 9, No. 2, 197-203.

Panofsky, H. A., 1951: Large-scale vertical velocity and divergence. Compendium of Meteorology. American Meteorological Society, Boston, Mass., 639-646.

Petterssen, S. and S. J. Smebye, 1971: On the development of extra tropical cyclones. Quart. J. Roy. Meteor. Soc., 97, 457-482.

Rasmusson, E. M., 1971: Mass, momentum, and energy budget equations for BOMAP computations. NOAA Technical Memorandum ERL BIMAP-3, U.S. Dept. of Commerce Publication, 32 pp.

Ritchie, A. A., 1975: A variational optimization analysis approach to continuous data assimilation. Ph.D. Thesis, University of Oklahoma, 98 pp.

Sasaki, Y. K., 1958: An objective analysis based on the variational method. Journ. Met. Soc. Japan, 36, No. 3, 77-88.

_____, 1970a: Some basic formalisms in numerical variational analysis. MWR, 98, 875-883.

_____, 1970b: Numerical variational analysis formulated under the constraints as determined by longwave equations and a low-pass filter. MWR, 98, 884-889.

_____, 1971: Low-pass and band-pass filters in numerical variational optimization. Jour. Met. Soc. Japan, 49, 766-773.

Sechrist, F. and R. A. Rudy, 1969: Kinetic energy changes in a developing cyclone, studies of large scale atmospheric energetics. Annual Report, University of Wisconsin, Madison, Wisconsin, 93-114.

Smith, P. J., 1971: An analysis of kinematic vertical motion. MWR, 99, No. 10, 715-724.

_____, 1973a: The kinetic energy budget over North America during a period of major cyclone development. Tellus, 25, No. 5.

_____, 1973b: Midlatitude synoptic-scale systems: their kinetic energy budgets and role in the general circulation. MWR, 101, No. 10, 757-762.

Thompson, P. D., 1961: Numerical Weather Analysis and Prediction. MacMillan Co., New York, 170 pp.

Trewartha, G. T., 1961: The Earth's Problem Climates. The University of Wisconsin Press, Madison, Wis., 329 pp.

Ward, J. H. and P. J. Smith, 1976: A kinetic energy budget over North America during a period of short synoptic wave development. MWR, 104, 836-848.

APPENDIX A

THE KINETIC ENERGY EQUATION

The kinetic energy equation in (x,y,p,t) coordinates can be derived from the horizontal equation of motion given below

$$\frac{\partial \vec{V}}{\partial t} + (\vec{V}\cdot\nabla)\vec{V} + \omega \frac{\partial \vec{V}}{\partial p} = - \nabla\varphi - f\vec{k} \times \vec{V} - \vec{F} \qquad (A.1)$$

where $\vec{F}$ is force per unit mass due to eddy and viscous stresses. The derivation proceeds by taking the dot product of this equation with the horizontal wind vector, $\vec{V}$, resulting in

$$\frac{\partial K}{\partial t} + \vec{V}\cdot\nabla K + \omega \frac{\partial K}{\partial p} = - \vec{V}\cdot\nabla\varphi - \vec{V}\cdot\vec{F} \ . \qquad (A.2)$$

The continuity equation after multiplying it by K may be written as

$$K\nabla\cdot\vec{V} + K \frac{\partial \omega}{\partial p} = 0 \ . \qquad (A.3)$$

Adding (A.2) and (A.3) yields the following form of the kinetic energy equation:

$$\frac{\partial K}{\partial t} + \nabla\cdot K\vec{V} + \frac{\partial K\omega}{\partial p} = - \vec{V}\cdot\nabla\varphi + \delta \qquad (A.4)$$

where δ represents the dissipation of kinetic energy due to the viscous terms in the horizontal equation of motion. The variables described by Eq. (A.4) are the sum of the mean values ($\bar{\vec{V}}$, $\bar{\omega}$, and $\bar{\varphi}$)

$\bar{\omega}$) and the small-scale motions ($\vec{V}'$, ω', abd φ'). The small-scale phenomena are always present, but not adequately represented by either the data or the gridded analysis. Therefore by defining the following relationships:

$$\begin{aligned} K &= \bar{K} + K' \\ \vec{V} &= \bar{\vec{V}} + \vec{V}' \\ \omega &= \bar{\omega} + \omega' \\ \varphi &= \bar{\varphi} + \varphi' \end{aligned} \tag{A.5}$$

and substituting into Eq. (A.4), the equation may be written as

$$\underbrace{\frac{\partial \bar{K}}{\partial t}}_{A} + \underbrace{\bar{\vec{V}} \cdot \nabla \bar{K}}_{B} + \bar{\omega} \frac{\partial \bar{K}}{\partial p} + \underbrace{\bar{\vec{V}} \cdot \nabla \bar{\varphi}}_{C} = \underbrace{\overline{\vec{V}' \cdot \nabla K'} + \overline{\omega' \frac{\partial K'}{\partial p}} + \overline{\vec{V}' \cdot \nabla \varphi'}}_{D'} + \delta \tag{A.6}$$

where Term D' represents the subgrid-scale processes. In this study Term D' will also include any error introduced by the analysis or computational techniques and any error due to inaccuracies in the data. Term D, used in the text, is defined as the sum of D' and δ.

APPENDIX B

THE MINIMIZATION OF THE FUNCTIONAL USED IN THE PATTERN CONSERVING TECHNIQUE OF OBJECTIVE ANALYSIS

This appendix was copied verbatum from Baxter's (1975) technical memorandum section I-3. This was done for several reasons. First, Baxter's FORTRAN program was used to produce most of the objectively analyzed fields. Also, there is nothing to be gained by changing notation in reproducing his derivations. Finally, Baxter's publication is difficult to obtain and it is necessary that some detail on the derivation of the finite difference equations used to represent the minimization process be given.

> We would like the properties of the guess field defined in Table 1 to match their counterparts in the final analysis. The distribution of emphasis among these properties is determined by their respective weights. To effect this matching, we shall minimize the following integral:

$$
\begin{aligned}
I \equiv \iint \; [\; & A_{i,j} \, (P^*_{i,j} - P_{i,j})^2 + \\
& B_{i,j} \, (P^*_{i,j+1} - P^*_{i,j} - \mu_{i,j})^2 + \\
& B_{i,j-1} \, (P^*_{i,j} - P^*_{i,j-1} - \mu_{i,j-1})^2 + \\
& C_{i,j} \, (P^*_{i+1,j} - P^*_{i,j} - \nu_{i,j})^2 + \\
& C_{i-1,j} \, (P^*_{i,j} - P^*_{i-1,j} - \nu_{i-1,j})^2 + \\
& E_{i,j} \, (P^*_{i-1,j+1} - P^*_{i,j} - \alpha_{i,j})^2 + \\
& E_{i+1,j-1} \, (P^*_{i,j} - P^*_{i+1,j-1} - \alpha_{i+1,j-1})^2 +
\end{aligned}
$$

$$F_{i,j}\,(P^*_{i+1,j+1} - P^*_{i,j} - \beta_{i,j})^2 +$$
$$F_{i-1,j-1}\,(P^*_{i,j} - P^*_{i-1,j-1} - \beta_{i-1,j-1})^2 +$$
$$D_{i,j}\,(P^*_{i+1,j} + P^*_{i-1,j} + P^*_{i,j+1} + P^*_{i,j-1} - 4P^*_{i,j} - L_{i,j})^2 +$$
$$D_{i-1,j}\,(P^*_{i,j} + P^*_{i-2,j} + P^*_{i-1,j+1} + P^*_{i-1,j-1} - 4P^*_{i-1,j} - L_{i-1,j})^2 +$$
$$D_{i+1,j}\,(P^*_{i+2,j} + P^*_{i,j} + P^*_{i+1,j+1} + P^*_{i+1,j-1} - 4P^*_{i+1,j} - L_{i+1,j})^2 +$$
$$D_{i,j-1}\,(P^*_{i+1,j-1} + P^*_{i-1,j-1} + P^*_{i,j} + P^*_{i,j-2} - 4P^*_{i,j-1} - L_{i,j-1})^2 +$$
$$D_{i,j+1}\,(P^*_{i+1,j+1} + P^*_{i-1,j+1} + P^*_{i,j+2} + P^*_{i,j} - 4P^*_{i,j+1} - L_{i,j+1})^2\ ]$$
$$dxdy \qquad (B.1)$$

In the above, the starred quantities are the analysis values we are seeking. Each term is a departure from the desired matching of differential properties. Extra terms have been added to account for the effect of changing $P^*_{i,j}$ on the differential properties computed at surrounding points. To minimize the integral, we simply take the first variation with respect to $P^*_{i,j}$, and set it to zero. The solution of the resulting equation will be the $P^*_{i,j}$ that will cause the integral to be minimized. The fact that each term is squared insures a minimum as opposed to a maximum value.

$$\frac{\delta I}{\delta P^*} = \iint [\ 2A_{i,j}\,(P^*_{i,j} - P_{i,j})$$
$$-2\,B_{i,j}\,(P^*_{i,j+1} - P^*_{i,j} - \mu_{i,j})$$
$$+\,2\,B_{i,j-1}\,(P^*_{i,j} - P^*_{i,j-1} - \mu_{i,j-1})$$
$$-\,2\,C_{i,j}\,(P^*_{i+1,j} - P^*_{i,j} - \nu_{i,j})$$
$$+\,2\,C_{i-1,j}\,(P^*_{i,j} - P^*_{i-1,j} - \nu_{i-1,j})$$
$$-\,2\,E_{i,j}\,(P^*_{i-1,j+1} - P^*_{i,j} - \alpha_{i,j})$$
$$+\,2\,E_{i+1,j-1}\,(P^*_{i,j} - P^*_{i+1,j-1} - \alpha_{i+1,j-1})$$

$$- 2\, F_{i,j}\, (P^*_{i+1,j+1} - P^*_{i,j} - \beta_{i,j})$$

$$+ 2\, F_{i-1,j-1}\, (P^*_{i,j} - P^*_{i-1,j-1} - \beta_{i-1,j-1})$$

$$- 8\, D_{i,j}\, (P^*_{i+1,j} + P^*_{i-1,j} + P^*_{i,j+1} + P^*_{i,j-1} - 4P^*_{i,j} - L_{i,j})$$

$$+ 2\, D_{i-1,j}\, (P^*_{i,j} + P^*_{i-2,j} + P^*_{i-1,j+1} + P^*_{i-1,j-1} - 4P^*_{i-1,j} - L_{i-1,j})$$

$$+ 2\, D_{i+1,j}\, (P^*_{i+2,j} + P^*_{i,j} + P^*_{i+1,j+1} + P^*_{i+1,j-1} - 4P^*_{i+1,j} - L_{i+1,j})$$

$$+ 2\, D_{i,j-1}\, (P^*_{i+1,j-1} + P^*_{i-1,j-1} + P^*_{i,j} + P^*_{i,j-2} - 4P^*_{i,j-1} - L_{i,j-1})$$

$$+ 2\, D_{i,j+1}\, (P^*_{i+1,j+1} + P^*_{i-1,j+1} + P^*_{i,j+2} + P^*_{i,j} - 4P^*_{i,j+1} - L_{i,j+1})\ ]$$

$$dxdy \overset{\text{set}}{=} 0 \qquad \text{(B.2)}$$

The terms in $\frac{\delta I}{\delta P^*}$ can be grouped into three categories:

1. Those involving $P^*_{i,j}$.
2. Those involving P^* at surrounding points.
3. Those not involving P^*.

$$S_{i,j}P^*_{i,j} \left\{ \begin{array}{l} [\, A_{i,j} + B_{i,j} + B_{i,j-1} + C_{i,j} + C_{i-1,j} + E_{i,j} \\ \quad + E_{i+1,j-1} + F_{i,j} + F_{i-1,j-1} + 16\, D_{i,j} + D_{i-1,j} \\ \quad + D_{i+1,j} + D_{i,j-1} + D_{i,j+1}\,]\ \ P^*_{i,j} \end{array} \right.$$

$$-H_{i,j} \left\{ \begin{array}{l} - B_{i,j}\, P^*_{i,j+1} - B_{i,j-1}\, P^*_{i,j-1} - C_{i,j}\, P^*_{i+1,j} - C_{i-1,j}\, P^*_{i-1,j} \\ - E_{i,j}\, P^*_{i-1,j+1} - E_{i+1,j-1}\, P^*_{i+1,j-1} - F_{i,j}\, P^*_{i+1,j+1} \\ - F_{i-1,j-1}\, P^*_{i-1,j-1} - 4\, D_{i,j}\, P^*_{i+1,j} - 4\, D_{i,j}\, P^*_{i-1,j} \\ - 4\, D_{i,j}\, P^*_{i,j+1} - 4\, D_{i,j}\, P^*_{i,j-1} + D_{i-1,j}\, P^*_{i-2,j} \\ + D_{i-1,j}\, P^*_{i-1,j+1} + D_{i-1,j}\, P^*_{i-1,j-1} - 4\, D_{i-1,j}\, P^*_{i-1,j} \\ + D_{i+1,j}\, P^*_{i+2,j} + D_{i+1,j} P^*_{i+1,j+1} + D_{i+1,j}\, P^*_{i+1,j-1} \\ - 4\, D_{i+1,j}\, P^*_{i+1,j} + D_{i,j-1}\, P^*_{i+1,j-1} + D_{i,j-1}\, P^*_{i-1,j-1} \\ + D_{i,j-1}\, P^*_{i,j-2} - 4\, D_{i,j-1}\, P^*_{i,j-1} + D_{i,j+1}\, P^*_{i+1,j+1} \\ + D_{i,j+1}\, P^*_{i-1,j+1} + D_{i,j+1}\, P^*_{i,j+2} - 4\, D_{i,j+1}\, P^*_{i,j+1} \end{array} \right.$$

$$-G_{i,j}\begin{cases} -A_{i,j}\,P_{i,j} + B_{i,j}\,\mu_{i,j} - B_{i,j-1}\,\mu_{i,j-1} + C_{i,j}\,\nu_{i,j} \\ -C_{i-1,j}\,\nu_{i-1,j} + E_{i,j}\,\alpha_{i,j} - E_{i+1,j-1}\,\alpha_{i+1,j-1} \\ +F_{i,j}\,\beta_{i,j} - F_{i-1,j-1}\,\beta_{i-1,j-1} + 4\,D_{i,j}\,L_{i,j} \\ -D_{i-1,j}\,L_{i-1,j} - D_{i+1,j}\,L_{i+1,j} - D_{i,j-1}\,L_{i,j-1} \\ -D_{i,j+1}\,L_{i,j+1} \end{cases} \qquad (B.3)$$

The minimization equation may be written as

$$S_{i,j}\,P^*_{i,j} - (G_{i,j} + H_{i,j}) = 0 \qquad (B.4)$$

In $H_{i,j}$, let us group together the coefficients of P* at each point.

$$\begin{aligned} -H_{i,j} = {} & D_{i-1,j}\,P^*_{i-2,j} + (-C_{i-1,j} - 4\,D_{i,j} - 4\,D_{i-1,j})\,P^*_{i-1,j} \\ & + (-C_{i,j} - 4\,D_{i,j} - 4\,D_{i+1,j})\,P^*_{i+1,j} \\ & + D_{i+1,j}\,P^*_{i+2,j} + (-E_{i,j} + D_{i-1,j} + D_{i,j+1})\,P^*_{i-1,j+1} \\ & + (-B_{i,j} - 4\,D_{i,j} - 4\,D_{i,j+1})\,P^*_{i,j+1} \\ & + (-F_{i,j} + D_{i+1,j} + D_{i,j+1})\,P^*_{i+1,j+1} \\ & + (-F_{i-1,j-1} + D_{i-1,j} + D_{i,j-1})\,P^*_{i-1,j-1} \\ & + (-B_{i,j-1} - 4\,D_{i,j} - 4\,D_{i,j-1})\,P^*_{i,j-1} \\ & + (-E_{i+1,j-1} + D_{i+1,j} + D_{i,j-1})\,P^*_{i+1,j-1} \\ & + D_{i,j-1}\,P^*_{i,j-2} + D_{i,j+1}\,P^*_{i,j+2} \end{aligned} \qquad (B.5)$$

Define:

$$\begin{aligned} X_{i,j} &\equiv C_{i,j} + 4\,(D_{i,j} + D_{i+1,j}) \\ Y_{i,j} &\equiv B_{i,j} + 4\,(D_{i,j} + D_{i,j+1}) \\ Z_{i,j} &\equiv -F_{i,j} + D_{i+1,j} + D_{i,j+1} \\ R_{i,j} &\equiv -E_{i+1,j} + D_{i,j} + D_{i+1,j+1} \end{aligned} \qquad (B.6)$$

Then

$$
\begin{aligned}
-H_{i,j} \approx\ & D_{i-1,j}\, P^{*}_{i-2,j} - X_{i-1,j}\, P^{*}_{i-1,j} - X_{i,j}\, P^{*}_{i+1,j} \quad \text{[I-4]} \\
& + D_{i+1,j}\, P^{*}_{i+2,j} + R_{i-1,j}\, P^{*}_{i-1,j+1} - Y_{i,j}\, P^{*}_{i,j+1} \\
& + Z_{i,j}\, P^{*}_{i+1,j+1} + Z_{i-1,j-1}\, P^{*}_{i-1,j-1} - Y_{i,j-1}\, P^{*}_{i,j-1} \\
& + R_{i,j-1}\, P^{*}_{i+1,j-1} + D_{i,j-1}\, P^{*}_{i,j-2} - D_{i,j+1}\, P^{*}_{i,j+2} \qquad \text{(B.7)}
\end{aligned}
$$

APPENDIX C

A VARIATIONAL APPROACH TO HYDROSTATICALLY ADJUSTING OBJECTIVELY ANALYZED HEIGHT AND TEMPERATURE FIELDS

The hydrostatic approximation can be made for atmospheric scales of motion where the ratio of the depth of a disturbance to its horizontal extent is less than one. This approximation was used in the derivation of the kinetic energy equation in Appendix A. To continue in this consistent manner the temperature and height fields are constrained to be hydrostatic. This was accomplished by the use of a variational formalism which Sasaki (1970a) refers to as the "strong constraint."

In non-dimensional form the formalism is given by

$$J = \Sigma\Sigma\Sigma[\tilde{\alpha}(\bar{T} - \tilde{\bar{T}})^2 + \tilde{\beta}(\Delta z - \tilde{\Delta z})^2 + \lambda(\frac{R}{g} \ln(\frac{p_o}{p_1})\bar{T} - \Delta z)] \qquad (C.1)$$

where $\bar{T}$ is the mean temperature of a pressure layer extending from p_o as the lower level of pressure to p_1, the upper pressure. Δz is the height between the two pressure levels. $\tilde{\alpha}$ and $\tilde{\beta}$ are observational weights. All the "~" are the observed values, while the non "~" are the analyzed quantities. λ is the Lagrange multiplier.

The last term in (C.1) is derived from the following integration of the hydrostatic relation

$$\int_{p_o}^{p_1} dp = -g \int_{z_{p_o}}^{z_{p_1}} \rho \, dz \tag{C.2}$$

or since

$$\rho = \frac{p}{RT} \tag{C.3}$$

then

$$\int_{p_1}^{p_o} \frac{dp}{p} = g \int_{z_{p_o}}^{z_{p_1}} \frac{dz}{RT} \tag{C.4}$$

If we assume that some mean temperature can be given by

$$\bar{T} = \frac{T_{z_{p_1}} + T_{z_{p_o}}}{2} \tag{C.5}$$

which is not a function of height then

$$\ln(p_o/p_1) - \frac{g}{R\bar{T}} \Delta z = 0 \tag{C.6}$$

where $\Delta z = z_{p_1} - z_{p_o}$.

The functional in this formalism is composed of terms weighted by $\tilde{\alpha}$ and $\tilde{\beta}$, and the third term which is the physical constraint in this case given by the hydrostatic equation. While the inclusion of the Lagrange multiplier in a product with the constraint must be met exactly, the $\tilde{\alpha}$ and $\tilde{\beta}$ represent conditions, known as weak constraints, which will be only approximately met (Sasaki, 1970a). The stationary value of the functional (C.1) is found by equating the first variation of the functional to zero. The variational operator, δ, is analogous to the operator in differential calculus.

The minimization of the functional then proceeds as follows:

$$\delta J = \Sigma\Sigma\Sigma[\, 2\tilde{\alpha}(\bar{T} - \tilde{\bar{T}})\,\delta\bar{T} + 2\tilde{\beta}(\Delta z - \tilde{\Delta z}) + \delta\lambda(\frac{R}{g}\ln(\frac{p_o}{p_1})\bar{T} - \Delta z) +$$

$$\lambda\,(\frac{R}{g}\ln(\frac{p_o}{p_1})\,\delta\bar{T} + \delta\Delta z] \quad . \tag{C.7}$$

Eq. (C.7) yields the following Euler-Lagrange equations:

$$2\tilde{\alpha}(\bar{T} - \tilde{\bar{T}}) + \lambda K = 0 \tag{C.8}$$

$$2\tilde{\beta}(\Delta z - \tilde{\Delta z}) - \lambda = 0 \tag{C.9}$$

$$K\bar{T} - \Delta z = 0 \tag{C.10}$$

where

$$K = \frac{R}{g}\ln(\frac{p}{p_1}) \quad . \tag{C.11}$$

Eliminating λ from the set of Euler equations will result in two equations where Δz and $\bar{T}$ are given in terms of the observed, "~", quantities.

$$\Delta z = \frac{\tilde{\alpha}\tilde{\bar{T}} + K\tilde{\beta}\,\tilde{\Delta z}}{(\frac{\tilde{\alpha} + K^2\tilde{\beta}}{K})} \tag{C.12}$$

$$\bar{T} = \frac{\tilde{\alpha}\tilde{\bar{T}} + K\tilde{\beta}\,\tilde{\Delta z}}{(\tilde{\alpha} + K^2\tilde{\beta})} \quad . \tag{C.13}$$

APPENDIX D

A VARIATIONAL APPROACH TO THE MASS CONTINUITY PROBLEM

In order to insure that the analyzed components of the horizontal wind field satisfy the mass continuity equation, a variational approach was used to adjust them to satisfy the mass continuity equation exactly. In other words a formalism with the continuity equation as a strong constraint was minimized. The functional for which the stationary value was found is given by

$$J = \iiint_{x\,y\,p} [\tilde{\alpha}(u-\tilde{u})^2 + \tilde{\alpha}(v-\tilde{v})^2]\, dxdydp$$
$$+ \iint_{x\,y} \{\lambda[\int_{p} (\frac{\partial u}{\partial x} + \frac{\partial v}{\partial y})\, dp + \omega_o]\}\, dxdy\,, \qquad (D.1)$$

where $\tilde{\alpha}$ is the observational weight on the wind components and is a function only of pressure. u and v are the analyzed horizontal wind components, while $\tilde{u}$ and $\tilde{v}$ are the observed horizontal wind components. λ is the Lagrange multiplier. ω_o is the lower boundary condition on the vertical motion and is equal to $\frac{\partial p}{\partial t}$.

Taking the first variation of (D.1) yields

$$\delta J = \iiint_{x\,y\,p} [2\tilde{\alpha}(u-\tilde{u})\,\delta u + 2\tilde{\alpha}(v-\tilde{v})\,\delta v]\, dxdydp$$

$$+\iint_x\int_y [\lambda \int_p (\frac{\partial\ \delta u}{\partial x} + \frac{\partial\ \delta v}{\partial y})\ dp]\ dxdy$$

$$+\iint_x\int_y [\delta\ \lambda \int_p (\frac{\partial u}{\partial x} + \frac{\partial v}{\partial x})\ dp + \omega_o]\ dxdy = 0\ . \qquad (D.2)$$

Integrating the second term by parts, where

$$\frac{\partial(\lambda\ \delta u)}{\partial x} = \lambda\ \frac{\partial\ \delta u}{\partial x} + \delta u\ \frac{\partial \lambda}{\partial x} \qquad (D.3)$$

and

$$\frac{\partial(\lambda\ \partial v)}{\partial y} = \lambda\ \frac{\partial\ \delta v}{\partial y} + \delta v\ \frac{\partial \lambda}{\partial y}\ . \qquad (D.4)$$

Then (D.2) may be written as

$$\iiint_x\int_y\int_p [2\tilde{\alpha}(u - \tilde{u})\delta u + 2\tilde{\alpha}(v - \tilde{v})\delta v]\ dxdydp$$

$$-\iiint_x\int_y\int_p [\frac{\partial \lambda}{\partial x}\ \delta u + \frac{\partial \lambda}{\partial y}\ \delta v]\ dxdydp$$

$$+\iint_x\int_y [\delta\lambda \int_p (\frac{\partial u}{\partial x} + \frac{\partial v}{\partial y})\ dp + \omega_o]\ dxdy$$

$$+\iint_x\int_y [\lambda\ \delta u \Big|_{x_o}^{x_1}]\ dydp + \iint_x\int_y [\lambda\ \delta v \Big|_{y_o}^{y_1}]\ dxdp = 0\ . \qquad (D.5)$$

Using a natural boundary condition where $\lambda = 0$, and for arbitrary values of δu, δv, and $\delta\lambda$, one may write the following Euler-Lagrange equations.

$$2\tilde{\alpha}(u - \tilde{u}) - \frac{\partial \lambda}{\partial x} = 0 \qquad (D.6)$$

$$2\tilde{\alpha}(v - \tilde{v}) - \frac{\partial \lambda}{\partial y} = 0 \qquad (D.7)$$

$$\int_p (\frac{\partial u}{\partial x} + \frac{\partial v}{\partial y})\ dp + \omega_o = 0\ . \qquad (D.8)$$

The finite difference analogues for (D.6) and (D.7) after solving for the analyzed component may be written as

$$u = \tilde{u} + \frac{1}{2\alpha} \nabla_x \lambda \tag{D.9}$$

and

$$v = \tilde{v} + \frac{1}{2\tilde{\alpha}} \nabla_y \lambda \tag{D.10}$$

where $$\nabla_x \equiv [(\ )_{i+1} - (\ )_{i-1}]/2d \tag{D.11}$$

and

$$\nabla_y \equiv [(\ )_{j+1} - (\ )_{j-1}]/2d \tag{D.12}$$

d is the grid distance.

The mass continuity constraint, (D.8), is given by

$$\sum_{k=1}^{k} \{[\overline{(\nabla_x u + \nabla_y v)} \Delta p_k\} + \omega_o = 0 \tag{D.13}$$

where the mean divergence of the layer has been substituted.

The mean observed divergence, $\overline{\tilde{DIV}}$, is computed simply as

$$\overline{\tilde{DIV}}_k = .5(D\tilde{I}V_{k+\frac{1}{2}} + D\tilde{I}V)_{k-\frac{1}{2}} \tag{D.14}$$

where $k+\frac{1}{2}$ and $k-\frac{1}{2}$ are the levels immediately above and below layer k.

Substituting (D.9) and (D.10) into (D.13) yields

$$\sum_{k=1}^{k} \{0.5[(\nabla_x \tilde{u} + \frac{1}{2\tilde{\alpha}} \nabla_x^2 \lambda + \nabla_y \tilde{v} + \frac{1}{2\tilde{\alpha}} \nabla_y^2 \lambda)_{k+\frac{1}{2}}$$

$$+ (\nabla_x \tilde{u} + \frac{1}{2\tilde{\alpha}} \nabla_x^2 \lambda + \nabla_y \tilde{v} + \frac{1}{2\tilde{\alpha}} \nabla_y^2 \lambda)_{k-\frac{1}{2}}] \Delta p_k\} + \omega_o = 0 \tag{D.15}$$

where $$\nabla_x^2 \equiv [(\ )_{i+2} + (\ )_{i-2} - 2(\ )_i]/4d \tag{D.16}$$

and

$$\nabla_y^2 \equiv [(\ )_{j+2} + (\ )_{j-2} - 2(\ )_j]/4d \ . \qquad \text{(D.17)}$$

Eq. (D.15) can be solved for λ, resulting in

$$\nabla_x^2 \lambda + \nabla_y^2 \lambda = \frac{-4\{\sum_{k=1}^{k} .5[D\tilde{I}V_{k-\frac{1}{2}} + D\tilde{I}V_{k+\frac{1}{2}}]\Delta p_k - \omega_o\}}{\sum_{k=1}^{k} [\frac{\Delta p_k}{\alpha_{k-\frac{1}{2}}} + \frac{\Delta p_k}{\alpha_{k+\frac{1}{2}}}]} \ . \qquad \text{(D.18)}$$

The Poisson equation, (D.18), was solved for the analysis grid using a sequential relaxation technique. The values of λ were then substituted back into (D.9) and (D.10) to solve for the analyzed values of u and v.

APPENDIX E

SENSITIVITY ANALYSIS

Errors in determining the values of the budget terms are a result of:

1) the inaccuracies in measurements of wind direction and speed, of geopotential, and of temperature;
2) the analysis procedure; and
3) the finite difference analogues used to represent the kinetic energy equation.

The effects of randomly distributed errors has been documented by Kurihara (1961), Kornegay and Vincent (1976), and others. Kornegay and Vincent tested the effects of random errors in the data on their budget results by adding random numbers to the data ($\pm$ 10° for wind direction, $\pm$ 20% for wind speed, and $\pm$ .5% for geopotential). They repeated their budget calculations for the same data altered by ten sets of random numbers and found that the kinetic energy budget remained essentially the same. For example, the upper and lower limits of the budget terms, vertically integrated for the volume, were:

Limits			Original Budget	Units
11.6 $\leq$	Kinetic Energy	$\leq$ 11.9	11.4	J m^{-2}
2.9 $\leq \lvert \rvert \leq$	Tendency	$\leq \lvert \rvert \leq$ 4.0	3.4	W m^{-2}
13.9 $\leq \lvert \rvert \leq$	Generation	$\leq \lvert \rvert \leq$ 18.4	17.1	W m^{-2}
-17.0 $\leq \lvert \rvert \leq$	Advection	$\leq \lvert \rvert \leq$ -14.9	-15.6	W m^{-2}
1.1 $\leq \lvert \rvert \leq$	Residual	$\leq \lvert \rvert \leq$ 6.7	1.9	W m^{-2}

As in all objective analysis techniques, PCT cannot represent precisely the meteorological parameters on a gridded field from irregularly distributed data points. Hopefully most of the error introduced by the objective analysis is random. However, the physical assumptions made by PCT and computational procedures employed could have led to a systematic error. One apparent systematic error occurs in data sparse areas where the first guess wind (a geostrophic wind) remains essentially unchanged by PCT, resulting in an analyzed wind which is greater than the "true wind" (which for our purposes we consider to be the gradient wind) for cyclonic curvature and an analyzed wind which is less than the "true wind" where flow is anti-cyclonic. Since the budget computations were made primarily in areas of cyclonic curvature, one might expect that in general the analyzed wind fields would be biased (too strong). To gain some insight into the effect of this kind of systematic error on the kinetic energy budget, a simple experiment was conducted.

All the wind fields were reanalyzed using only 90% of the geostrophic wind as the first guess for PCT (test run #1). A second test was run using 75% of the geostrophic wind (test run #2). Two periods, which represent extremes in the characteristics of the storm and of the data were examined. The first was when the horizontal advection of kinetic energy was negative (0000 GMT, 14 February) and when the storm was in an area of relatively high data density. The second was where advection of kinetic energy was positive (1200 GMT, 15 February) and the storm volume was in an area of minimum data coverage. Figure 61 shows the original

budget values for the entire storm volume, and the two test runs for 0000 GMT, 14 February. In Figure 61b are plotted the budget terms from the original analysis and for tests #1 and #2 for 1200 GMT, 15 February.

From test period 1, it is apparent that even at 25% reduction of the first guess wind, which represents the maximum expected difference between the gradient and geostrophic winds, the general character of the budget remains essentially unchanged. As might be expected the advection term is altered more than the generation term by changes in the first guess wind field. This occurs since both the wind components and the kinetic energy are affected by changes in the wind analysis. The generation term decreases by 21% and 32% from the original value with 10% and 25% reductions, respectively, in the first guess wind field, while reductions of 26% and 58%, respectively, in the advection of kinetic energy is observed. The reduced values of the kinetic energy results in a slight decrease in the magnitude of the tendency. The most encouraging observation is the continued near balance of the generation and advection of kinetic energy, as in the original budget values.

In test period 2 the percent changes in the budget terms were higher than in test period 1. This was primarily due to the decreased data density. For example, in period 1 a 10% reduction of first guess wind resulted in a 12% decrease of kinetic energy, and a 16% reduction in period 2. In other words, in the second period examined, the data were less abundant and were less

effective in restoring the altered first guess to its original value when compared with period 1. The budget terms behaved in a similar manner, with their combined effect leading to a 52% reduction (for period 2) in the residual. However, the essential features of the budget were not affected: a relatively large negative residual; negative tendency; positive advection; and a small value for the generation term. For the 25% reduction of the first guess wind the generation became slightly negative.

The results of the sensitivity analysis show that the bias introduced by a systematic error, such as an overestimate of the "true wind" in cyclonic flow by a geostrophic first guess, is not sufficient to change the general features of the kinetic energy budget.

Table 1. Kinetic energy budgets by period for Smith's (S) and Petterssen and Smebye (P & S). Units are 10^5 J·m^{-2} for k and W·m^{-2} for other terms. (from Smith, 1973)

Study	$\bar{k}$	$\frac{\partial \bar{k}}{\partial t}$	$-\bar{V}\cdot\bar{k}V$	$\frac{-\partial \omega k}{\partial p}$	$-\bar{V}\cdot\nabla\bar{\phi}$	D
			Prestorm period			
S	14.5	−1.1	2.3	0.0	5.8	−9.2
P&S	27.8	−5.4	−13.1	−1.5	17.3	−8.1
			Growth period			
S	19.2	6.5	12.0	0.0	10.0	−15.5
P&S	27.0	2.8	−9.7	−1.0	19.8	−6.3
			Decay period			
S	19.0	−3.6	9.5	0.0	0.3	−13.4
P&S	26.3	−2.8	−9.4	−1.0	16.0	−8.4
			Total system			
S	17.4	−0.1	6.9	0.0	6.1	−13.1
P&S	27.0	−1.3	−10.6	−1.1	17.9	−7.5

Table 2. Kinetic energy balance of various types of cyclonic disturbances. (k) in units of 10^5 J·m^{-2} and others in W·m^{-2}. (from Kung and Baker, 1975)

Flow pattern	Type	Pressure layer (mb)	$[k]$	$\left[\frac{\partial k}{\partial t}\right]$	$[\nabla \cdot Vk]$	$\left[\frac{\partial \omega k}{\partial p}\right]$	$-[\nabla \cdot \nabla\phi]$	$[E]$
Developing cyclones	C1, C4	100–350	8·63	0·35	2·56	−0·66	4·00	1·75
		350–750	5·65	0·13	0·81	0·56	2·42	0·92
		750–surface	0·76	0·09	−0·10	0·06	2·42	2·37
		Total	15·04	0·57	3·27	−0·04	8·84	5·04
Mature cyclones	C2, C5	100–350	8·39	0·21	1·73	−0·43	3·59	2·08
		350–750	5·81	0·36	−0·04	0·31	2·87	2·23
		750–surface	0·89	0·08	0·04	0·10	3·09	2·87
		Total	15·09	0·65	1·73	−0·02	9·55	7·18
Occluded cyclones	C3, C6	100–350	8·56	−0·09	0·48	−0·26	2·86	2·75
		350–750	5·96	0·34	0·08	0·24	1·61	0·92
		750–surface	0·84	0·05	0·10	−0·01	2·69	2·56
		Total	15·36	0·30	0·66	−0·03	7·16	6·23
Closed low at 500mb	C1, C2, C3	100–350	8·15	0·02	0·48	−0·35	2·94	2·80
		350–750	5·54	0·43	−0·28	0·27	1·88	1·43
		750–surface	0·83	0·07	0·00	0·05	2·79	2·68
		Total	14·52	0·52	0·20	−0·03	7·61	6·91
Open cyclonic wave at 500mb	C4, C5, C6	100–350	8·92	0·24	2·50	−0·49	3·94	1·68
		350–750	6·12	0·16	0·70	0·41	2·72	1·46
		750–surface	0·82	0·08	0·05	0·05	2·77	2·59
		Total	15·86	0·48	3·25	−0·03	9·43	5·73

Table 3. Cyclone vicinity budget for the period 1200 GMT, April 12 to 0000 GMT, April 15, summarized with cyclone system budget. Units are the same as in Table 1. (from Smith, 1973)

Layer (mb)	$\frac{\partial k}{\partial t}$	$-\mathbf{v}\cdot k\mathbf{v}$	$-\frac{\partial \omega k}{\partial p}$	$-\mathbf{v}\cdot\nabla\phi$	D
400–200	−0.9	17.5	1.4	7.5	−27.3
600–400	1.9	4.9	−0.6	1.1	−3.5
800–600	2.1	0.7	−0.1	0.7	0.8
sfc–800	0.6	0.8	−0.7	8.9	−8.4
sfc–200	3.7	23.9	0.0	18.2	−38.4
Cyclone system sfc–200	−0.1	6.9	0.0	6.1	−13.1

Table 4. Summary of the data set. This includes only the data to be used in this study and does not reflect the entire data set available for this research.

APPROX. #	TYPE	LEVELS (mbs)	OBSERVATION TIMES	PARAMETERS & REPORTING RESOLUTION
25	AMTEX surface	Sea Level	every 6 hrs	1,2,3,4,5
86	ships	Sea Level	every 6 hrs	1,2,3,4,6,7
9	AMTEX RAOBS	1000,850 700,500 400,300 250,200 150,100	every 6 hrs	a,b,c,d,e
110	*RAOBS	(same as above)	every 6 hrs	a,b,c,d,e
900	*other surface	Sea Level	every 6 hrs	1,2,3,4,5
250	*other ships	Sea Level	every 6 hrs	1,2,3,4,6,7
100	*military aircraft	one flight level (meters)	irregular	b,c,d,e

*from the AFGWC data base.

1 = sea level pressure (.1mb)
2 = air temperature (.1°C)
3 = wind direction (10°)
4 = wind speed (.1 m/s)
5 = six hour precip (.1mm)
6 = sea surface temp (.1°C)
7 = height of wind wave(.1m)

a = height of pressure surface (.1m)
b = wind direction (10°)
c = wind speed (.1m/s)
d = air temperature (1°C)
e = dewpoint (.1°C)

Table 5. Summary of "3-D Neph" data.

Type Low Cloud	Maximum Tops
Type Middle Cloud	Minimum Bases
Type High Cloud	Total % Cloud Cover
Present Weather	% Cloud Cover by Layer (for 15 layers)

Table 6. Definition of variables used in Eq. (4.2). "X" is any scalar variable.

Analyzed Quantities	First Guess Quantities	Relative Weight	Remarks
$X^*_{i,j}$	$X_{i,j}$	$A_{i,j}$	
$\mu^*_{i,j} = X^*_{i,j+1} - X^*_{i,j}$	$\mu_{i,j} = X_{i,j+1} - X_{i,j}$	$B_{i,j}$	Gradient in y-direction
$\nu^*_{i,j} = X^*_{i+1,j} - X^*_{i,j}$	$\nu_{i,j} = X_{i+1,j} - X_{i,j}$	$C_{i,j}$	Gradient in x-direction
$\alpha^*_{i,j} = X^*_{i-1,j+1} - X^*_{i,j}$	$\alpha_{i,j} = X_{i-1,j+1} - X_{i,j}$	$E_{i,j}$	Gradient in diagonal ("SE to NW")
$\beta^*_{i,j} = X^*_{i+1,j+1} - X^*_{i,j}$	$\beta_{i,j} = X_{i+1,j+1} - X_{i,j}$	$F_{i,j}$	Gradient in diagonal ("SW to NE")
$L^*_{i,j} = X^*_{i+1,j} + X^*_{i-1,j} + X^*_{i,j+1} + X_{i,j-1} - 4\,X^*_{i,j}$	$L_{i,j} = X_{i+1,j} + X_{i-1,j} + X_{i,j+1} + X_{i,j-1} - 4\,X_{i,j}$	$D_{i,j}$	Laplacian

Table 7. Root-mean square errors in radiosonde computed height and density at specified pressure. (from Lenhard, 1973)

Pressure (mb)	Height error (m)	Density error (%)
700	2.3	.08
500	4.6	.10
300	8.5	.12
200	11.7	.10
100	15.2	.09

Table 8. Definition of variables in Eq. (4.6). See Fig. 10 for location of point i,j for the different variables.

Analyzed Variables	First Guess Variables	Weights	Quantity Represented
$u^*_{i,j}$	$u_{i,j}$	$A_{i,j}$	Horizontal wind component in: 1) x-direction
$v^*_{i,j}$	$v_{i,j}$	$A_{i,j}$	2) y-direction
$d^*_{i,j}$	$d_{i,j}$	$D_{i,j}$	Divergence of horizontal wind
$q^*_{i,j}$	$q_{i,j}$	$Q_{i,j}$	Vorticity of horizontal wind
$e^*_{i,j} = u^*_{i-1,j+1} - u^*_{i,j}$	$e_{i,j} = u_{i-1,j+1} - u_{i,j}$	$E_{i,j}$	Gradient along the "SE-NW" diagonal of 1) u-component
$\hat{e}^*_{i,j} = v^*_{i-1,j+1} - v^*_{i,j}$	$\hat{e}_{i,j} = v_{i-1,j+1} - v_{i,j}$	$E_{i,j}$	2) v-component
$f^*_{i,j} = u^*_{i,j+1} - u^*_{i,j}$	$f_{i,j} = u_{i,j+1} - u_{i,j}$	$F_{i,j}$	Gradient in y-direction of 1) u-component
$\hat{f}^*_{i,j} = v^*_{i,j+1} - v^*_{i,j}$	$\hat{f}_{i,j} = v_{i,j+1} - v_{i,j}$	$F_{i,j}$	2) v-component
$g^*_{i,j} = u^*_{i+1,j+1} - u^*_{i,j}$	$g_{i,j} = u_{i+1,j+1} - u_{i,j}$	$G_{i,j}$	Gradient along the "SW-NE" diagonal of 1) u-component
$\hat{g}^*_{i,j} = v^*_{i+1,j+1} - v^*_{i,j}$	$\hat{g}_{i,j} = v_{i+1,j+1} - v_{i,j}$	$G_{i,j}$	2) v-component
$h^*_{i,j} = u^*_{i+1,j} - u^*_{i,j}$	$h_{i,j} = u_{i+1,j} - u_{i,j}$	$H_{i,j}$	Gradient in x-direction of 1) u-component
$\hat{h}^*_{i,j} = v^*_{i+1,j} - v^*_{i,j}$	$\hat{h}_{i,j} = v_{i+1,j} - v_{i,j}$	$H_{i,j}$	2) v-component

Table 9. Cyclone vicinity budget from study by Smith (1973). Units are Wm^{-2}.

Layer (mb)	$\frac{\partial K}{\partial t}$	$-\vec{V}_3 \cdot \nabla K$	$-\vec{V}_2 \cdot \nabla \varphi$	R
SFC - 800	0.6	0.1	8.9	-8.4
800 - 600	2.1	0.6	0.7	0.8
600 - 400	1.9	4.3	1.1	-3.5
400 - 200	-0.9	18.9	7.5	-27.3
SFC - 200	3.7	23.9	18.2	-38.4

Table 10. Kinetic energy budget for AMTEX storm vicinity from 0000 GMT, 13 February to 1200 GMT, 15 February 1975. Units are the same as Table 9.

Layer (mb)	$\frac{\partial K}{\partial t}$	$-\vec{V}_3 \cdot \nabla K$	$-\vec{V}_2 \cdot \nabla \varphi$	R
SFC - 800	0.8	-0.6	2.5	-1.1
800 - 600	1.0	-0.9	0.1	1.8
600 - 350	2.0	-4.7	3.6	3.1
350 - 225	-2.0	-4.6	7.1	-4.5
225 - 100	-4.7	-6.3	6.6	-5.0
SFC - 100	-2.9	-17.1	19.9	-5.7

Table 11. Same as Table 10 except for 0000 GMT, 13 February to 0000 GMT, 15 February.

Layer (mb)	$\frac{\partial K}{\partial t}$	$-\vec{V}_3 \cdot \nabla K$	$-\vec{V}_2 \cdot \nabla \varphi$	R
SFC - 800	0.9	-0.7	2.3	-0.7
800 - 600	1.3	-1.0	0.3	2.0
600 - 350	3.0	-5.9	4.5	4.4
350 - 225	-1.0	-6.7	8.4	-0.7
225 - 100	-4.1	-8.7	7.3	-2.7
SFC - 100	0.1	-23.0	22.8	2.3

Table 12. Time-mean, area-average cyclone vicinity kinetic energy budget for 11-24 April 1970. Budget quantities are in Wm^{-2}. (from Ward and Smith, 1976)

Layer (mb)	$\frac{\partial K}{\partial t}$	$-\vec{V}_3 \cdot \nabla K$	$-\vec{V}_2 \cdot \nabla \varphi$	R
SFC - 800	0.0	0.0	2.3	-2.3
800 - 600	0.4	-0.3	1.8	-1.1
600 - 400	1.1	2.6	-0.3	-1.2
400 - 200	1.3	11.5	-6.0	-4.2
200 - 100	-0.1	4.0	0.7	-4.8
SFC - 100	2.7	17.8	-1.5	-13.6

Table 13. Same as Table 12 except for 13-18 April 1970. (from Ward and Smith, 1976)

Layer (mb)	$\frac{\partial K}{\partial t}$	$-\vec{V}_3 \cdot \nabla K$	$-\vec{V}_2 \cdot \nabla \varphi$	R
SFC - 800	0.0	0.2	1.0	-0.9
800 - 600	0.0	0.4	1.7	-1.9
600 - 400	2.1	8.3	-0.6	-5.6
400 - 200	2.1	17.8	-13.1	-10.0
200 - 100	0.4	4.6	-3.0	-3.9
SFC - 100	4.5	31.3	-14.0	-22.3

Table 14. Kinetic energy budget for AMTEX storm vicinity. K is in 10^5 Jm^{-2}. Budget quantities are in Wm^{-2}.

Day/Hr	(GMT) K	$\frac{\partial K}{\partial t}$	$-V_3 \cdot \nabla K$	$-V_2 \cdot \nabla \varphi$	R	Layer (mbs)
13/0000	53.1	-9.1	-42.1	12.9	19.7	Upper(100-500)
	2.4	2.5	-0.8	2.5	0.8	Lower(500-SFC)
Total	55.5	-6.6	-42.9	15.4	20.5	
13/1200	49.4	-7.4	-29.4	26.1	-4.5	Upper
	2.3	1.5	-1.1	0.9	1.7	Lower
Total	51.7	-6.3	-30.5	27.0	-2.8	
14/0000	46.2	3.0	-26.4	25.8	3.6	Upper
	3.7	2.5	-1.9	2.9	0.6	Lower
Total	49.9	5.5	-28.3	28.7	4.2	
14/1200	49.7	2.0	-21.2	24.3	-1.1	Upper
	5.6	1.0	-3.4	3.7	0.7	Lower
Total	55.3	3.0	-24.6	28.0	-0.4	
15/0000	47.2	-7.9	3.8	11.8	-23.5	Upper
	5.8	0.7	-2.0	2.9	-0.2	Lower
Total	53.0	-7.2	1.8	14.7	-23.7	
15/1200	39.8	-18.3	13.3	3.0	-34.6	Upper
	5.8	0.1	-1.0	2.8	-1.7	Lower
Total	45.6	-18.2	12.3	5.8	-36.3	

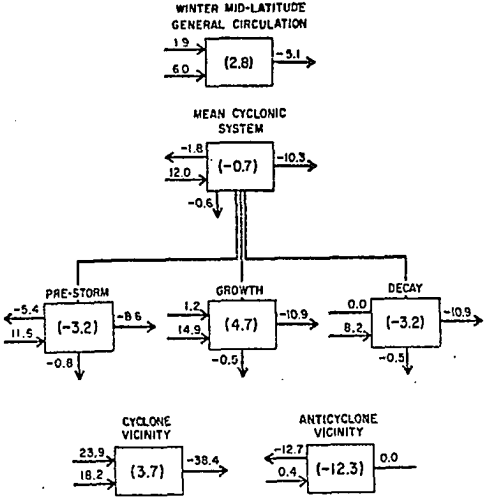

Fig. 1. Summary of kinetic energy budgets ($W \cdot m^{-2}$) for general circulation and various synoptic systems. The upper left arrow is horizontal transport, lower left is generation, right is dissipation, bottom is vertical transport, and the interior value is net time change. Arrows pointing outward (negative values) correspond to processes decreasing the kinetic energy. (from Smith, 1973)

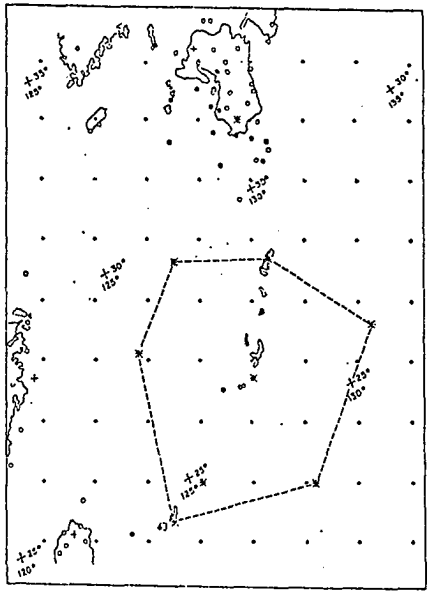

Fig. 2. The analysis grid in vicinity of the AMTEX with observation sites. o surface (AMTEX). * RAOB (AMTEX). o surface (regular synoptic). + RAOB (regular synoptic).

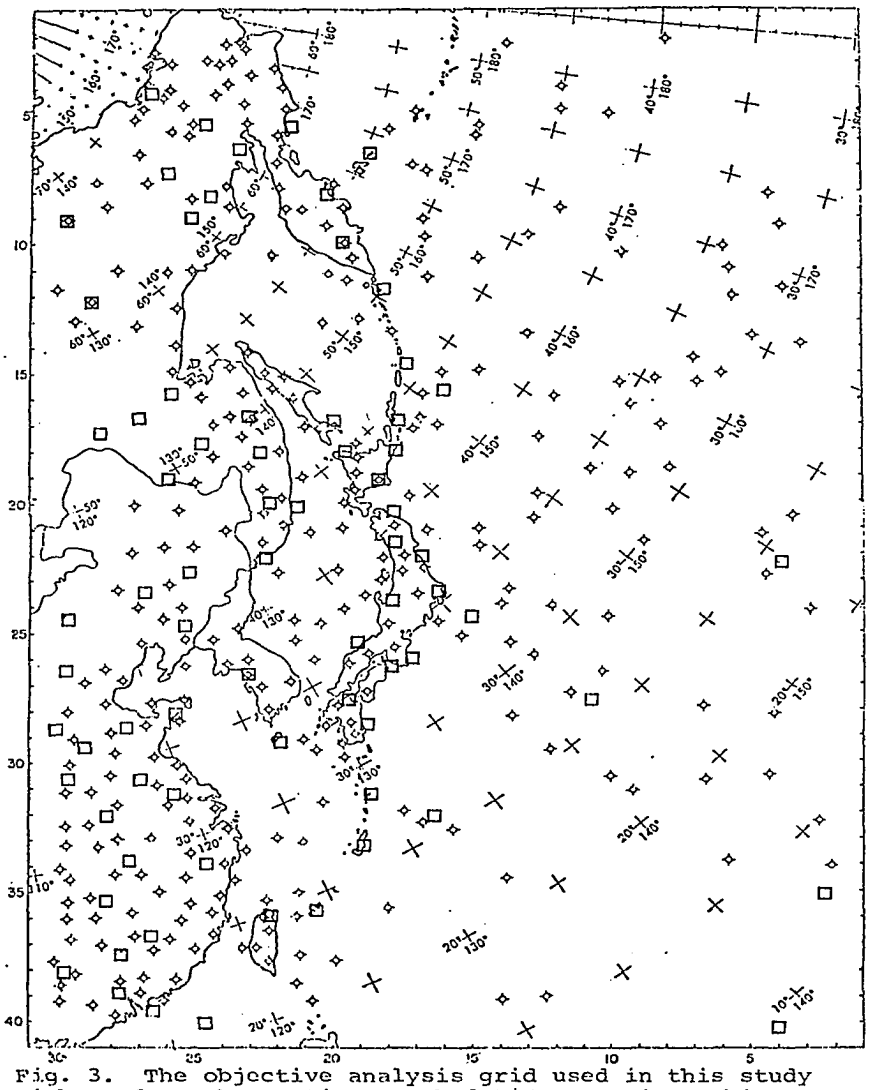

Fig. 3. The objective analysis grid used in this study with surface observations marked "✧", transient ship reports marked "✧", and upper air observations given by "□". The transient ship reports which are indicated on the map are representative of the position and frequency per analysis period. Not all surface observations sites are marked due to the high density in some areas.

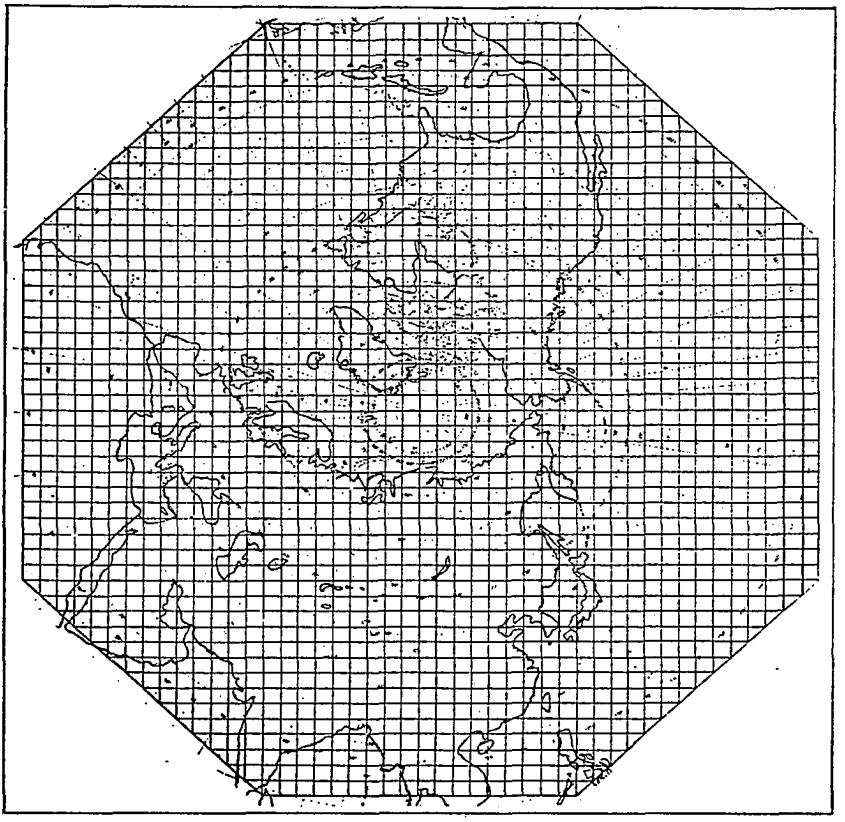

Fig. 4. The standard polar stereographic AFGWC analysis grid. The mesh size is 381 km at the standard latitude, 60°N.

Level in mbs		Parameters Analyzed
10 -		Z,T,U/V
30 -		Z,T,U/V
50 -		Z,T,U/V
70 -		Z,T,U/V
100 -		Z,T,U/V
150 -	ω	Z,T,U/V
200 -		Z,T,U/V
250 -	ω	Z,T,U/V
300 -		Z,T,U/V
400 -	ω	Z,T,U/V
500 -		Z,T,U/V,Td
600 -	ω	
700 -		Z,T,U/V,Td
775 -	ω	
850 -		Z,T,U/V,Td
925 -	ω	
1000 -		Z,T,U/V,Td

ω, vertical velocity
Z, height
T, temperature
Td, dew-point depression
U/V, wind components

Fig. 5. Vertical resolution of the AFGWC objective analysis model with symbols indicating where parameters are analyzed.

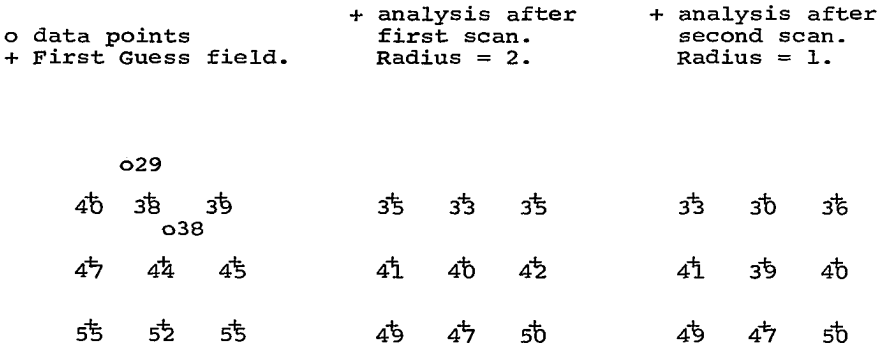

Fig. 6. Example of how a data point might alter a first guess field when a Cressman type of analysis is applied on successive scans. Radius of influence of the data is changed with each successive scan.

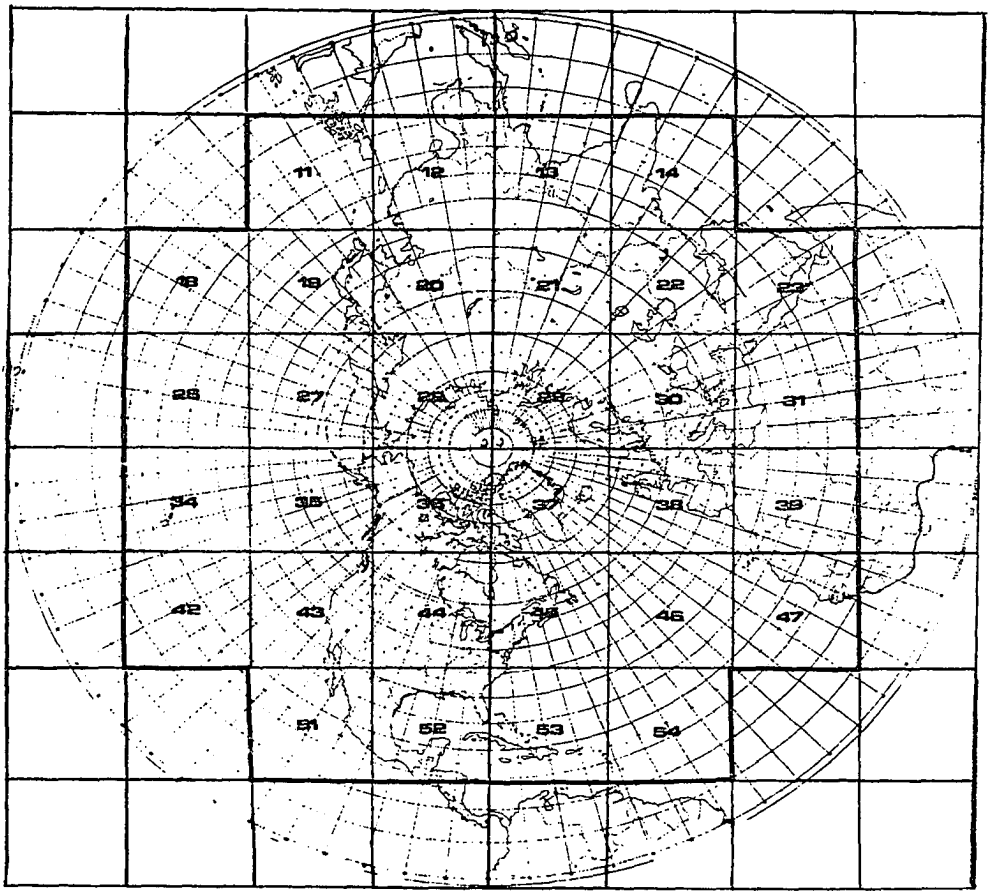

Fig. 7. Outline of the gridded cloud analyses boxes. Grid spacing is one-eighth of the standard AFGWC mesh. See Fig. 4.

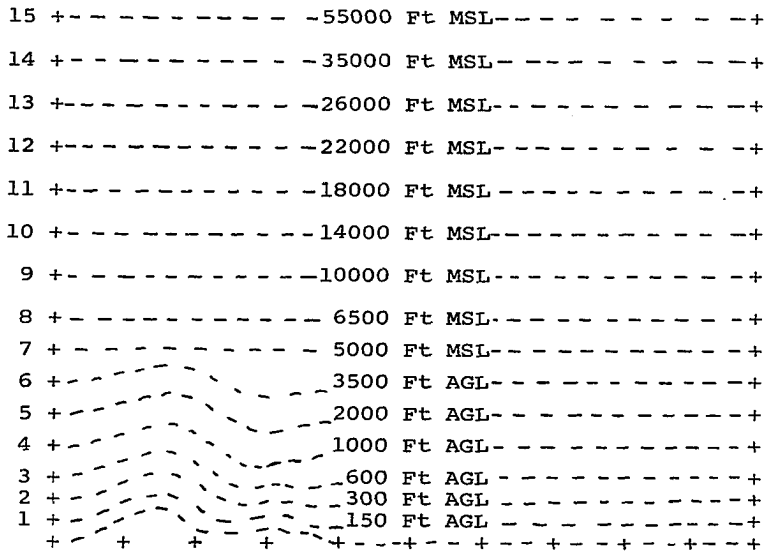

Fig. 8. Spatial resolution of the three dimensional cloud analysis program. Horizontal resolution is 48 km.

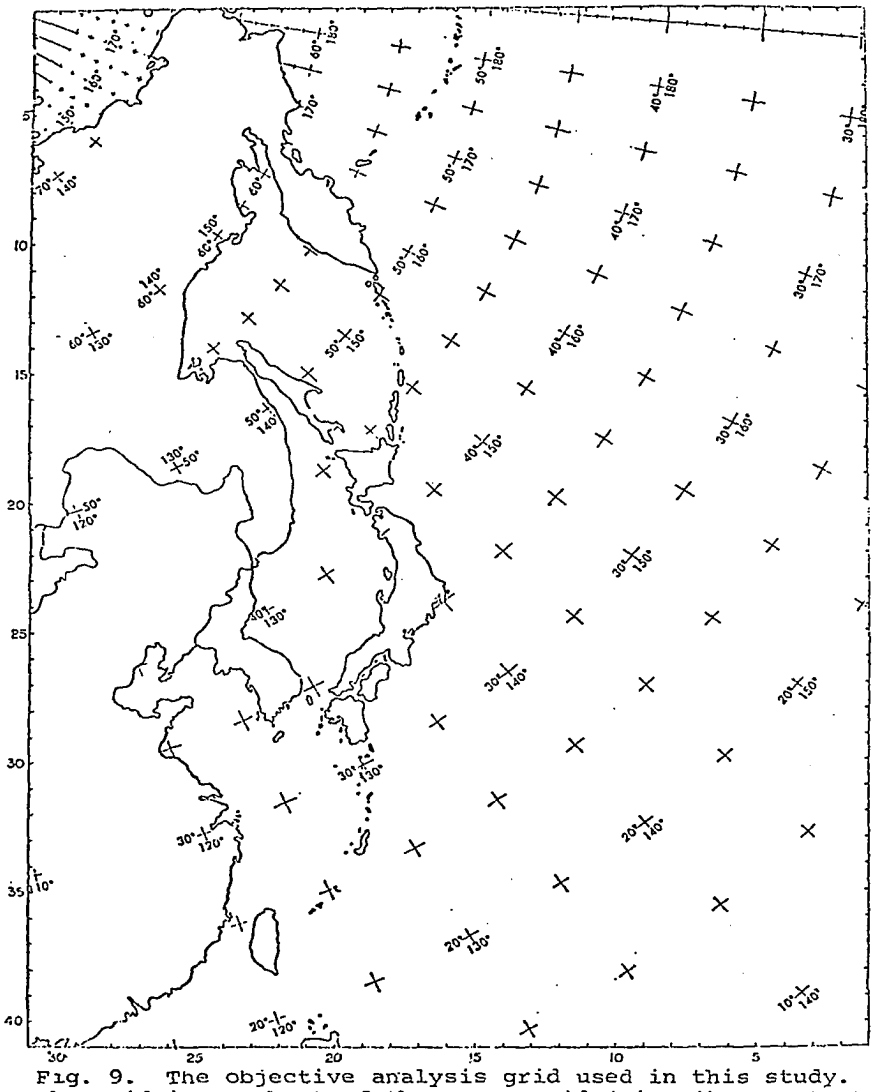

Fig. 9. The objective analysis grid used in this study. The grid is a subset of the AFGWC grid (Fig. 4) except at half-mesh (190.5 km) grid spacing.

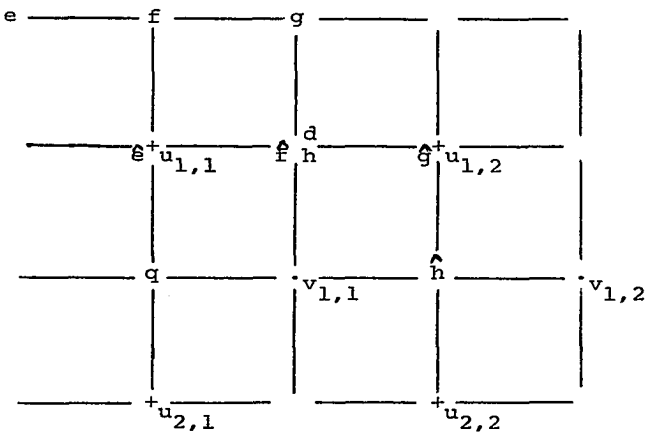

Fig. 10. The relative location of the wind components (u and v), the gradients in all directions (e, $\hat{e}$, f, $\hat{f}$, g, $\hat{g}$, h, and $\hat{h}$), the vorticity (q), and the divergence (d) terms on the staggered grid used for solving Eq. (4.6). See Table 8. Variables are on their respective grid point (1,1) unless otherwise indicated.

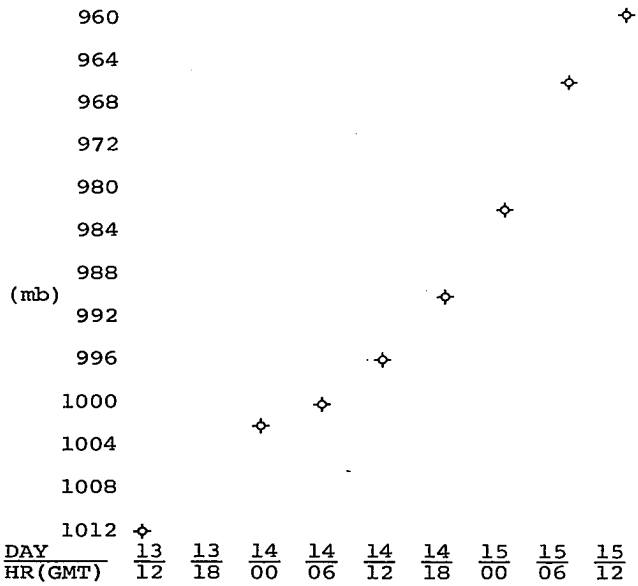

Fig. 11. Central low pressure of the cyclone which developed in the East China Sea during the AMTEX 1975 plotted every six hours starting at 1200 GMT, 13 February 1975.

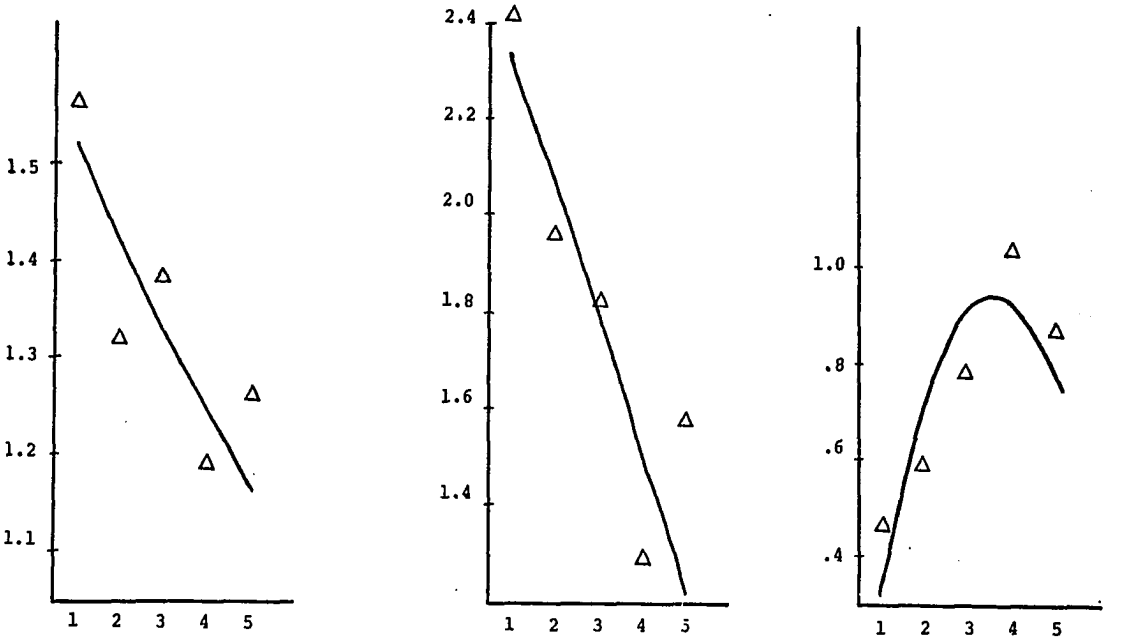

Fig. 12. Examples of second degree curve fitting to kinetic energy of three different grid points, which are located along the storm's path. Units of kinetic energy are in 10^5 J m^{-2}.

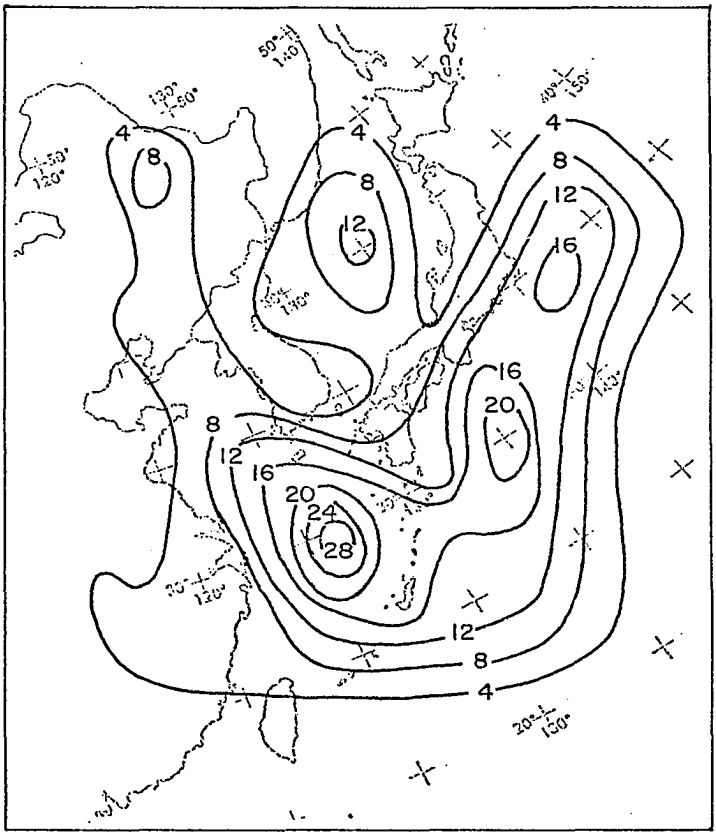

Fig. 13. Frequency of cyclone formation. The value of any isoline at any point represents the number of cyclones that formed within a radius of 2.5 latitude degrees from that point in the months October through April, 1932-37. (Trewartha, 1961)

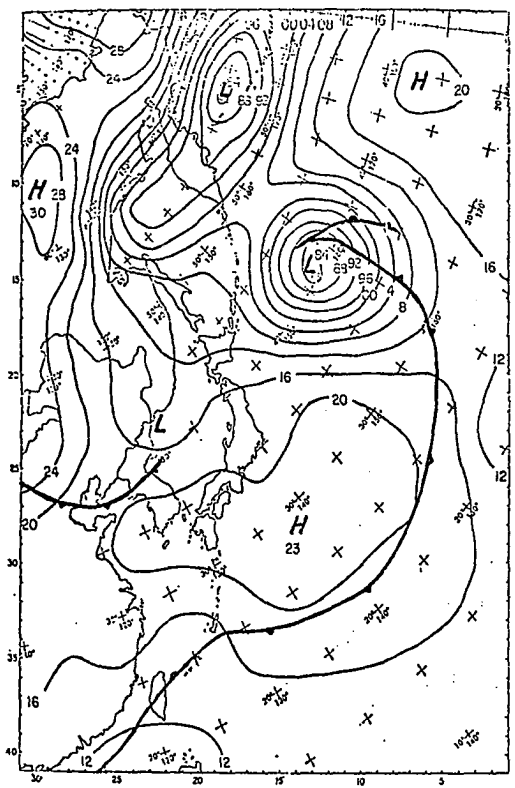

Fig. 14. Sea level surface analysis with surface fronts, 1200 GMT, 13 February 1975. Units of isobars are in millibars.

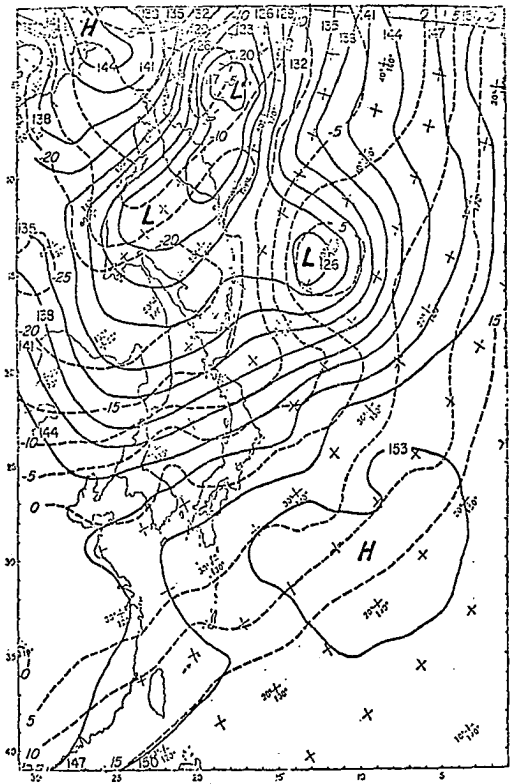

Fig. 15. 850-mb height analysis (solid curves in decameters) and temperature analysis (dashed curves in °C) for 1200 GMT, 13 February 1975.

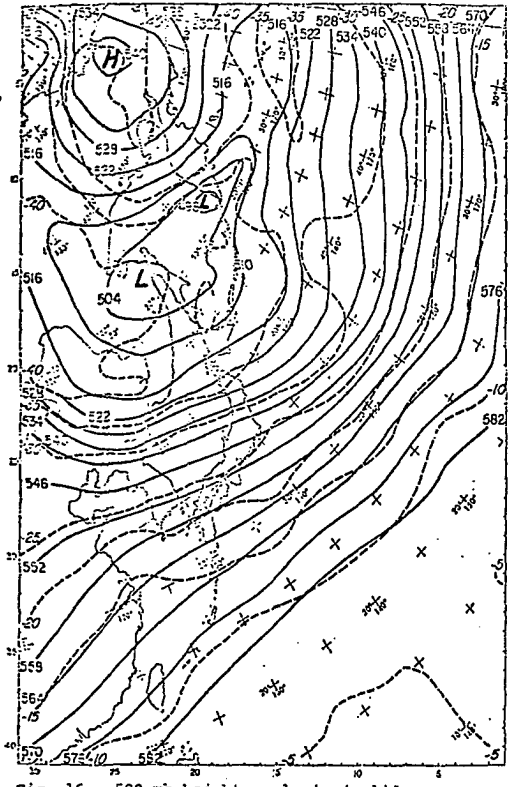

Fig. 16. 500-mb height analysis (solid curves in decameters) and temperature analysis (dashed curves in °C) for 1200 GMT, 13 February 1975.

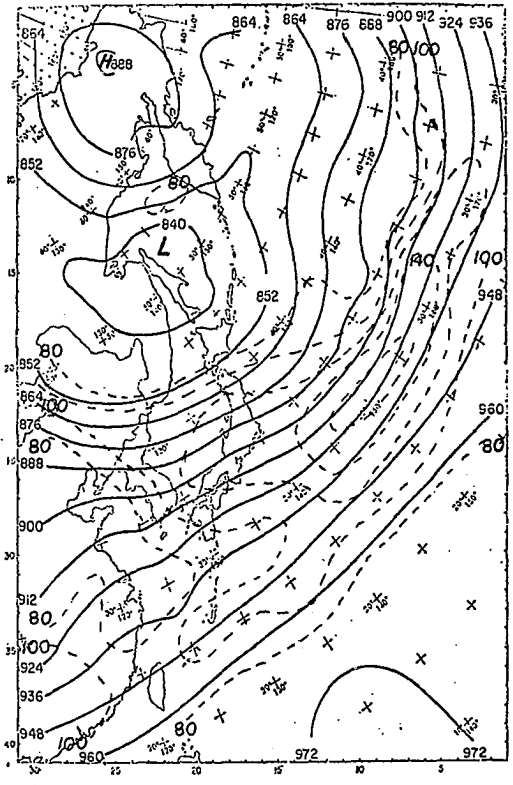

Fig. 17. 300-mb height analysis (solid curves in decameters) and isotach analysis (dashed curves in knots) for 1200 GMT, 13 February 1975.

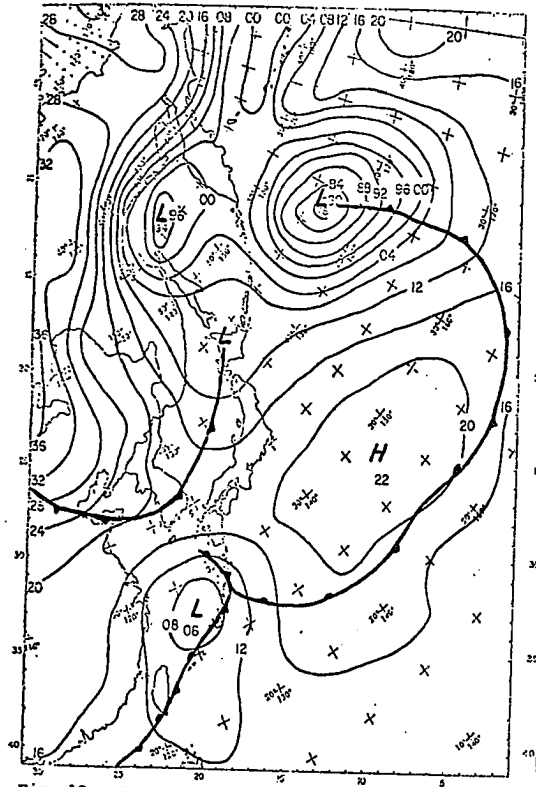

Fig. 18. Same as Fig. 14 except for 0000 GMT, 14 February 1975. (Surface)

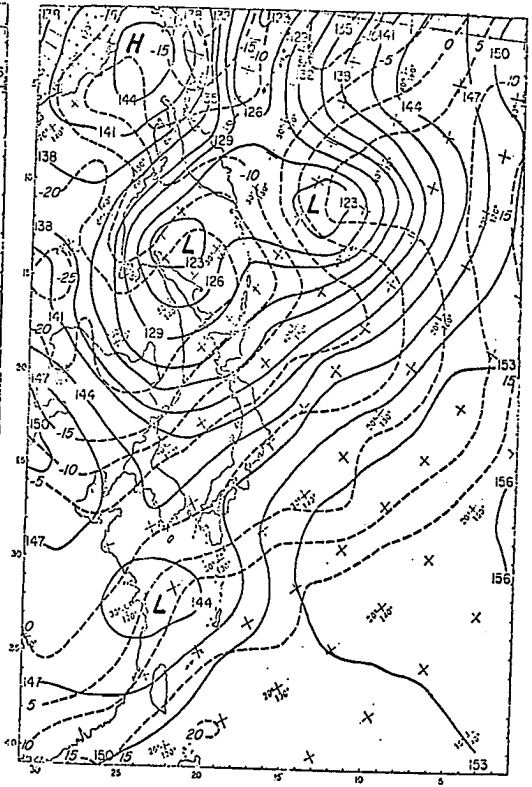

Fig. 19. Same as Fig. 15 except for 0000 GMT, 14 February 1975. (850-mb)

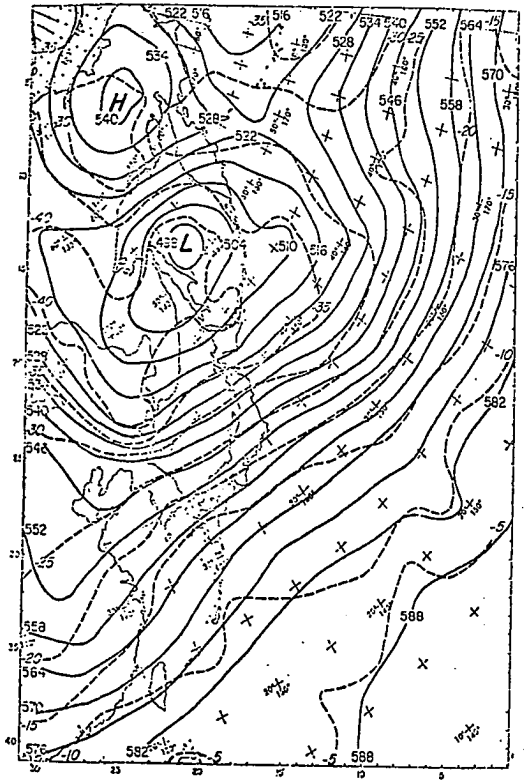

Fig. 20. Same as Fig. 16 except for 0000 GMT, 14 February 1975. (500-mb)

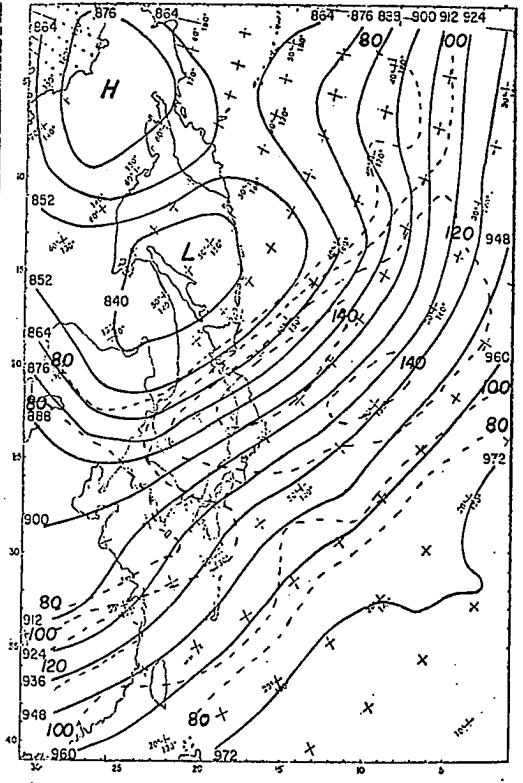

Fig. 21. Same as Fig. 17 except for 0000 GMT, 14 February 1975. (300-mb)

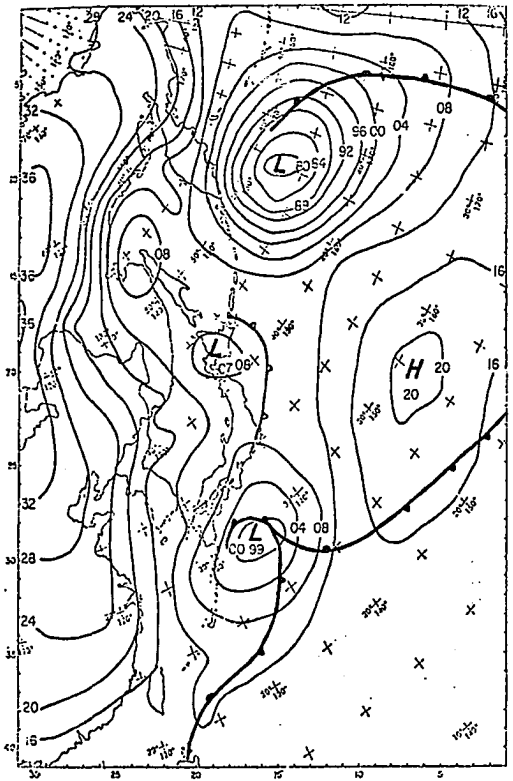

Fig. 22. Same as Fig. 14 except for 1200 GMT, 14 February 1975. (Surface)

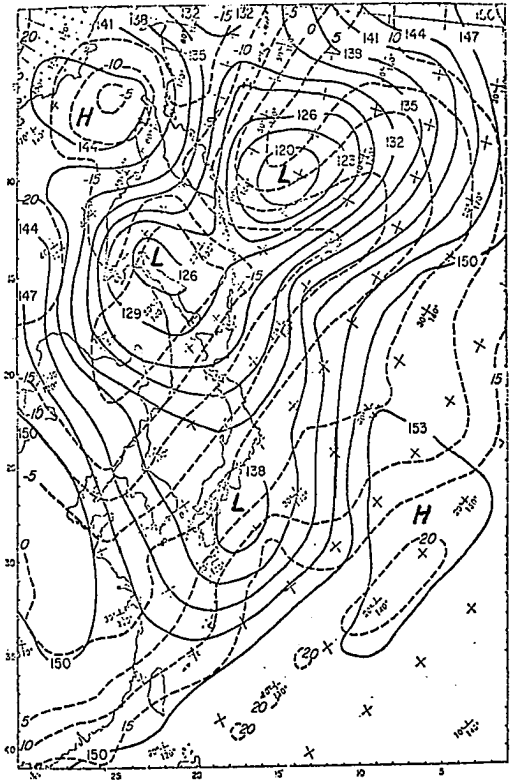

Fig. 23. Same as Fig. 15 except for 1200 GMT, 14 February 1975. (850-mb)

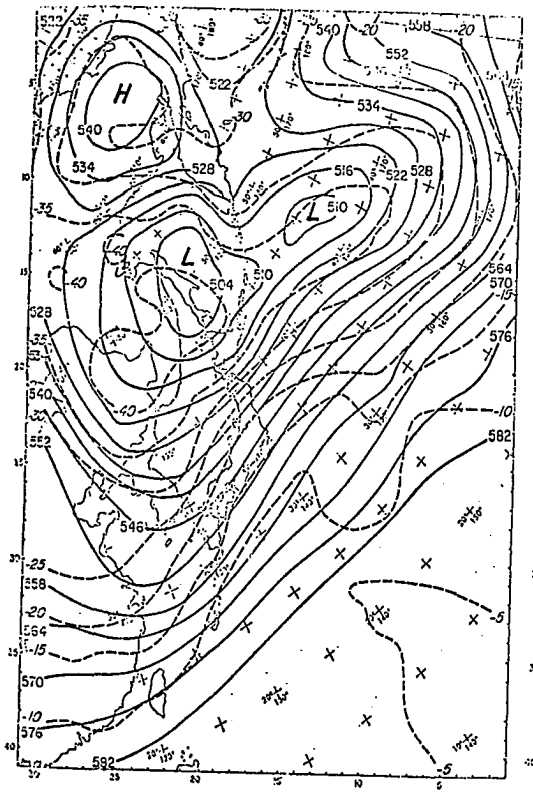

Fig. 24. Same as Fig. 16 except for 1200 GMT, 14 February 1975. (500-mb)

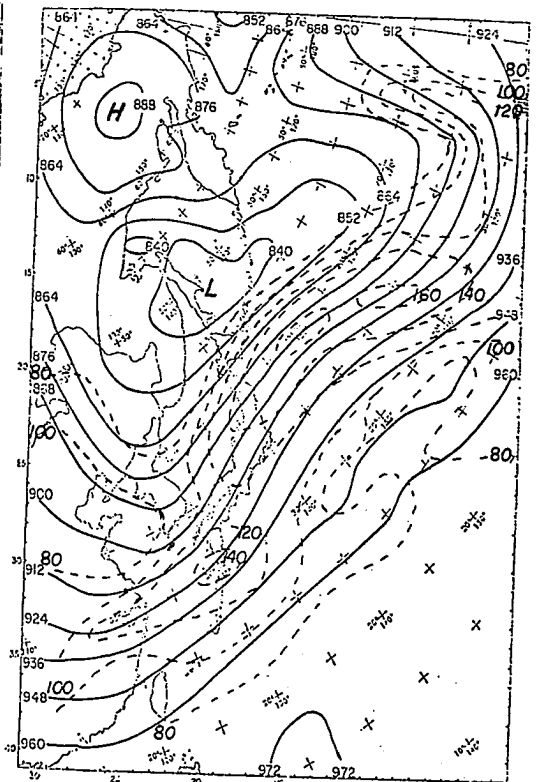

Fig. 25. Same as Fig. 17 except for 1200 GMT, 14 February 1975. (300-mb)

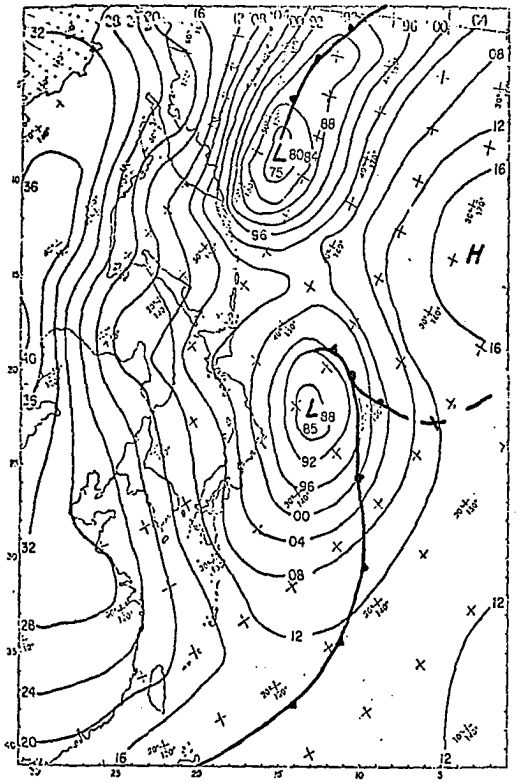

Fig. 26. Same as Fig. 14 except for 0000 GMT, 15 February 1975. (Surface)

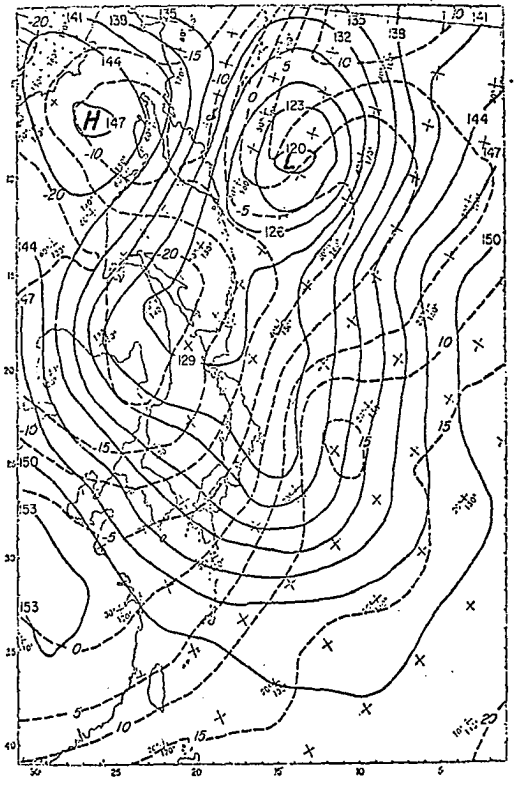

Fig. 27. Same as Fig. 15 except for 0000 GMT, 15 February 1975. (850-mb)

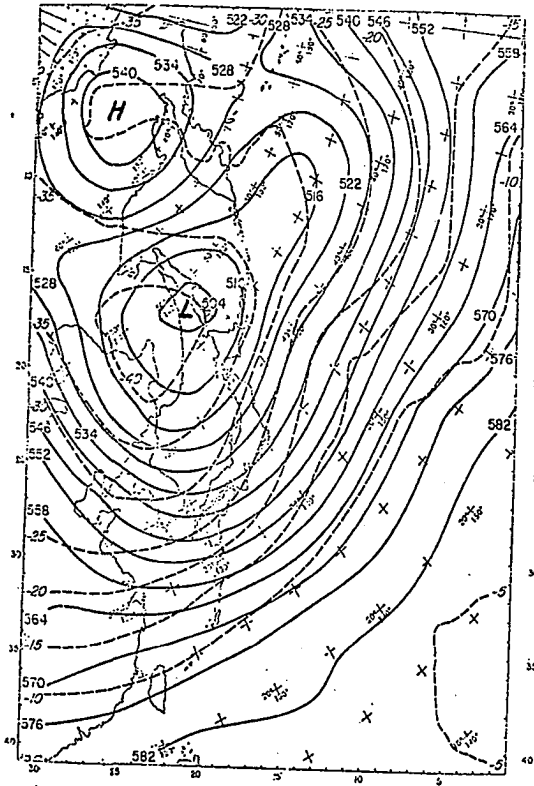

Fig. 28. Same as Fig. 16 except for 0000 GMT, 15 February 1975. (500-mb)

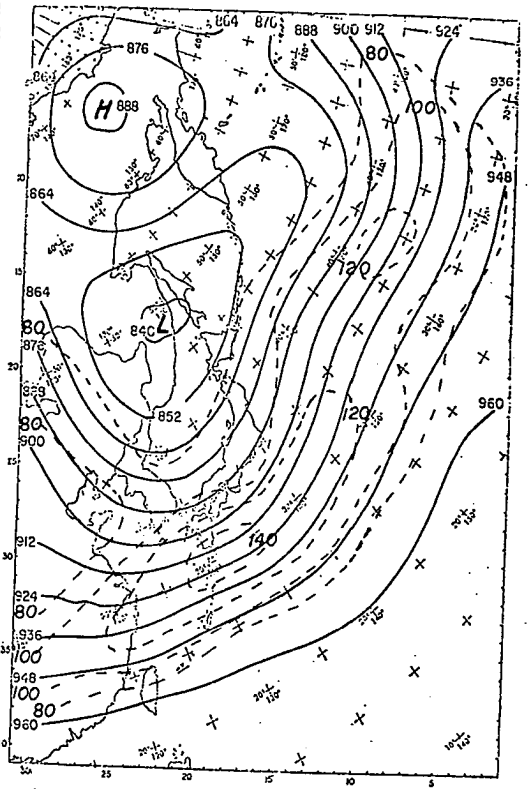

Fig. 29. Same as Fig. 17 except for 0000 GMT, 15 February 1975. (300-mb)

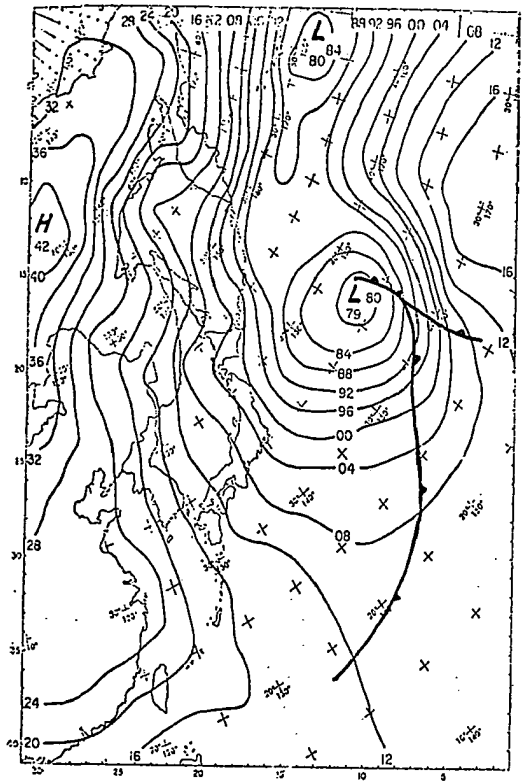

Fig. 30. Same as Fig. 14 except for 1200 GMT, 15 February 1975. (Surface)

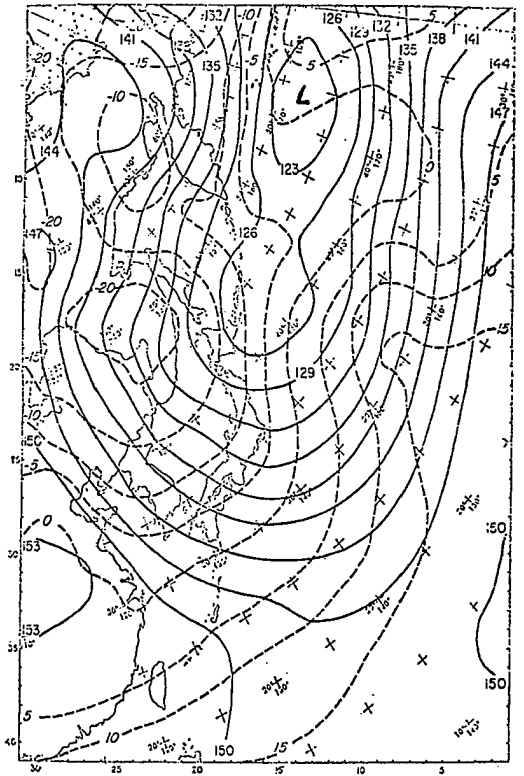

Fig. 31. Same as Fig. 15 except for 1200 GMT, 15 February 1975. (850-mb)

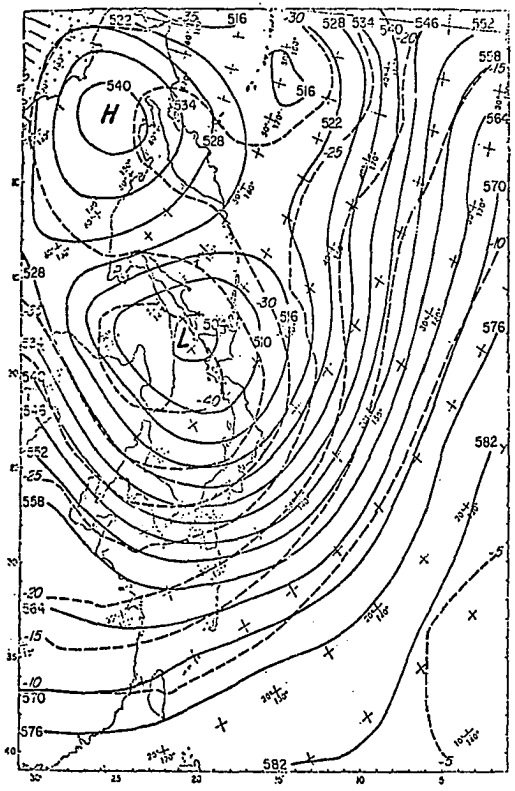

Fig. 32. Same as Fig. 16 except for 1200 GMT, 15 February 1975. (500-mb)

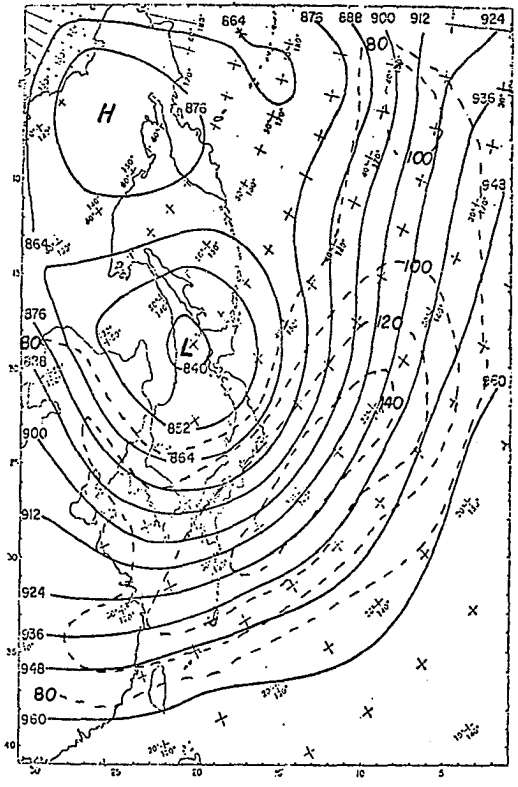

Fig. 33. Same as Fig. 17 except for 1200 GMT, 15 February 1975. (300-mb)

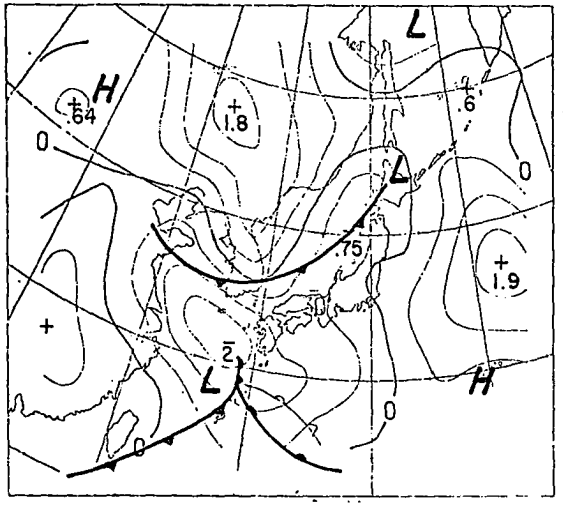

Fig. 34. The JMA 700-mb vertical motions for 0000 GMT, 14 February 1975 with surface pressure centers and surface fronts. Vertical motion centers are in μb S^{-1}, and contours are approximately .55 μb S^{-1}.

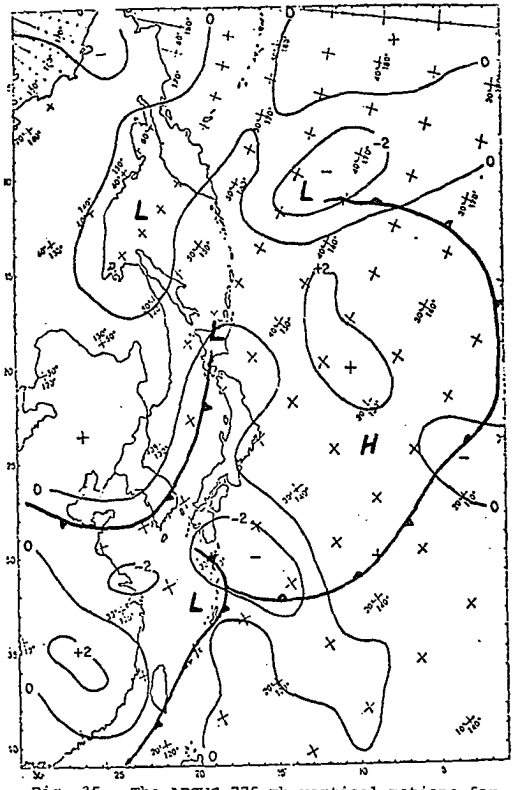

Fig. 35. The AFGWC 775-mb vertical motions for 0000 GMT, 14 February 1975 with surface pressure conters and surface fronts. Vertical motion contours are in μb S^{-1}.

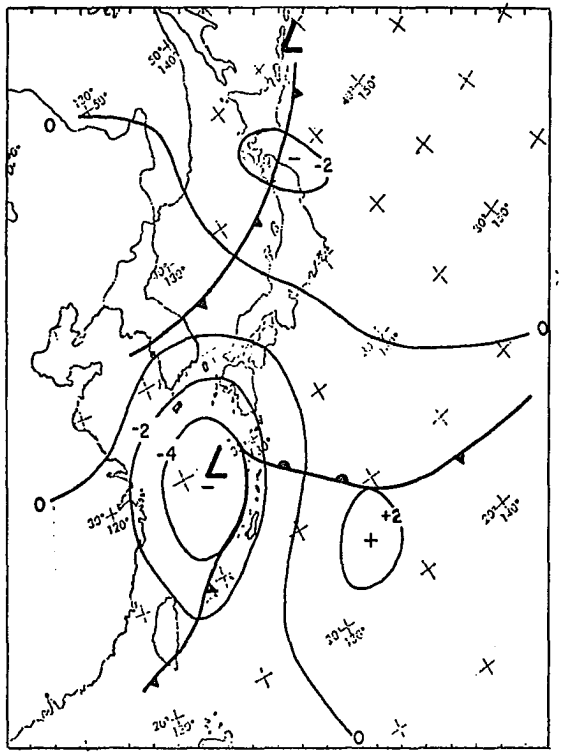

Fig. 36. 775-mb vertical motions computed kinematically from subjectively analyzed horizontal winds for 0000 GMT, 14 February 1975 with surface pressure centers and surface fronts. Vertical motion contours are in μb S^{-1}.

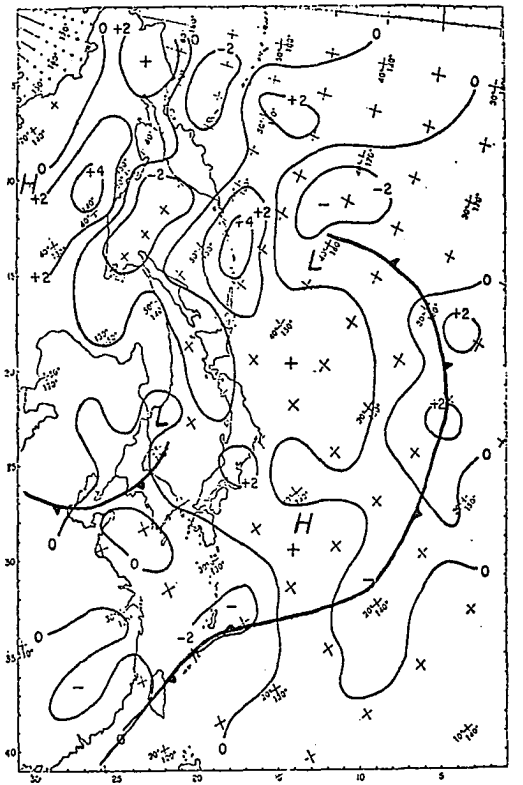

Fig. 37. The PCT 775-mb vertical motions for 1200 GMT, 13 February 1975 with surface pressure centers and surface fronts. Vertical motion contours are in μb S^{-1}.

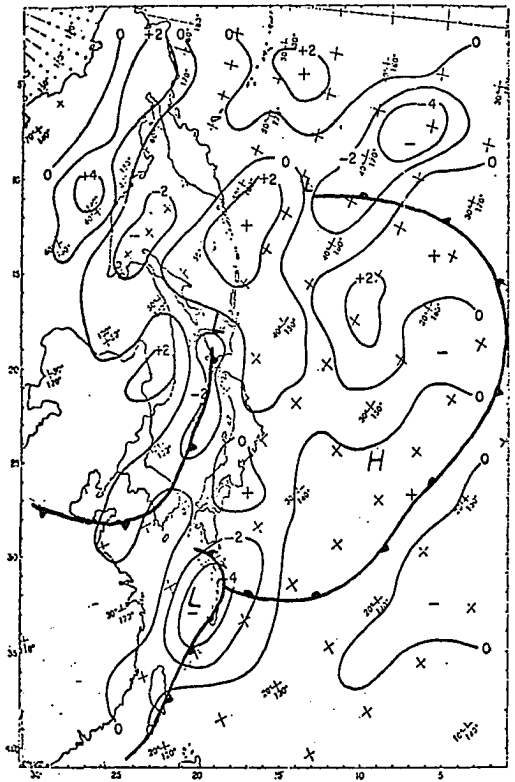

Fig. 38. Same as Fig. 37 except for 0000 GMT, 14 February 1975.

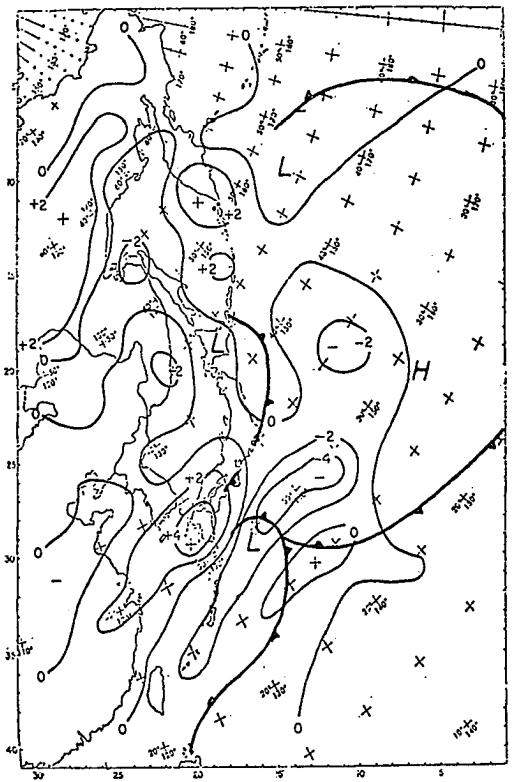

Fig. 39. Same as Fig. 37 except for 1200 GMT, 14 February 1975.

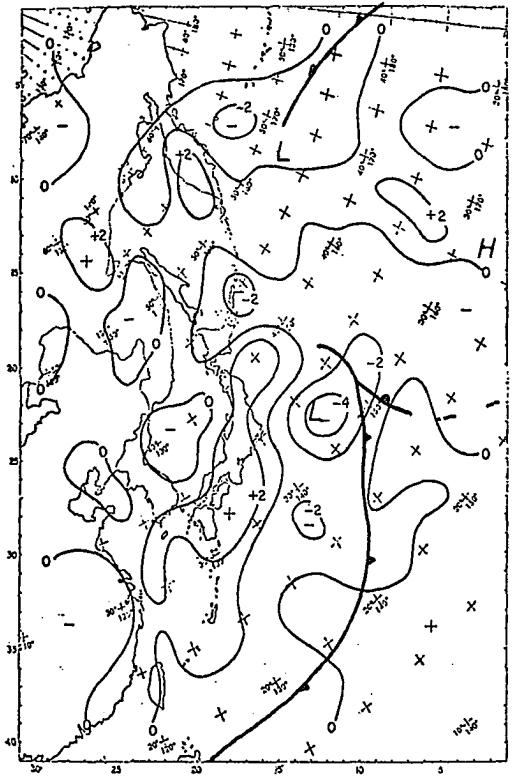

Fig. 40. Same as Fig. 37 except for 0000 GMT, 15 February 1975.

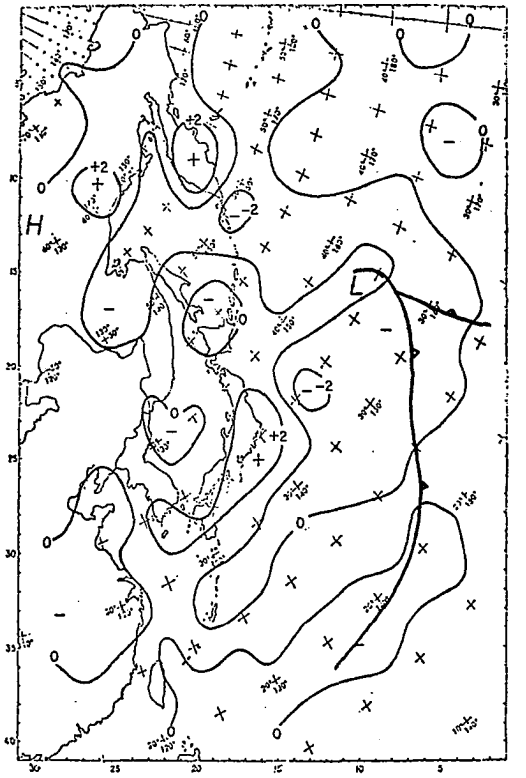

Fig. 41. Same as Fig. 37 except for 1200 GMT, 15 February 1975.

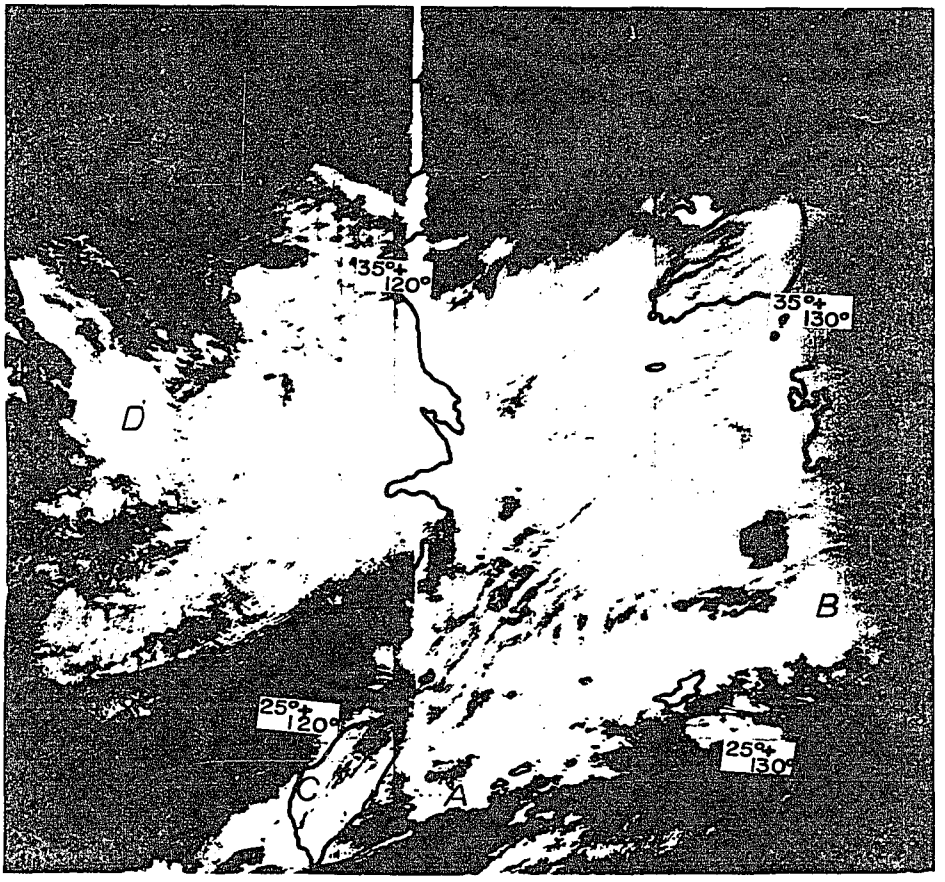

Fig. 42. The DMSP (Defense Meteorological Satellite Program) satellite photograph valid 0332 GMT, 14 February 1975.

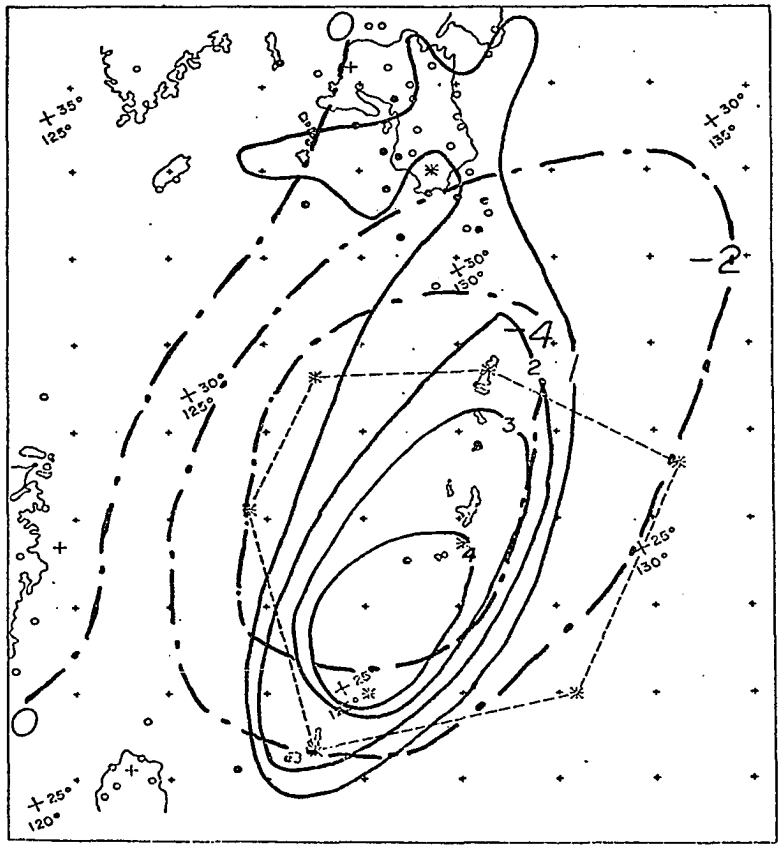

Fig. 43. Precipitation analysis (solid curves in cm of precipitation) for the period from 0000 GMT, 14 February to 0600 GMT, 14 February 1975. Vertical velocities (broken curves in $\mu b\ s^{-1}$) are taken from the PCT analysis for 0000 GMT, 14 February 1975.

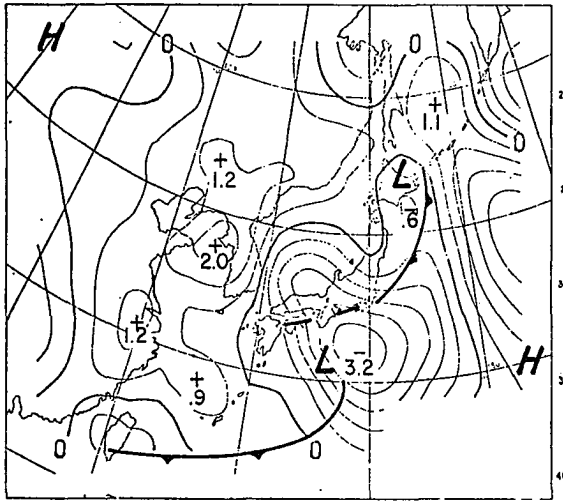

Fig. 44. Same as Fig. 34. (JMA 700-mb ω_s) except for 1200 GMT, 14 February 1975.

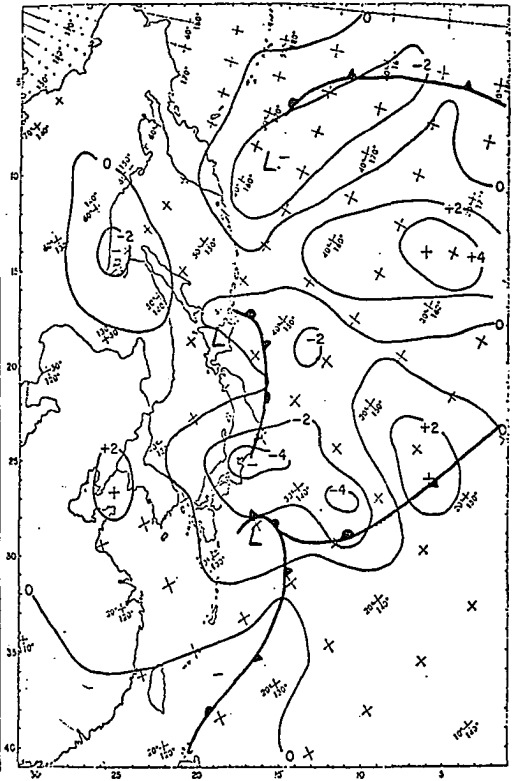

Fig. 45. Same as Fig. 35. (AFGWC 775-mb ω_s) except for 1200 GMT, 14 February 1975.

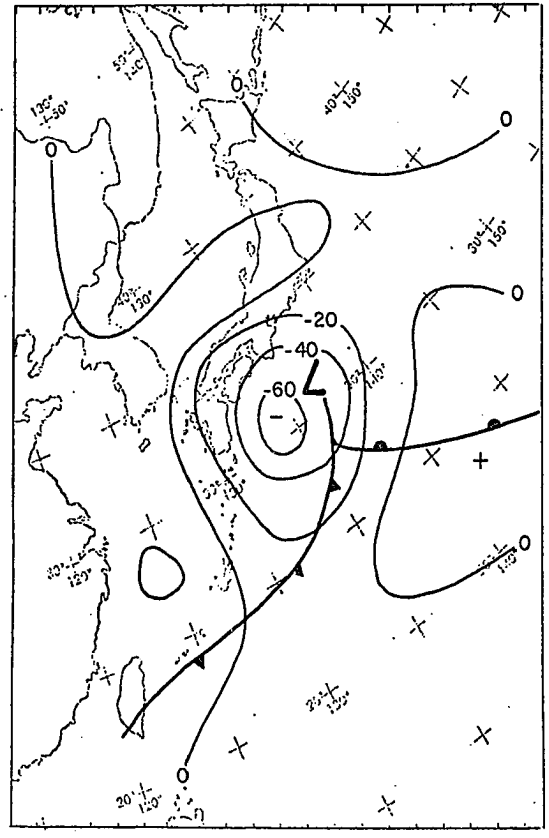

Fig. 46. Same as Fig. 36. (Subjective 775-mb ω_s) except for 1200 GMT, 14 February 1975.

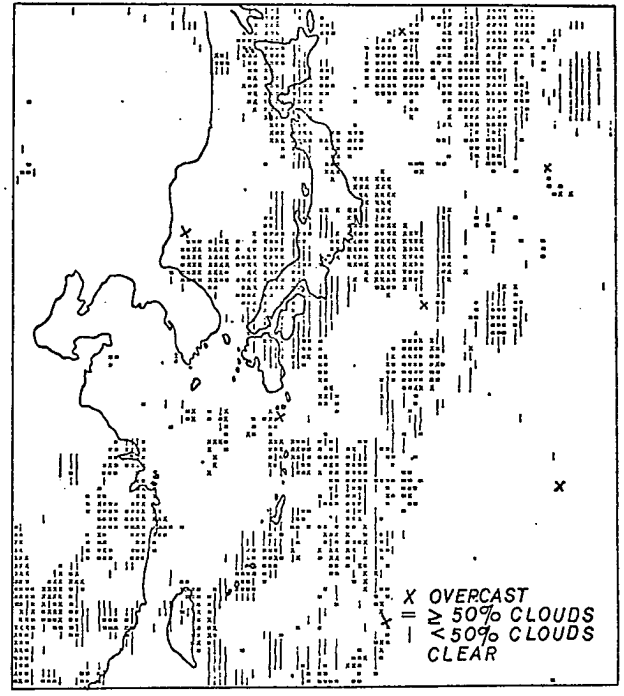

Fig. 47. Cloud analysis for the 800- to 700-mb layer from AFGWC's 3-D Neph analysis model. Valid 1200 GMT, 14 February 1975.

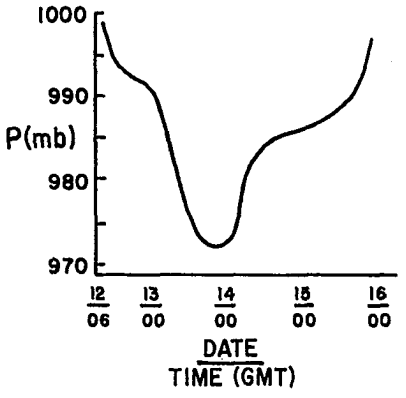

Fig. 48. Central pressure of major cyclone in millibars as a function of time in six hour increments. (from Smith, 1973).

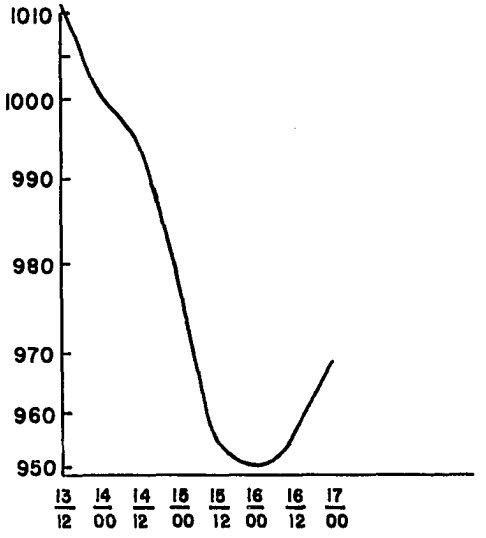

Fig. 49. Same as 48 except for AMTEX storm.

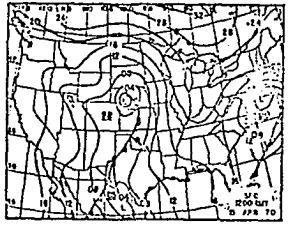

Fig. 50. Sea level analysis for 1200 GMT, 15 April 1970. Isobars are in 4 mb increments.

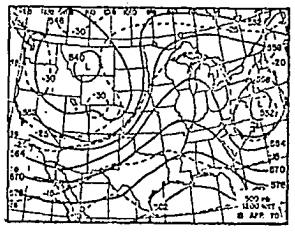

Fig. 51. The 500 mb height and temperature analysis for 1200 GMT, 15 April 1970. Height contours are in 6 dam intervals (solid). Isotherms are in 5°C increments (dashed).

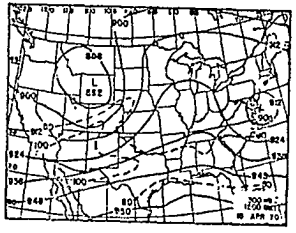

Fig. 52. The 300 mb height and isotach analysis for 1200 GMT, 15 April 1970. Height contours are in 12 dam intervals (solid). Isotachs are in 20 kt increments (dashed).

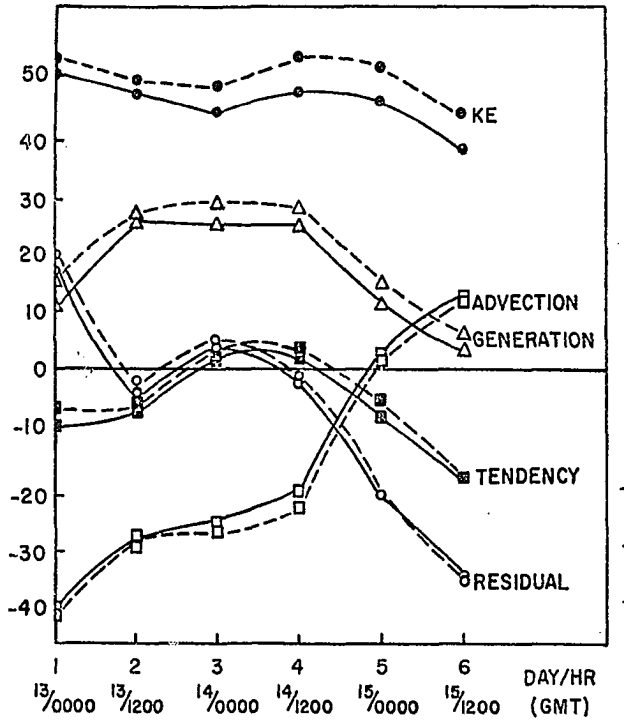

Fig. 53. The kinetic energy budget terms for the AMTEX storm vicinity as a function of time. Units are Wm^{-2} for budget terms and 10^5 Jm^{-2} for kinetic energy. (---Surface to 100 mb. ——500 mb to 100 mb)

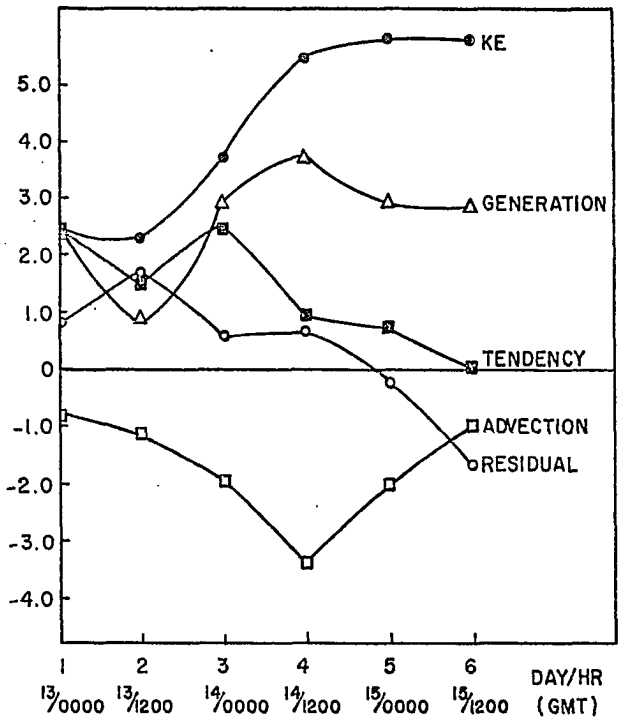

Fig. 54. The kinetic energy budget terms for the AMTEX storm vicinity as a function of time. Units are the same as Fig. 53. (——Surface to 500 mb)

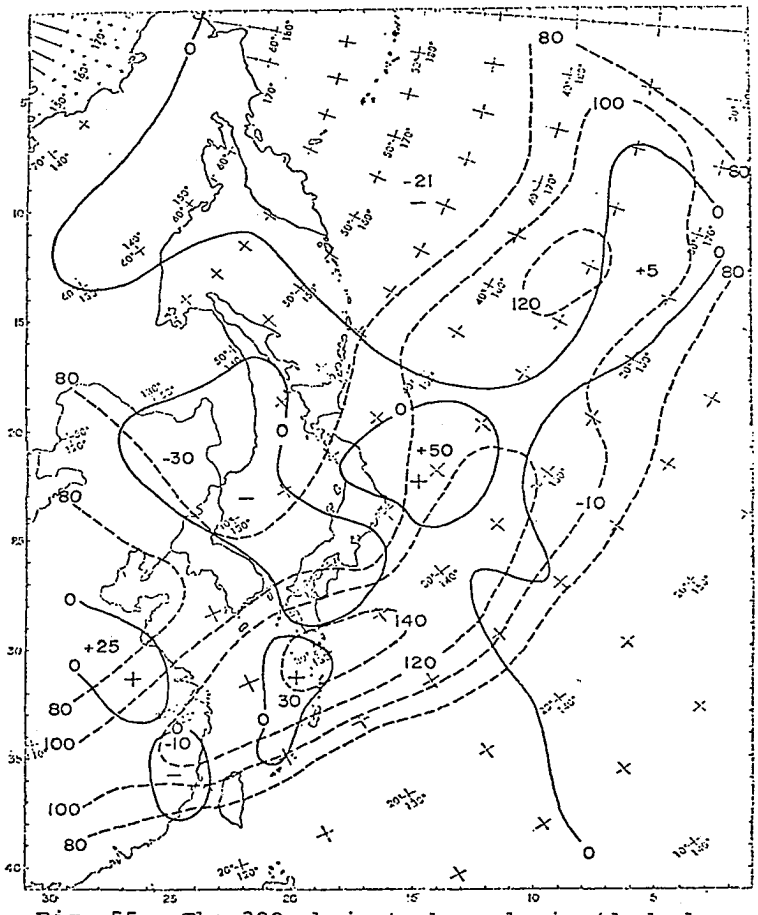

Fig. 55. The 300-mb isotach analysis (dashed curves in knots) and the generation of kinetic energy for a 100-mb layer centered at 300 mb (solid lines with central values given in Wm^{-2}) for 0000 GMT, 15 February 1975.

UMI

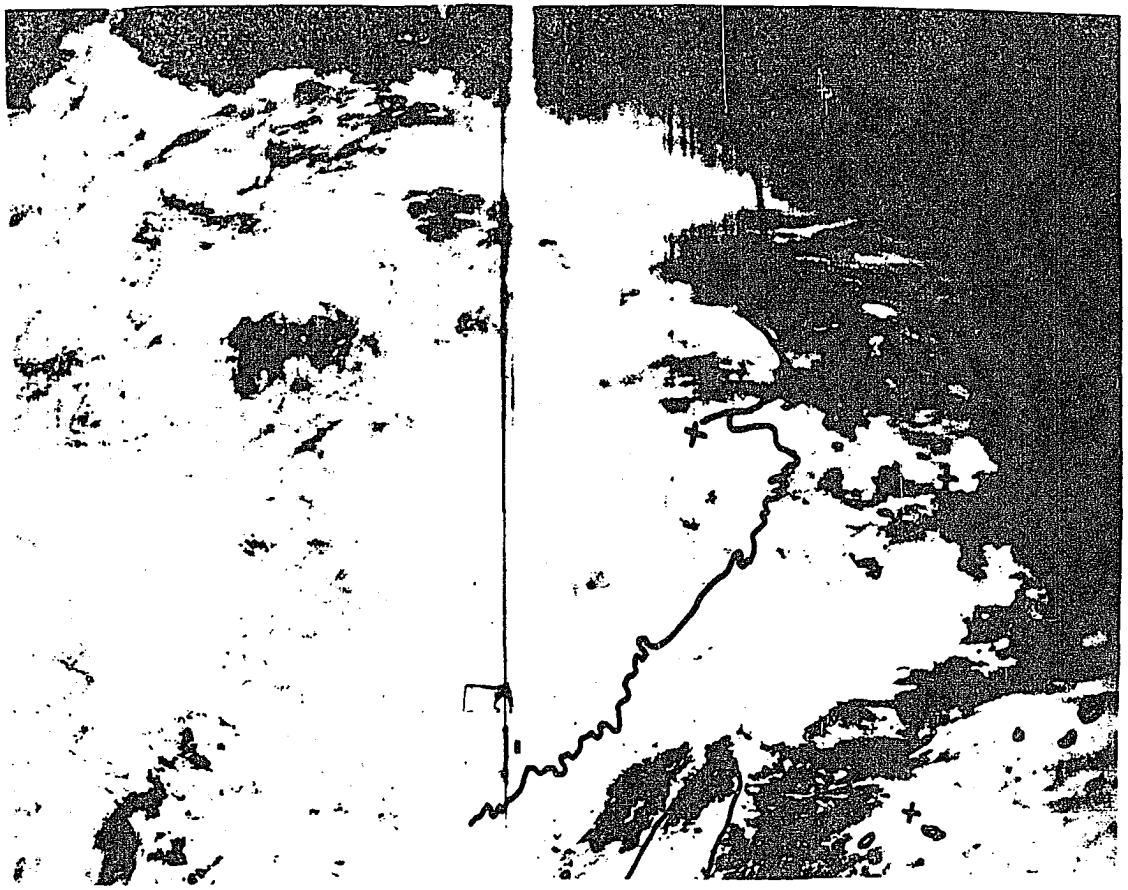

Fig. 56. The DMSP satellite photograph valid 0351 GMT, 13 February 1975.

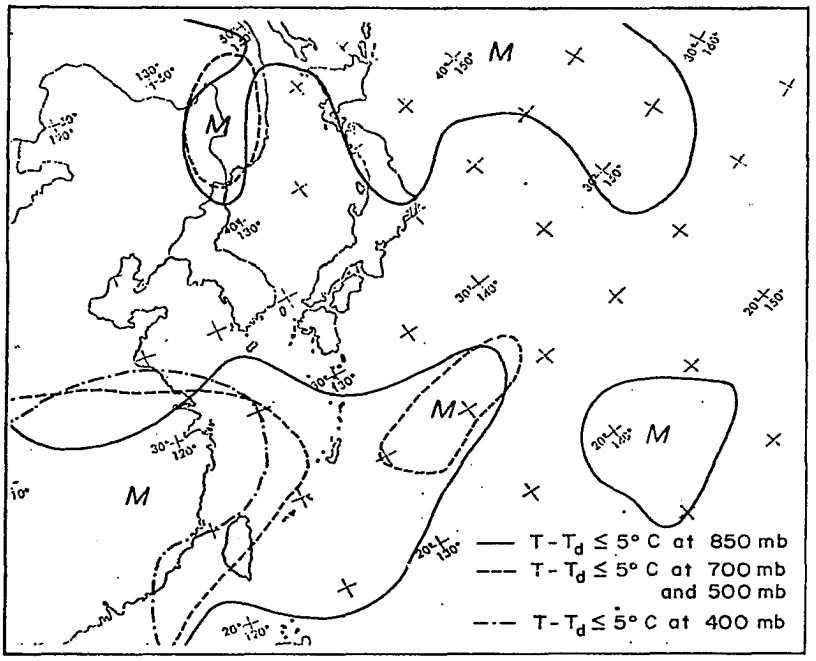

Fig. 57. Temperature - dew point spread analysis for 0000 GMT, 13 February 1975. "M"'s indicate areas of moisture, i.e., ≤ 5°C spread.

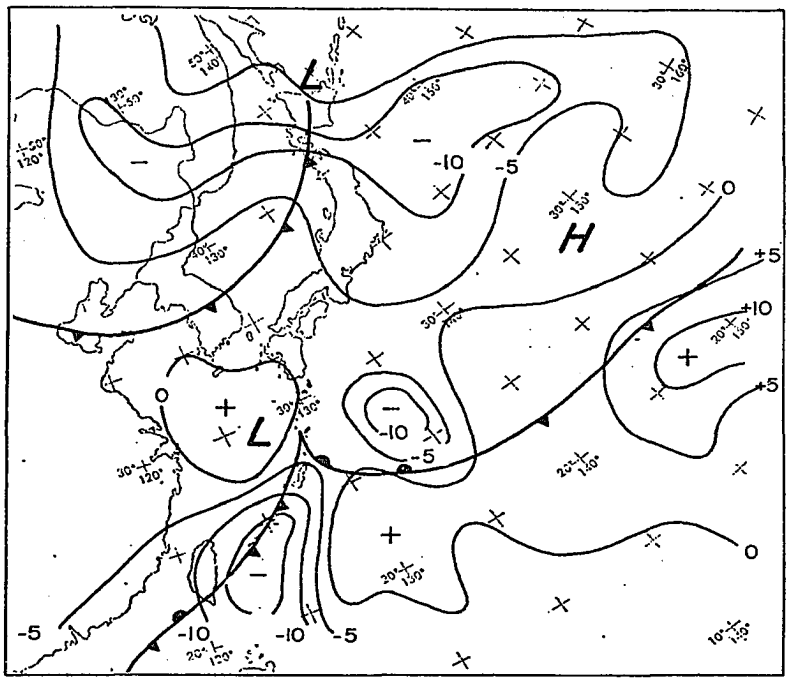

Fig. 58. Vertical change in kinetic energy with respect to pressure $(\frac{\partial K}{\partial p})$ from surface to 850 mb. Valid 0000 GMT, 14 February 1975. Units are $M^2\ s^{-2}\ mb^{-1} \times 10$.

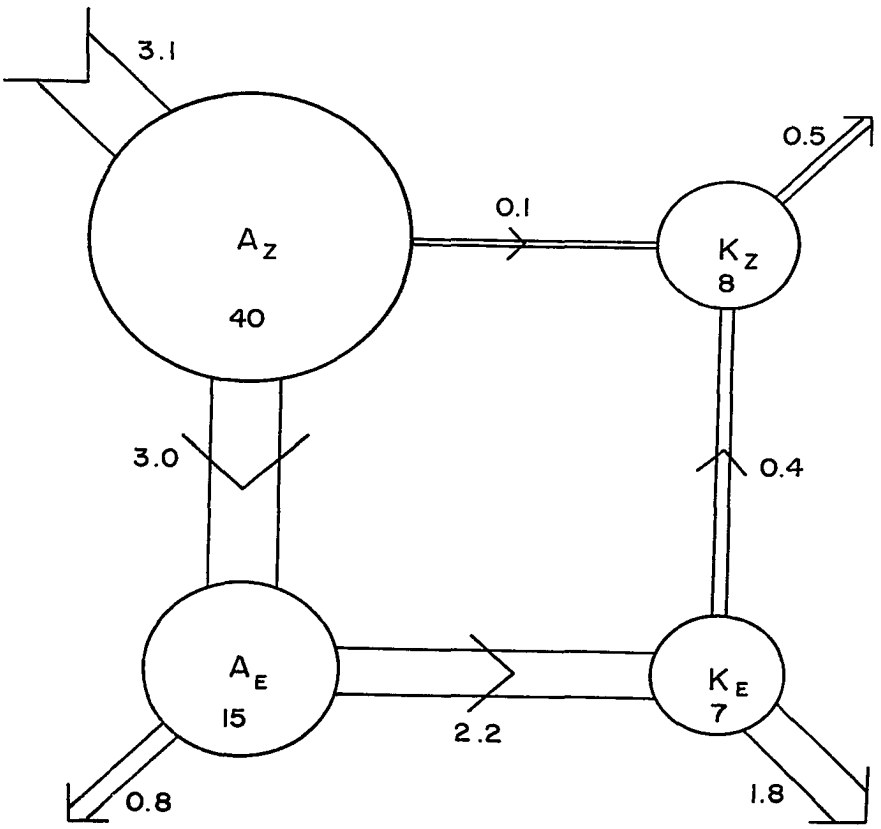

Fig. 59. The energy cycle of the atmosphere as estimated by Oort (1964a). Values of energy are in units of 10^5 joules m^{-2}, and values of generation, conversion and dissipation are in watts m^{-2}. The estimated value of conversion from A_Z to K_Z is smaller than the probable error of the estimate. (from Lorenz, 1967)

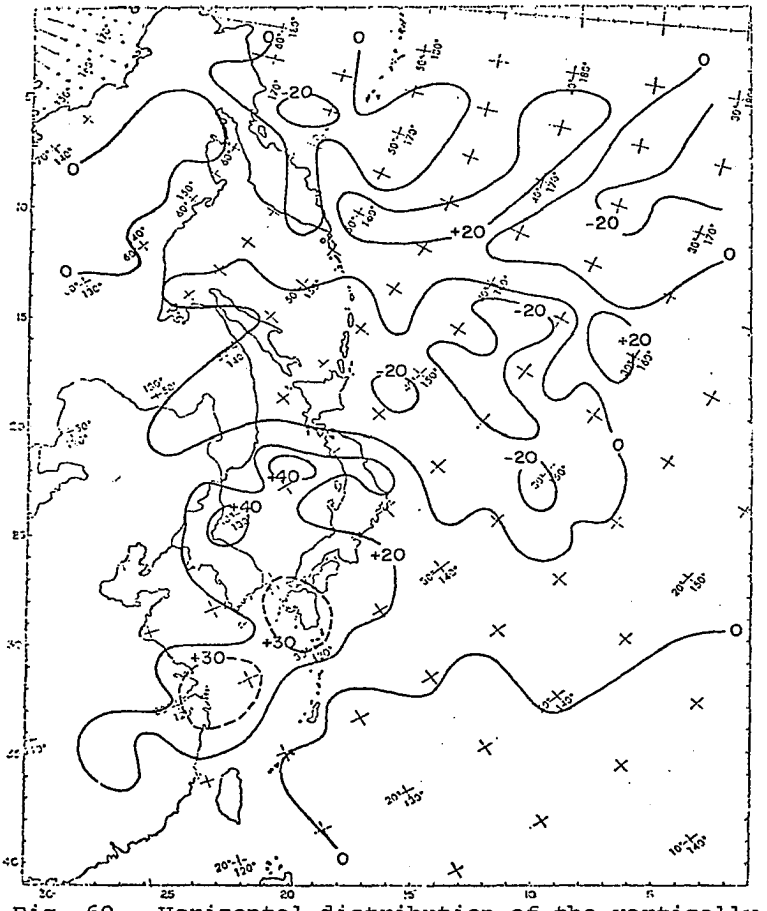

Fig. 60. Horizontal distribution of the vertically integrated generation of kinetic energy for 0000 GMT, 14 February 1975. Units are in Wm^{-2}.

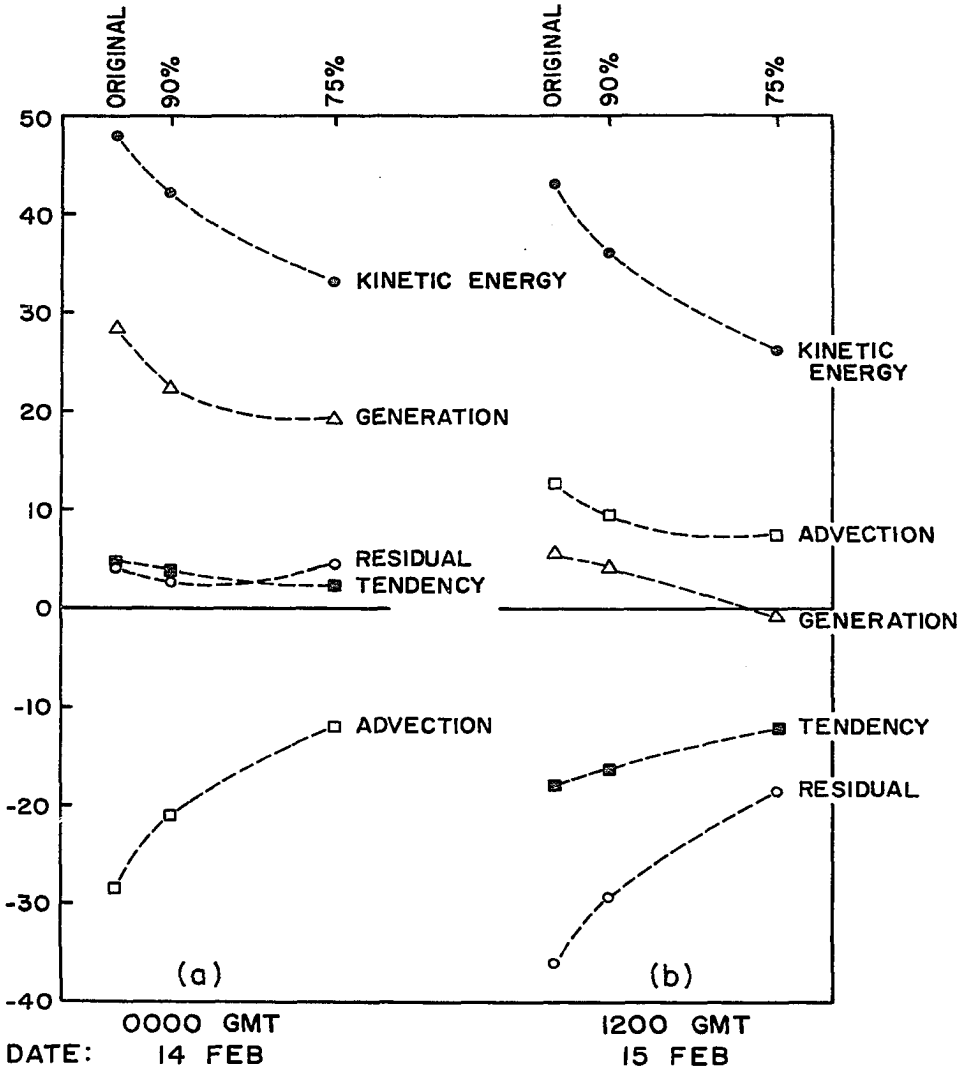

Fig. 61. The sensitivity of budget terms to % changes in the geostrophic wind as first guess for the wind analysis. Kinetic energy is in 10^5 J·m^{-2}. Other terms are in W·m^2.